Universitat de Girona

METHODOLOGY FOR THE EXPERIMENTAL CHARACTERISATION OF MODE I DELAMINATION UNDER DIFFERENT LOADING RATES

Sergio Alonso Medina Escobar

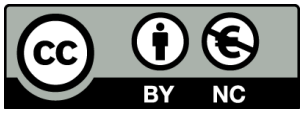

Universitat de Girona

Doctoral Thesis

METHODOLOGY FOR THE EXPERIMENTAL CHARACTERISATION OF MODE I DELAMINATION UNDER DIFFERENT LOADING RATES

Sergio Alonso Medina Escobar

2022

Universitat de Girona

Doctoral Thesis

Methodology for the experimental characterisation of mode I delamination under different loading rates

Sergio Alonso Medina Escobar

2022

Doctoral Program in Technology

Advisors:

Dr. Norbert Blanco Villaverde
Universitat de Girona

Dr. Emilio V. González Juan
Universitat de Girona

Thesis submitted for the degree of Doctor of Philosophy

Sergio Alonso Medina Escobar

Methodology for the experimental characterisation of mode I delamination under different loading rates

Doctoral Thesis, 2022

Doctoral Program in Technology

Advisors: Dr. Norbert Blanco Villaverde and Dr. Emilio V. González Juan

Universitat de Girona

AMADE Research Group

Escola Politècnica Superior

Dept. d'Enginyeria Mecànica i de la Construcció Industrial

Carrer de Maria Aurèlia Capmany i Farnés, 61 - Campus Montilivi

17003 Girona

... con amor y cariño para ti mamá.

> *All we have to decide is what to do with the time that is given us.*

— **Gandalf** —
(The Fellowship of the Ring
by J.R.R. Tolkien)

Acknowledgement

I would like to express my sincere gratitude to my advisors Dr. Norbert Blanco and Dr. Emilio González for this challenging but gratifying journey of five years of PhD. A time full of ups and downs, but they have always been by my side, it has been a pleasure to have a mama and papa like you. Also, I am extremely grateful to Dr. Albert Turon for the opportunity to come to Girona and join AMADE. I would also like to thank to Dr. Pere Maimí for all the guidance with his clever ideas, and Dr. Jordi Renart and Dr. Carlos Sarrado for the discussions. I express my sincere gratitude to Dr. Jose Artero and Dr. Jesús Pernas from Universidad Carlos III de Madrid for the interest and collaboration with the high rates testing. Additionally, I would like to thank all the members at the AMADE research laboratory and the UC3M labs who have helped in successfully completing the experimental campaign.

During my research stay at the Fraunhofer Institute for High-Speed Dynamics - EMI in Germany, I had a great support from Dr. Michael May, and despite the rough situation due to COVID, I enjoyed my stay there. Immense thanks to Philipp, Sally and Patrick for all the help and the nice shared moments in the lab and in Freiburg, the experience was amazing because of you!

This section is never complete if I don't thank all my dear colleagues at the AMADE group, the people who has pass by all these years. The atmosphere at the Uni has been superb thanks to all of you. A special thanks to all my dear flatmates during all these years, we definitely had an amazing time at home. Countless gratitude to my PhD life friends: Aravind, Javi, Juan José, Jaqueline, Magda, Laura, Jordi, Younes, Edwin. I met them by fortune and I am immensely fortunate to keep their friendship.

My greatest and most emotional show of thankfulness to my family, in especial to my mom, the inspiration and motivation to follow the academic life so far, no gratitude is enough. As importantly, thanks to Natalia and Júlia, my new home. They have support me with endless love despite the several rough times during the last year due to the thesis. I love you, my girls.

Preface

The work contained in this Ph.D. thesis was conducted at the AMADE research group (Department of Mechanical Engineering and Industrial Construction, University of Girona, Spain). The thesis was carried out with the financial support from the predoctoral grant IFUdG2017/43 from the University of Girona. The author also acknowledges the financial support from the Spanish Ministerio de Ciencia, Innovación y Universidades through the project RTI2018-099373-B-100.

A part of the thesis is dedicated to the BEDYN project that was led by Dassault Aviation, in collaboration with the Universidad Carlos III de Madrid (UC3M), Compoxi and AMADE research group (Universitat de Girona). This project has received funding from the Clean Sky 2 Joint Undertaking (JU) under grant agreement No. 886519. The JU receives support from the European Union's Horizon 2020 research and innovation programme and the Clean Sky 2 JU members other than the Union.

Part of the research presented in this thesis was developed during the Ph.D. candidate's research stay at the Fraunhofer Institute for High-Speed Dynamics, Ernst-Mach-Institute (Freiburg, Germany) with the financial support from the mobility grant MOB19 from the University of Girona.

Outcomes & Publications

The scientific contribution outcomes of the present Ph.D. is presented below:

Peer-reviewed journal articles

- **S.A. Medina**, E.V. González, N. Blanco. Transition time threshold for Double Cantilever Beam specimens under high loading rates. ***Engineering Fracture Mechanics***, 107754 (2021) 249. doi: `doi.org/10.1016/j.engfracmech.2021.107754`.

- **S.A. Medina**, E.V. González, N. Blanco, J. Pernas-Sánchez, J.A. Artero-Guerrero. Guided Double Cantilever Beam test method for intermediate and high loading rates in composites. *Submitted for publication in* ***International Journal of Solids and Structures***, (2022).

- **S.A. Medina**, E.V. González, N. Blanco, P. Maimí, J. Pernas-Sánchez, J.A. Artero-Guerrero, P. Hahn, M. May, E. de Blanpré, V. Jacques. Rate-dependency analysis of mode I delamination by means of different data reduction strategies for the GDCB test method. *Submitted for publication in* ***Composite Structures***, (2022).

Patents

- **S.A. Medina**, E.V. González, N. Blanco. Dispositivo para ensayo de tenacidad a la fractura en modo-I con velocidad de carga controlada. Device for mode-I fracture toughness testing with controlled loading rate. *Publication Number WO/2022/003219*, (6$^{\text{th}}$ January 2022). `https://patentscope.wipo.int/search/en/detail.jsf?docId=WO2022003219`

Conferences

- **S.A. Medina**, E.V. González, N. Blanco, P. Hahn, M. May. Development of a new dynamic testing method for mode-I interlaminar fracture toughness under high loading rates. 10$^{\text{th}}$ International Conference on Composites Testing and Model Identification (Comptest 2021). Virtual - Lille (France).
  International Conference. Oral presentation.

- **S.A. Medina**, E.V. González, N. Blanco, J. Pernas-Sánchez, J.A. Artero-Guerrero. Rate-dependency behaviour of the mode-I interlaminar fracture toughness in composite laminates. 1$^{\text{st}}$ Virtual ESIS TC4 Conference on Fracture of Polymers, Composites and Adhesives (ESIS TC4 2021). Virtual - Les Diablerets (Switzerland).
  International Conference. Oral presentation.

- **S.A. Medina**, E.V. González, N. Blanco, J. Pernas-Sánchez, J.A. Artero-Guerrero, V. Jacques, E. de Blanpré. Analysis of the rate-dependency of the mode I interlaminar fracture toughness in composite laminates using different data reduction strategies. 20$^{\text{th}}$ European Conference on Composite Materials (ECCM20 2022). Lausanne (Switzerland).
  International Conference. Oral presentation.

Declaration

Universitat de Girona

Dr. Norbert Blanco Villaverde, Full Professor at Universitat de Girona,

and

Dr. Emilio V. González Juan, Associate Professor at Universitat de Girona,

hereby CERTIFY that:

The work entitled *Methodology for the experimental characterisation of mode I delamination under different loading rates*, submitted for the doctoral degree by Sergio Alonso Medina Escobar, has been conducted under our supervision and fulfils the requirements for the *International Doctorate*.

Norbert Blanco Villaverde
Universitat de Girona

Emilio V. González Juan
Universitat de Girona

Girona, October 2022

Contents

List of Figures

List of Tables

Abstract

The rate-dependent behaviour of the interlaminar fracture toughness of fibre reinforced composites has been a matter of research during the last decades. However, the results obtained so far are not conclusive and further analysis is required. In parallel, the correct characterisation of these material properties should promote the development of reliable constitutive models for the simulation of dynamic events.

The research carried out in this thesis starts by trying to identify and understand the governing parameters involved in dynamic testing of mode I fracture toughness. With this in mind, a time-based threshold criterion is proposed to determine when dynamic effects might be neglected during the analysis of a high loading rate Double Cantilever Beam (DCB) test. The criterion compares the time after which inertia effects can be neglected in the specimen, known as transition time, versus the time for the initiation of fracture propagation. Three different methods are considered for determining the transition time: an analytical approach, a numerically-based method and a graphic method through FE simulations. Good agreement is found when comparing the derived expressions with the results of numerical simulations. It is also demonstrated that the transition time is affected by the velocity profile. The proposed criterion and approach to determine the transition time are useful tools to define when a quasi-static data reduction scheme can be used, providing an initial framework to mark off the analysis of high-rate tests.

An analysis of the specific literature regarding the test methods shows that there is no consensus on the appropriate methodology to characterise the interlaminar fracture toughness of composite materials under high-strain

rates. In this thesis a new test method, the Guided Double Cantilever Beam (GDCB), is presented to measure the mode I fracture toughness in composites laminates and brittle adhesively bonded joints under intermediate/high loading rates. The proposed device guarantees a symmetric crack opening and thus pure mode I propagation during high loading rate testing. When used in a dynamic servo-hydraulic testing machine with controllable displacement rate, a constant opening velocity can be driven. The GDCB testing method is validated against a quasi-static DCB test, showing a good agreement between the results. In addition, the test method has been satisfactorily used under intermediate/high loading rates, showing the good performance of the device. The GDCB device has been patented with patent number WO/2022/003219.

The loading-rate mechanical response of the mode I delamination in composites and adhesively bonded joints has been also investigated. Using the GDCB test method, three different data reduction strategies have been assessed: a displacement-based formulation, a near-crack-tip displacement formulation, and a numerical assessment method based on the deformed shape of the arms of the specimen. The methods are developed to account for the dynamic effects which may be present during the test. Small differences between the three different methods can be noticed when comparing the results. Meanwhile, no clear rate-dependency of the fracture toughness has been evidenced for the composite laminate nor the adhesively bonded joint used.

Finally, a methodology for the dynamic mode I characterisation of composites and brittle adhesively bonded joints has been proposed. The methodology is established for a wide range of loading rates: from quasi-static to high loading rates (up to 30 m/s opening loading rates). The methodology covers the test methods, the data reduction methods, and the test set-up to obtain the parameters required in the data reduction.

Resum

La caracterització de la tenacitat a la fractura interlaminar dels materials compostos respecte la velocitat de deformació ha estat un tema rellevant de recerca durant les últimes dècades. Tot i així, els resultats obtinguts fins ara no són concloents i es fa necessari continuar investigant sobre el tema. Al mateix temps, una correcta catacterització d'aquestes propietats permetria el desenvolupament de models constitutius adaptats per a la simulació d'esdeveniments dinàmics.

El treball de recerca durant aquesta tesi parteix de la identificació i la comprensió dels paràmetres de govern involucrats en els assajos dinàmics de tenacitat a la fractura en mode I. Amb això en ment, es proposa un criteri de temps límit o llindar amb la finalitat de determinar quan es poden menysprear els efectes dinàmics durant l'anàlisi d'un assaig de doble biga en voladiu (o de l'anglès, Double Cantilever Beam, DCB) en assaigs amb alta velocitat d'aplicació de la càrrega. El criteri compara el temps després del qual es poden menysprear els efectes d'inèrcia, conegut com temps de transició, amb el temps transcorregut per a l'inici de la propagació de la fractura. En concret, es consideren tres mètodes diferents per a determinar el temps de transició: un mètode analític, un mètode basat en una anàlisi numèrica i un mètode gràfic per mitjà de simulació per elements finits. Al comparar els resultats de les expressions obtingudes amb els resultats de simulacions numèriques es troba un comportament similar entre ells. També es demostra que el temps de transició es veu afectat pel perfil de velocitat de càrrega. Finalment, es pot esmentar que tant el criteri límit com la metodologia proposada per a determinar el temps de transició són eines útils per a definir quan es pot utilitzar un esquema de reducció de dades quasi-estàtic. Això permet un marc inicial per a delimitar l'anàlisi de les proves sota condicions de càrrega a alta velocitat.

De l'anàlisi específica de la bibliografia dels mètodes d'assaig es pot concloure

que no existeix un consens sobre quin és el millor mètode d'assaig per a caracteritzar la tenacitat a la fractura interlaminar en materials composits a alte velocitat de càrrega. En aquesta tesi es presenta un nou mètode d'assaig, el Guided Double Cantilever Beam (GDCB), o assaig de doble biga en voladiu guiat, per a mesurar aquesta tenacitat a la fractura interlaminar en mode I en laminats compòsits i unions adhesives sota velocitats de càrrega mitjanes/altes. El dispositiu proposat garanteix una obertura simètrica de l'esquerda i, per tant, una propagació en mode I pur durant els assajos a alta velocitat de càrrega. Quan s'utilitza en una màquina servohidráulica d'assajos dinàmics, es pot assolir una velocitat d'obertura constant dels braços. El mètode d'assaig GDCB es valida comparant amb un assaig quasi-estàtic de DCB, obtenint una bona concordança entre els resultats d'ambdós mètodes. A més, el dispositiu GDCB ha estat patentat amb el número de patent WO/2022/003219.

També s'ha investigat la resposta mecànica a la velocitat de càrrega de la delaminació en mode I en compòsits i unions adhesives. Fent ús del mètode d'assaig GDCB proposat, s'avaluen tres estratègies diferents de reducció de dades: una formulació basada en el desplaçament dels braços en el punt d'aplicació de la càrrega, una formulació local en base als desplaçaments dels braços prop de la punta d'esquerda, i un mètode d'avaluació numèrica basat en els desplaçaments experimentals dels braços. Tots ells pretenen tenir en comptes els efectes dinàmics presents durant l'assaig. Comparant els resultats obtinguts amb els tres mètodes es poden detectar petites diferències. Així i tot, no s'ha evidenciat una clara dependència de la tenaticat a fractura amb la velocitat de càrrega per al material compost ni tampoco per la unió adhesiva utilitzada.

Finalment, s'ha proposat una metodologia per a la caracterització dinàmica en mode I de laminats compostos i unions adhesives de baix comportament plàstic. La metodologia s'estableix per a un ampli rang d'assajos, des de quasi-estàtics fins a velocitats de càrrega elevades (velocitats d'obertura dels braços de fins a 30 m/s). La metodologia cobreix els mètodes d'assaig, els

mètodes de reducció de dades i la instrumentació de l'assaig per a obtenir els paràmetres necessaris en la reducció de dades.

Resumen

El comportamiento de la tenacidad a la fractura interlaminar respecto a la tasa de deformación en materiales compuestos ha sido un tema de investigación relevante durante las últimas décadas. Sin embargo, los resultados obtenidos hasta ahora no son concluyentes, siendo necesaria una mayor investigación. Sumado a ello, la correcta caracterización de estas propiedades debería promover el desarrollo de modelos constitutivos más confiables para la simulación de eventos dinámicos.

La investigación llevada a cabo en esta tesis parte de la identificación y comprensión de los parámetros de gobierno involucrados en los ensayos dinámicos de tenacidad a la fractura en modo I. A partir de ello, se propone un criterio límite basado en el tiempo, con el fin de determinar cuándo los efectos dinámicos durante el análisis de un ensayo de doble viga en voladizo (o del inglés, Double Cantilever Beam, DCB) durante ensayos con una alta velocidad de aplicación de la carga pueden ser despreciados. El criterio compara el tiempo a partir del cual se pueden despreciar los efectos inerciales, conocido como tiempo de transición, con el tiempo transcurrido para iniciar la propagación de la fractura. En concreto, se consideran tres métodos distintos para determinar el tiempo de transición: un método analítico, un método basado en un análisis numérico y un método gráfico a través de simulación por elementos finitos. Al comparar los resultados de las expresiones obtenidas con resultados de simulaciones numéricas se encuentra un comportamiento similar entre ellos. También, se demuestra que el tiempo de transición se ve afectado por el perfil de velocidad de aplicación de la carga. Finalmente, se puede decir que tanto el criterio límite como la metodología propuesta para determinar el tiempo de transición son herramientas útiles para definir cuándo se puede utilizar un esquema de reducción de datos cuasi-estático. Esto permite definir un marco inicial para delimitar el análisis de los ensayos a altas tasas de aplicación de la carga.

Un análisis específico de la bibliografía relacionada con los métodos de ensayos permite determinar que no existe consenso sobre el método de ensayo para caracterizar la tenacidad a la fractura interlaminar en materiales compuestos bajo altas tasas de aplicación de la carga. En esta tesis se presenta un nuevo método de ensayo, el Guided Double Cantilever Beam (GDCB), o ensayo de doble viga en voladizo guiado, para medir dicha tenacidad a la fractura interlaminar en modo I en laminados compuestos y uniones adhesivas bajo tasas de aplicación de carga intermedias/altas. El dispositivo propuesto garantiza una apertura simétrica de los brazos de la probeta y, por lo tanto, un modo I puro a la hora de propagar la grieta durante los ensayos a alta velocidad. Cuando el dispositivo se usa en una máquina servohidráulica de ensayos dinámicos con tasa de desplazamiento controlable, se puede conseguir una velocidad de apertura constante de los brazos. El método de ensayo GDCB se ha validado respecto a un ensayo cuasi-estático de DCB, mostrando una buena concordancia entre los resultados. Además, el dispositivo GDCB has sido patentado con número de patente WO/2022/003219.

Adicionalmente, se ha investigado la respuesta mecánica de la tasa de aplicación de la carga de la deslaminación en modo I en materiales compuestos y uniones adhesivas. Usando el método de ensayo GDCB, se evaluaron tres estrategias diferentes para la reducción de datos: una formulación basada en el desplazamiento de los brazos en el punto de aplicación de la carga, una formulación de desplazamiento de los brazos cercana a la punta de la grieta y un método de evaluación numérica basado en los desplazamientos de los brazos a lo largo de la probeta. Estos métodos se han desarrollado para tener en cuenta los efectos dinámicos que pueden estar presentes durante el ensayo. Al comparar los resultados obtenidos por los tres métodos se pueden detectar pequeñas diferencias. Aun así, no se ha evidenciado una clara dependencia de la tenacidad a fractura con la tasa de aplicación de la carga, ni para el laminado compuesto ni para la unión adhesiva utilizada.

Por último, se ha definido una metodología para la caracterización dinámica

en modo I de compuestos laminados y uniones adhesivas de baja plasticidad. La metodología se establece para un amplio rango de ensayos, desde ensayos cuasi-estáticos hasta altas tasas de aplicación de la carga (tasas de apertura de los brazos de hasta 30 m/s). La metodología cubre los métodos de ensayo, los métodos de reducción de datos y la instrumentación del ensayo para obtener los parámetros requeridos en la reducción de datos.

Part I

Introduction & Literature review

1 Introduction

1.1 Overview & Motivation

The use of composite materials for structural applications in several industries has experienced a large increase in the last decades, being a suitable material for new solutions in engineering applications. In the same way, the use of structural adhesives to bond polymer composites has grown within the aerospace and automotive industries. However, further improvement in the knowledge of the mechanical behaviour of these materials under dynamic conditions at different strain rates is required for more accurate and reliable designs. In order to predict and study the dynamic behaviour of composite structures and adhesively bonded structures different methods have been developed. The use of Finite Element (FE) simulation tools is one of the main design methodologies for these structures. The accuracy of the FE predictions relies, in part, on the material properties and the implemented constitutive laws. Generally, the material properties required for the numerical analysis are characterised under quasi-static loading conditions [1], however, these properties are usually used to feed constitutive models for the dynamic simulation of a given structure. Therefore, it is necessary to develop suitable test methods to obtain reliable input data for the material models used for dynamic loading. It has been demonstrated that the use of rate-dependent material models significantly influences the numerical prediction of the structure behaviour [2], such as in crash and impact simulations [3].

In addition, diverse experimental test set-ups have evidenced different strain rate dependency of key properties such as stiffness and strength, even for the same material and conditions [4]. These differences in the values obtained are basically due to: the data reduction method applied, different test set-ups can be used, and measuring reliable forces and crack growths at high strain

rates is challenging. Most of the test set-ups for high strain rates derive from quasi-static test methods although they may be inappropriate since different phenomena, mainly dynamic effects, are present. This clearly shows that the composites at high rate testing have many difficulties and challenges which need to be solved.

One of the main concerns of composite structures is their weakness against debonding of individual plies causing delamination. When using the numerical analysis to study, predict or design against delamination, one of the material properties required is the interlaminar mode I fracture toughness. This material property has been extensively studied in composite materials under quasi-static loading conditions [5–8], commonly using the Double Cantilever Beam (DCB) test. Different standards have been defined for the quasi-static mode I interlaminar testing of FRPs (fibre reinforced polymers), such as ISO 15024:2001 [9], ASTM D5528-13 [10] and JIS K 7086:1993 [11]. For dynamic loading cases, the information available about the behaviour of polymer-based composite materials is limited. Most of the studies carried out need to be improved since the base hypotheses are not adequate, such as the use of governing equations without taking into account a dynamic framework. It is important to define a framework for each analysis since the rate-dependency of these properties must be characterised using the appropriate method depending of the strain rate desired, as shown in Fig. 1.1. Hence, it is important to understand the effect of the governing parameters to account for the proper dynamic considerations during dynamic testing.

Whilst there seems to be consensus to determine the rate-dependent in-plane properties [12], there still remain many open questions regarding the measurement of rate-dependent fracture toughness in composite materials, such as for mode I delamination. Unlike for quasi-static loading, no protocols and standard test methods have yet been defined.

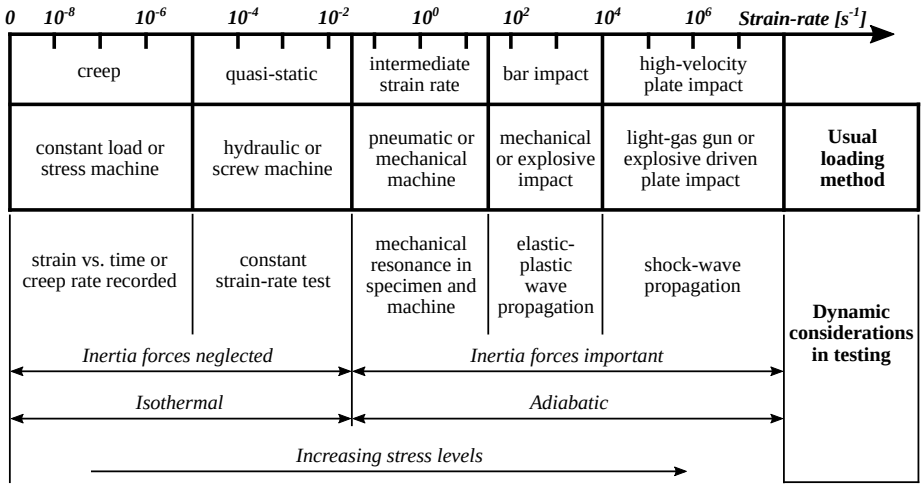

Fig. 1.1: Dynamic aspects of testing according to the strain rate (Image adapted from: Sierakowski [13]).

1.2 Objective

The thesis aims to define a methodology to characterise the loading rate dependency of the mode I interlaminar fracture toughness of laminate composites and adhesively bonded joints, where no standard has been defined and a lack of comprehensive characterisation methods regarding the rate effect of materials is still present.

1.3 Scope

The purpose of the thesis is to contribute to the study of the dynamic response of composites, especially with the interlaminar fracture toughness. The thesis deals with the study of the governing parameters that can affect delamination for different loading rates (quasi-static to high-rates). Even though, not all of them can be considered for the proposal of the methodology, as the cases of transient loading and heat. Besides, a threshold where a dynamic framework for the data reduction method can be set for mode I delamination testing is required.

The development of a test set-up that allows to capture the dynamic effects on the interlaminar fracture toughness in the material is needed. The test set-up should avoid the problems found in the literature from the previous tests used. In addition, a suitable data reduction method must be defined to capture the real behaviour at the different loading rates, especially at high-rates where the dynamic contribution can take an important role.

1.4 Thesis Layout

This thesis is structured in three parts. The first part (Chapter 1 and 2) includes the introduction and the literature review. The second part (Chapter 3 to 6) describes in detail the development to obtain a methodology for mode I dynamic testing, which is the final outcome of the thesis. Finally, the third part (Chapter 7 and 8) concludes the thesis including an assessment of the achievements made and suggestions for future work.

Describing the chapters, Chapter 2 provides a brief literature review regarding the mode I fracture toughness with a view to the dynamic testing and analysis, that helps to identify the gaps and needs for the topic. An study of the parameters involved in dynamic analysis is presented in this chapter. Chapter 3 deals with the first step when testing under dynamic loading that is to know if the corresponding dynamic test can be analysed using a quasi-static framework. This chapter allows to understand the role of some of the parameters involved in dynamic analysis described in the previous chapter. Chapter 4 and 5 present a test method for the mode I delamination at high-rates. Chapter 4 is focused on the development of the testing device and the test set-up, meanwhile, Chapter 5 presents different data reduction methods. Chapter 6 resumes the work done in Chapters 3, 4 and 5, to present the proposed methodology for dynamic mode I testing, giving response to the objective of the thesis. The thesis is concluded in Chapter 7 with the concluding remarks, and in Chapter 8 with prospective ideas for future work.

Literature review

2

2.1 Dynamic properties in composites

During the last decades, the effect of strain rate over the elastic and strength properties in polymer-based composites has been extensively studied. Works like the ones performed by Jacob et al. [14] and Körber [12] give a review about the studies done over polymer composite materials and unidirectional carbon-epoxy material systems, respectively. Emphasis has been given to compression (more experimental data found) since the response of the materials is strongly influenced by the behaviour of the matrix, but studies on tension and shear properties are also included.

For compression, Hsiao and Daniel used a drop-weight tower [15] and a Split-Hopkinson Pressure Bar (SHPB) [16] for high strain rate experiments on carbon-epoxy laminates. They found no strain rate effect for the longitudinal compressive modulus but reported a significant increase for longitudinal compressive strength. Besides, the transverse compressive modulus and strength were found to increase with increasing the strain rate. Similar conclusions were reached by Hosur et al. [17], Bing and Sun [18], Wiegand [19] and Koerber et al. [20], and more recently by Koerber et al. [20] and Ploeckl et al. [21] on the dynamic behaviour of the compressive modulus and strength in composites. These studies were carried out mainly using a SHPB but in some cases in order to obtain medium strain rates hydraulic machines were used.

For in-plane tension, Harding and Welsh [22], and Taniguchi et al. [23] used a tensile SHPB apparatus and found no significant strain rate effects over unidirectional carbon-epoxy laminates. Gilat et al. [24] and Taniguchi et al. [23] studied the transverse tensile properties, reporting that both, transverse

tensile modulus and strength, increase with increasing the strain rate. For the case of dynamic in-plane shear, where no common standard exists, Staab and Gilat [25], Gilat et al. [24], Taniguchi et al. [23], Shokrieh and Omidi [26] and more recently by Tsai and Sun [27] conducted dynamic tests. These studies are difficult to assess since the test itself presents some limitations and important considerations that may difficult the comparison.

When focused in the fracture behaviour of composite laminates, three different types of fracture toughness must be considered: the interlaminar, the intralaminar and the translaminar. In the interlaminar fracture, the crack propagates in between the plies, whereas in the intralaminar case, the crack is located inside the plies (longitudinal or transverse intralaminar matrix crack). In the translaminar fracture, the crack grows perpendicular to the fibres which implies the fracturing of fibres, and it can be due to tensile or compressive loads.

The dynamic interlaminar fracture toughness of composite materials has received less attention and few research analysis are present in the literature. Nevertheless, as it is the main topic of this thesis, a specific review of this subject is presented in Section 2.2. For the dynamic intralaminar fracture toughness, some studies has been carried out using different set-ups [28–34]. In her work, McCarroll [28] used a servo-hydraulic machine to test carbon-epoxy Compact Tension (CT) specimens but the results were overshadow by the scatter. Kuhn et al. [29] and Leite et al. [31] used Double-Edge Notched Compression (DENC) specimens in a SHPB for carbon-epoxy materials obtaining that the fibre compressive failure increases with high-rate loading. Kuhn et al. [30] and Leite et al. [32] presented an equivalent study for the fibre tensile failure using Double-Edge Notched Tension (DENT) specimens with a small increase at high strain rate. Catalanotti et al. [33] performed an equivalent study over an E-Glass polymer composite material system, obtaining a significant increase of the dynamic fracture toughness in tension and compression loading. Yoo et al. [34] defined the characterisation of the

dynamic intralaminar fracture toughness of composites by means of a high-speed servo-hydraulic test machine, as an alternative to the SHPB testing from previous works. Finally, regarding the translaminar fracture toughness, Laffan et al. [35] presented a review for the characterisation of the fracture toughness associated with the translaminar (fibre-breaking) failure modes of continuously reinforced laminated composites. More recently, Hoffmann et al. [36] used a dynamic CT test on a SHPB to determine the translaminar fracture toughness of a composite cross-ply.

2.2 Dynamic interlaminar fracture toughness of composites

The interlaminar fracture toughness of composite materials has been the subject of few studies for the dynamic loading. Strain rate effects on the Mode I, Mode II, and Mixed Mode (I/II) fracture toughness of FRP composites were summarised by Cantwell and Blyton [37] and Jacob et al. [4]. They showed that the changes in loading rate may affect the fracture toughness due to the effect of strain rate over the properties of the matrix. As Jadhav et al. [38] specified in their work, delamination and matrix cracking are the principal modes of failure of composite specimens when loaded dynamically out of the plane, which agrees with the behaviour reported previously [4, 37]. Some studies for dynamic loading have been limited to reporting the results and no attempt was made to explain the trends of the results by the test conditions or dynamic effects. The review work by May [1] presents a description of the different test configurations and specimens proposed through the years to assess the mode I dynamic interlaminar fracture toughness in terms of the strain rate or loading rate desired. In addition, Jiang and Vecchio [39] made a review for the dynamic fracture toughness tests using the SHPB apparatus in different materials including composites.

Despite the work done, from the different experimental research that has been performed to study the mode I loading rate effects in composite laminates, it can be concluded that there is no agreement on the trend of fracture toughness

with regard to loading rate. In some cases, it was noticed that with an increase of the loading rate there was an increase in the mode I fracture toughness [40–43], in some other cases a decrease in the mode I fracture toughness was found [44–47], and in some other studies no effect was observed [47–50]. Besides, the results of some studies have been inconclusive about the rate dependency of the fracture toughness. For example, Aliyu and Daniel [41] reported an increasing fracture toughness when increasing loading rates in AS4/3501-6 carbon composite laminates, while Smiley and Pipes [46] reported the opposite trend for the same material, using the same DCB test method. From the analysis of these previous results it can be concluded that testing and monitoring under high loading rates still require some improvements.

Additionally, the rate dependency of the fracture toughness in DCB type tests has been presented mainly by means of three different types of rates: the loading rate of specimen arms, the crack propagation velocity, and the crack opening displacement rate [1]. The challenge comes when comparing data reported with different types of rates, since there is not always a clear correlation between them. On the one hand, the use of the loading rate of the specimens arms is the most common way to report results, mainly, because it is easy to obtain it from testing. However, it is the least relevant since it describes the rate dependency with the behaviour far from the crack tip. On the other hand, the crack propagation velocity can directly be measured and it may represent in a better way the rate dependency since it is located at the crack tip. Nevertheless, when the data is required for rate-dependent cohesive zone models in numerical analysis, the crack propagation velocity cannot be used because the calculations are based on a local out-of-plane strain rate [3]. For these cases, the crack opening displacement rate is preferred, although, it is the most difficult rate to be measured.

Over the last decades, several test set-ups have been proposed. Even so, the Double Cantilever Beam (DCB) [9] test method (Fig. 2.1) is the most common adopted set-up for the analysis of the dynamic fracture toughness

of composites in mode I loading. The test set-ups reported in the literature include a wide range of loading and boundary conditions, including screw driven [51] or hydraulic test machines, modified Charpy and Izod impact tests, drop weight impact tower [52] and Hopkinson bar apparatus [53]. The desired loading rate defines the equipment and specimen configuration to be used as shown in Fig. 1.1 of Section 1.1.

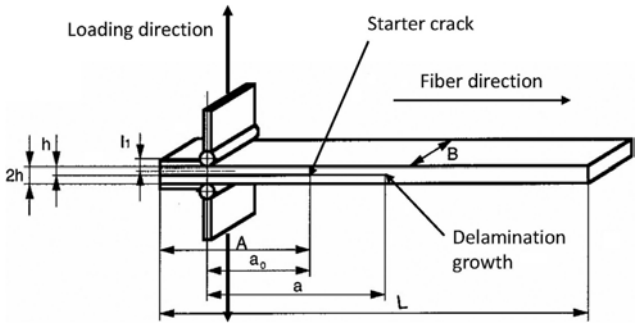

Fig. 2.1: Schematic of the standardised Double Cantilever Beam specimen for determining the quasi-static mode I fracture toughness (source: ISO 15024:2001 [9]).

The following subsections include a description of the issues associated to the dynamic characterisation of the mode I fracture toughness and the different options proposed in the literature to overcome them. Each subsection is focused on a main issue, and only the most relevant ones are presented.

2.2.1 Symmetrical opening behaviour

Blackman et al. [48, 54] used a DCB specimen in a servo-hydraulic testing machine to obtain high loading rates for their research. Applying the displacement-based approach for the mode I fracture energy, the displacement at loading point and the crack propagation was recorded using high-speed video cameras. Despite that the analysis was formulated to consider the dynamic effects, the high-speed images for monitoring the test behaviour showed that the deformation of the two arms of the specimen in the DCB was no longer symmetrical and the degree of asymmetry increased as the test velocity was increased [54]. Thus, it becomes a mixed-mode test and a

mode I analysis cannot longer be used. This unsymmetrical response is due to inertial effects affecting mainly one of the two arms of the specimen, the one where the machine displacement is applied. The asymmetrical behaviour can be seen in Fig. 2.2. Moreover, unstable crack growth was evidenced. Other authors had the same issue about the symmetry of the DCB test under high loading rates [50, 55] and it can be evidenced in Fig. 2.3.

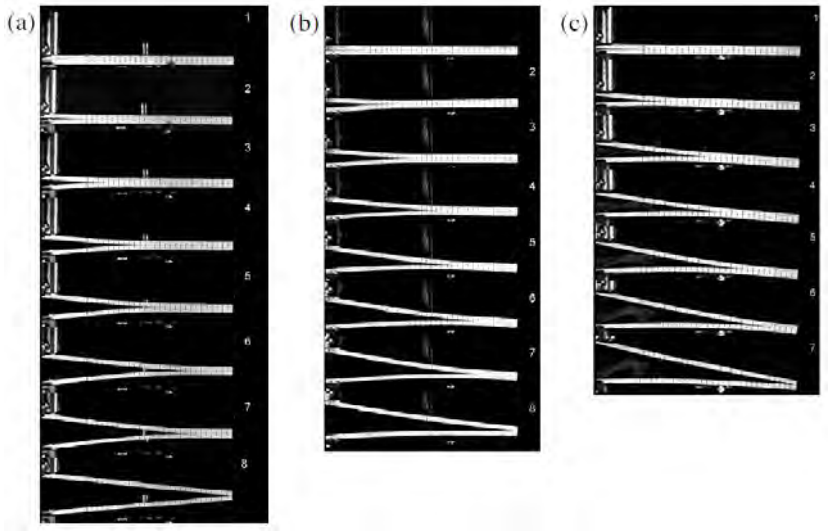

Fig. 2.2: High speed video photographs for a HTS-XD4600 DCB joint tested at (a) 0.1 m/s, (b) 3.6 m/s and (c) 15 m/s (source: Blackman et al. [55]).

To solve the issue of the symmetrical opening, Hug et al. [56] defined a complex device to amplify the quasi-static loads, based on the DCB test method. However, due to the inertia effect of the fixture, the loading rate was limited to 1.6 m/s. Thereafter, some authors used an internal wedge test (wedge-insert inside the DCB specimen), shown in Fig. 2.4. In this type of test, the crack length, defined as the distance from the load application point to the crack tip, is almost constant during the test, yielding to a crack growth stabilization and opening symmetry [47, 53, 57–59]. The internal wedge technique has proven to be especially useful for characterising material systems exhibiting pronounced stick-slip fracture behaviour. The drawback

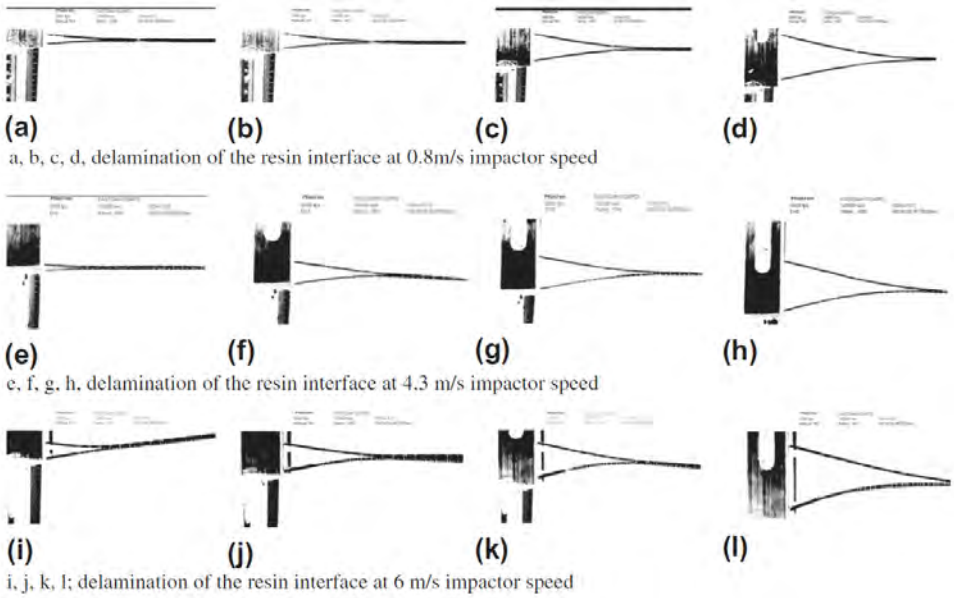

Fig. 2.3: Side view of an untufted DCB response at various high rates (source: Colin de Verdiere et al. [50]).

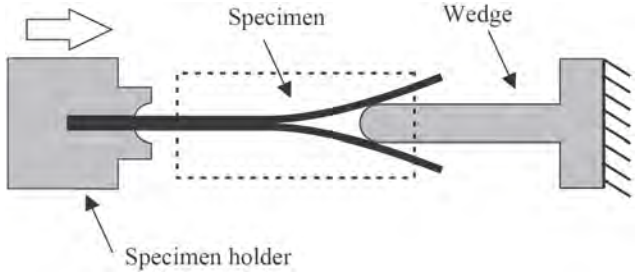

Fig. 2.4: Illustration of internal wedge test configuration (source: Isakov et al. [53]).

of this test method is the friction between the crack surfaces and the wedge while it is driven between the two arms, which is difficult to measure. May [1] reported that the wedge-insert fracture method is the most promising method for achieving mode I interlaminar fracture at elevated rates, being able to use the standard DCB specimen configuration and at the same time achieving symmetric loading.

Additionally, new proposals based on an external wedge falling method for a DCB specimen in a drop-weight tower were developed (Fig. 2.5), allowing a symmetrical opening of the specimen [52, 60–62], and removing the surface to surface friction between the wedge and the crack surfaces by using two external loading blocks. The loading method is, however, not free of friction, due to contact between the rollers and the wedges as well as the bearing blocks. The authors managed to minimise the friction by the use of smooth wedge surfaces and tight tolerance machining and lubrication. In spite of that, the load is of an impact nature, generating load vibrations and pulses, without constant opening velocity and unstable crack growth when using a drop-weight tower machine. Liu et al. [63] proposed a symmetrically opened DCB test for high loading rates using a dual electromagnetic Hopkinson bar system, as shown in Fig. 2.6), solving the issues of the friction between the crack surfaces and the wedge, but limited to the use of this particular test device.

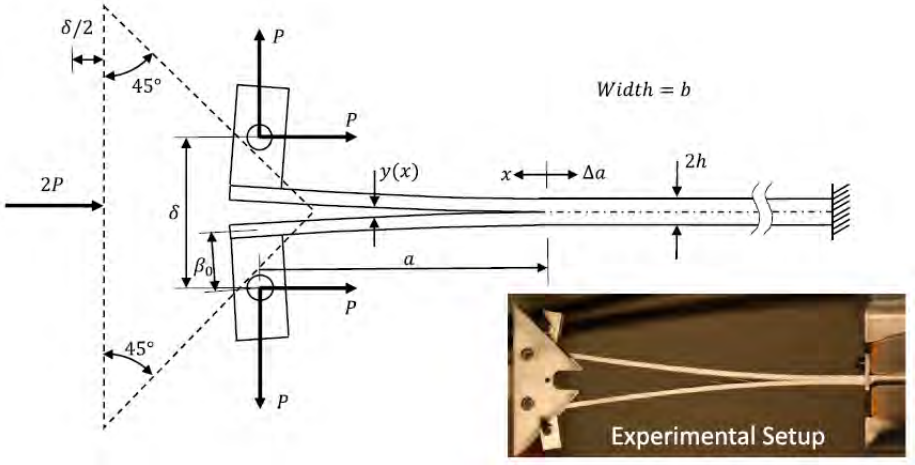

Fig. 2.5: External wedge falling method schematic and picture (source: Thorsson et al. [52]).

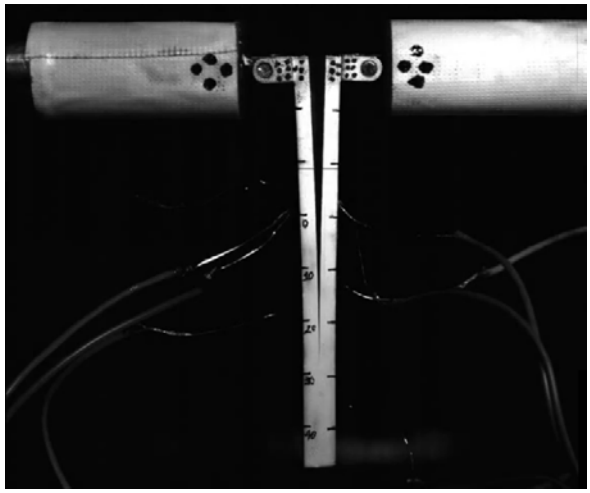

Fig. 2.6: Dynamic DCB experiment using the dual electromagnetic Hopkinson bar and subjected to symmetrical loadings by the two loading bars (source: Liu et al. [63]).

2.2.2 Dynamic effects in load and displacement monitoring

One issue associated with testing at high rates is related to the appropriate measuring of the applied load, so it can be used as an input for the data reduction. Typically, the load measured in such situations oscillates with important amplitudes at high frequencies due to the dynamic effects [48, 50, 55] and it cannot be filtered because it is not clear which oscillations are spurious and which not, as seen in Fig. 2.7 for a tufted non-crimp fabric (NCF), Fig. 2.8 for a PEEK/carbon-fibre composite, and Fig. 2.9 for a HTS-XD4600 DCB joint. Therefore, the signal from the load cell cannot be considered as representative of the material response and a load-independent data reduction approach is needed.

Due to all of the above, it seems more accurate the measurement of the displacement and perform a data reduction strategy with a load-independent method. However, a special care must also be taken when the displacement is recorded. The values of displacement can be affected by dynamic accelerations and oscillation effects [48, 64]. Blackman et al. [48] compared the displacement

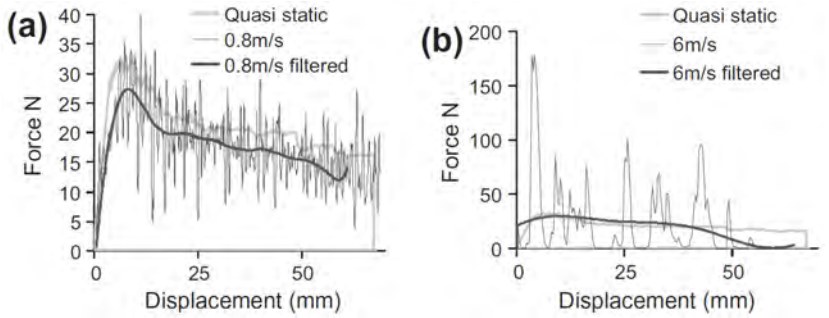

Fig. 2.7: Load response versus displacement for the tufted NCF at different loading rates: (a) 0.8 m/s and (b) 6 m/s with standard load cell set-up (source: Colin de Verdiere et al. [50]).

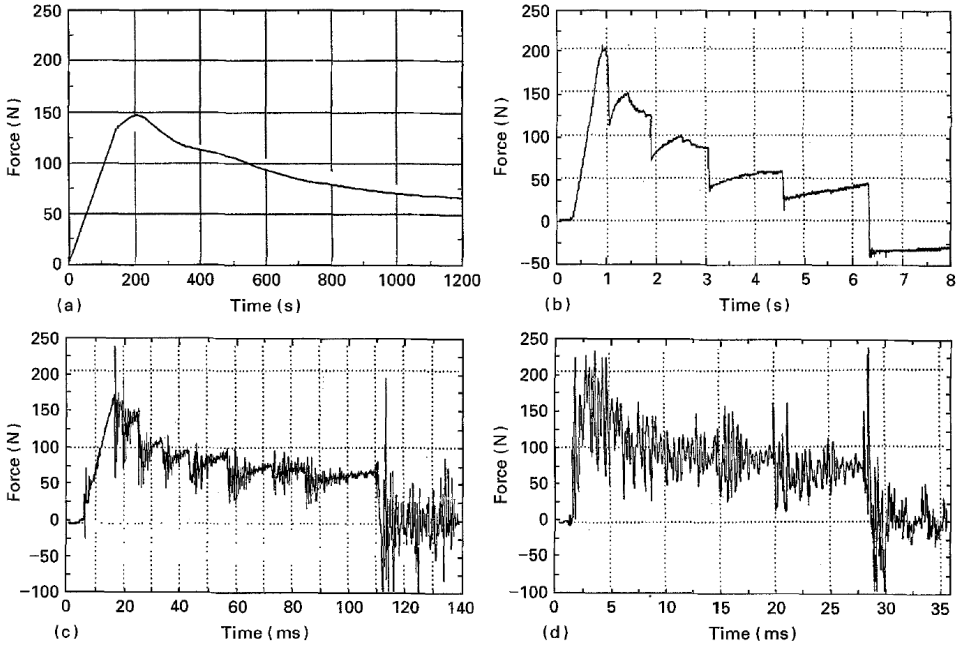

Fig. 2.8: Typical load versus time traces for PEEK/carbon-fibre composite tests conducted at a tester displacement rate of (a) 3.3×10^{-5} m/s, (b) 1×10^{-2} m/s, (c) 5×10^{-1} m/s, (d) 2 m/s (source: Blackman et al. [48]).

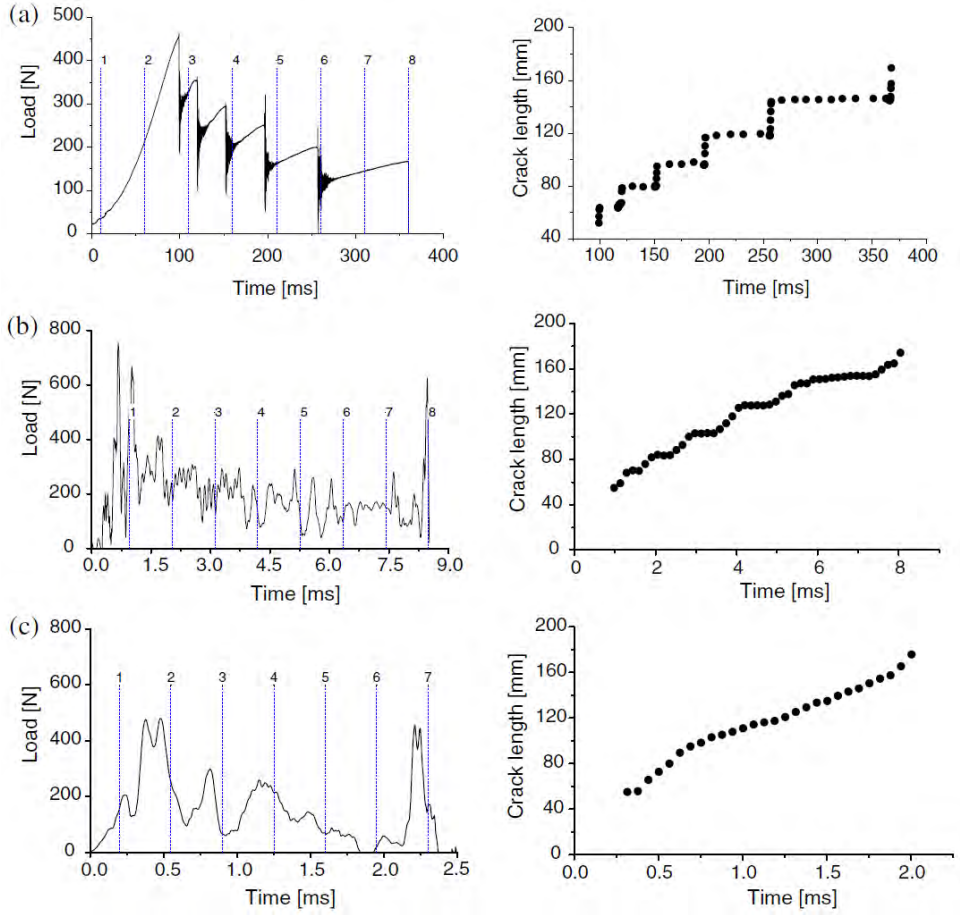

Fig. 2.9: Load versus time record for a HTS-XD4600 DCB joint tested at (a) 0.1 m/s, (b) 3.6 m/s and (c) 15 m/s (source: Blackman et al. [55]).

recorded through the test machine and the one monitored by high-speed photography. It was found that at low testing rates the response is the same (Fig. 2.10a), whereas at high testing rates the measurement of displacement in the testing machine is underestimated (Fig. 2.10b). An accurate usage of high-speed cameras must be done in order to capture the loading-point displacement.

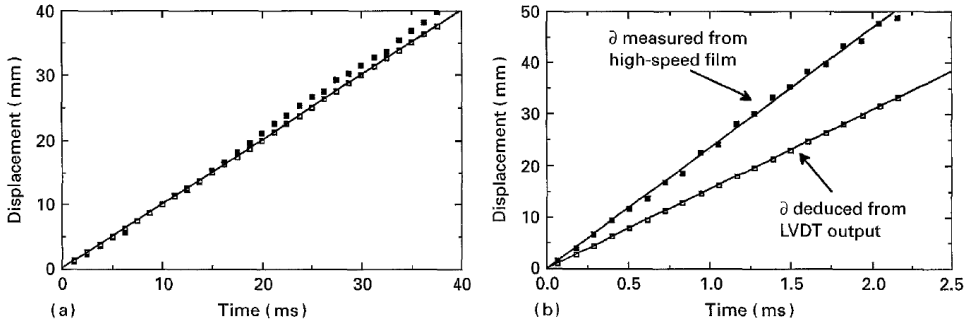

Fig. 2.10: Displacement versus time from tests conducted using an adhesively bonded DCB specimen at a tester displacement rate of (a) 1 m/s, (b) 15 m/s (source: Blackman et al. [48]).

2.2.3 Crack tip measurements

It has been probed that the use of specific set-up for data acquisition, such as the use of high-speed cameras or Digital Image Correlation (DIC), can increase the accuracy of the relevant measurements of the parameters involved in the data analysis [12, 65, 66]. The crack length during propagation is a common parameter in the data reduction methods, especially when load-independent data reduction approaches are used. As the case of quasi-static testing, crack tip propagation for high-rate analysis is usually measured optically by crack length monitoring, in this case by means of high-speed cameras [50, 52, 55, 64]. However, clear visibility of the crack is difficult for certain composite materials and adhesives, being challenging to follow this method. Other researchers, such as Lißner et al. [66] and Ben Salem et al. [67], relied upon measuring the crack length measurement using DIC recordings to avoid the crack length monitoring.

Other approach can be the estimation of the crack length by means of beams theory or measurement of the compliance. Isakov et al. [53] used a high-speed camera in an internal wedge DCB experiment (WDCB) to obtain the fracture energy by using an equivalent crack length measuring the deformation of the arms as shown in Fig. 2.11. Oshima et al. [62] and Riezzo et al. [59] used a quasi-static compliance calibrated analysis where the crack length is obtained

analytically by means of a compliance expression that uses the strain gauges attached to the specimen to calculate the load over the bending strain. Using this technique to obtain the fracture energy under dynamic loading needs careful consideration.

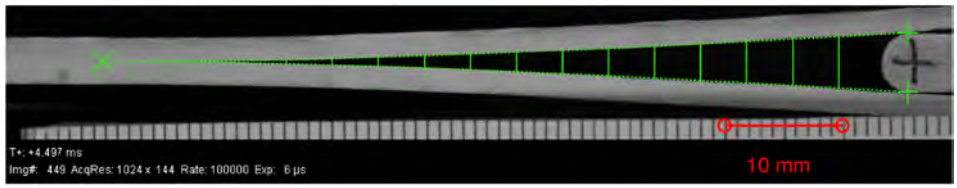

Fig. 2.11: Example of a high-speed video frame with superimposed visualization of the optical tracking and fitting based on the beam theory (source: Isakov et al. [53]).

2.2.4 Data reduction methods

The data reduction methods for mode I tests under quasi-static conditions are normally based on Linear Elastic Fracture Mechanics (LEFM). This is the case of the international standards ISO 15024:2001 [9] (Fig. 2.1), widely used to characterise the propagation of interlaminar cracks in fibre-reinforced composites, and ISO 25217:2009 [68], used to determine the fracture energy of adhesively bonded joints. According to [48], different correction factors must be included in the determination of the mode I interlaminar fracture energy, G_{Ic}, for the DCB test. The equation for the "corrected-load" method can be expressed as:

$$G_{\mathrm{Ic}} = \frac{12FP^2\left(a+\chi h\right)^2}{E_{11}b^2h^3} \tag{2.1}$$

and for the "corrected-displacement" method as:

$$G_{\mathrm{Ic}} = \frac{3}{2}\frac{F}{N}\frac{P\delta}{b\left(a+\chi h\right)} \tag{2.2}$$

where F and N are the correction factors for the large deflection and end-block effect, b is the width of the specimen and $2h$ is the combined thickness of fibre composite arms, a is the crack length, χ is the correction factor for end-rotation and deflection of the crack tip, P is the load required to induce

crack growth, δ is the displacement and E_{11} is the axial modulus of the fibre composite arms.

As LEFM is a very reliable method for quasi-static analyses, different authors have used the same approach for dynamic tests too. However, this approach does not account for the dynamic effects present during high-rate loading tests. This is one of the major reasons for so different results present in the literature. Interpreting results from dynamic fracture experiments is complex because of three factors: a) the inertia of the specimen and additional elements bonded to it, b) the time dependence of the material, and c) reflected stress waves that alter the stress state at the crack tip. However, most data reduction methods for deriving the fracture toughness were developed with quasi-static observations in mind. Since the quasi-static data reductions are not reliable for most of the cases, a deeper analysis of these dynamic effects is required. It has been shown that the data reduction method used is a key factor to correctly account for the dynamic effects during a dynamic characterisation of the fracture energy [1, 54].

An important remark about the experimental analysis of high-rate tests, in especial with inertia effects, is that the applied load cannot be measured accurately because of signal oscillations, as it has been explained in Section 2.2.2. For that reason, Blackman et al. [48] developed a load-independent (displacement-based) analysis for the dynamic DCB fracture toughness. In a first step of their research, they used a simple displacement-based LEFM analysis, which does not require a direct knowledge of the load:

$$G_{\mathrm{Ic}} = \frac{3}{16}\frac{F}{N^2}\frac{E_{11}h^3\delta^2}{(a+\chi h)^4} \tag{2.3}$$

Afterwards, an energy analysis in which the dynamic effect for the same DCB test was included [54, 55]. They proposed two cases for the analysis of dynamic fracture toughness where the kinetic energy in the moving specimen arms was significant when compared to the fracture energy: case 1, unstable crack growth (prior to crack propagation when the crack speed is zero in

stick slip events); and case 2, stable crack growth (for steady-state crack propagation where there is a velocity contribution from the crack motion). Finally, they expressed the dynamically-corrected fracture energy G_{Ic} for fast-rate unstable fracture as:

$$G_{\mathrm{Ic}} = \frac{3}{4}\frac{F}{N^2}\frac{E_{11}h^3t^2\left(\dot{\delta}/2\right)^2}{(a+\chi h)^4} - \frac{33}{140}\frac{E_{11}h\left(\dot{\delta}/2\right)^2}{{c_{\mathrm{o}}}^4} \tag{2.4}$$

and for the fast-rate stable fracture as:

$$G_{\mathrm{Ic}} = \frac{3}{4}\frac{F}{N^2}\frac{E_{11}h^3t^2\left(\dot{\delta}/2\right)^2}{(a+\chi h)^4} - \frac{111}{280}\frac{E_{11}h\left(\dot{\delta}/2\right)^2}{{c_{\mathrm{o}}}^4} \tag{2.5}$$

where $\dot{\delta}$ is the applied velocity, t is the time and c_{o} is the longitudinal wave velocity. In both cases the right term accounts for the kinetic energy and the left term is the quasi-static fracture energy.

Although the previous dynamic analysis was proposed several years ago, most authors still use the expression from Eq. (2.3) for G_{Ic} ignoring the dynamic effects [57, 60, 61, 69, 70]. In the work of Isakov et al. [53] it is proved that using a quasi-static framework is valid for their test and loading rates. They showed that the contribution of the kinetic energy can be assumed to be minimal for all the tested loading rates and only being important for loading rates above 30 m/s. Only a few works present in the literature include the kinetic effects in the analysis. Thorsson et al. [52] included the kinetic energy contribution to their modified wedge-insert fracture (MWIF) method using simple beam theory. The expression for G_{Ic} at high rates was expressed by:

$$G_{\mathrm{Ic}} = \frac{3P\delta}{2ba}\left(1 - \frac{{\beta_{\mathrm{o}}}^2\cos^2\left(\frac{3\delta}{4a}\right)}{a^2}\right) - \frac{33\rho h\dot{\delta}^2}{560} \tag{2.6}$$

where β_{o} is the initial moment arm linked to the axial force generated in this test.

Some other analysis have been performed using different strategies and theories to account for the dynamic mode I fracture toughness. Riezzo et al. [59]

performed dynamic wedge-insert tests using a thermal-mechanical physical system (based on a hydraulic system) to obtain the interlaminar fracture toughness in composite laminates. They used a quasi-static calibrated compliance curve with a load-dependent analysis to obtain the fracture energy in dynamic tests. Because wedge-insert test involves friction between the wedge and the cracked surfaces of the specimen, the load was measured indirectly by means of strain gauges attached to the specimen. The expression for G_{Ic} at high rates was defined as:

$$G_{\mathrm{Ic}} = \frac{3P^2}{4b^2h}\frac{\sqrt[3]{(bCa)^2}}{\alpha} \tag{2.7}$$

where C is the experimental compliance and α is the corresponding fitting parameter of the compliance.

Lißner et al. [66] used the J-integral theory to measure the fracture energy of adhesive interfaces in a SHPB using the expression of Eq. (2.8). However, assuming that the equations derived from quasi-static equilibrium are valid for high-rate analysis, no dynamic effect was considered.

$$J_{\mathrm{Ic}} = \frac{12P^2a^2}{E_{11}b^2h^3} + \frac{P}{b}(\theta_1 - \theta_2) \tag{2.8}$$

In the previous equation, θ_1 and θ_2 are the beam rotations obtained through DIC recordings.

A relevant concluding remark for this section is that although different analytical approaches have been used in the literature, there is no clear evidence on how the dynamic effects affect the characterisation of the mode I fracture toughness in fibre-reinforced composites.

2.3 Parameters involved in dynamic delamination

In order to study dynamic fracture events, and especially dynamic crack growth, it is important to identify the main parameters that can have an effect in the analysis. This section presents the different parameters involved in a dynamic delamination under mode I loading in terms of an energy balance.

In the general case, dynamic fracture mechanics contains three complex features: inertia forces, rate-dependent material behaviour, and reflected stress waves. Inertia effects are important when the displacement-rate changes suddenly or the crack grows rapidly; a portion of the work that is applied to the specimen is converted to kinetic energy. When the displacement-rate changes abruptly or the crack grows rapidly, stress waves propagate through the material and reflect off free surfaces, such as the specimen boundaries and the crack plane. Reflecting stress waves influence the local crack-tip stress and strain fields which, in turn, affect the fracture behaviour [71]. In addition, during dynamic events an extra portion of the work applied can be converted to heat. Linked to the localised heating in regions of the material in the vicinity of the crack tip, heat is important when the energy dissipation is restricted by a relatively short loading time (assimilated to an adiabatic process), and when materials with viscoelastic or plastic behaviour are involved.

Using the dynamic fracture mechanics approach, an energy balance allows to identify the contribution of dynamic effects and time-dependent material behaviour in contrast with a quasi-static case. It will be useful later on this thesis to propose a data reduction method for the test developed.

A general energy balance can be defined in the case of a DCB test, as the one shown in Fig. 2.1, or a driven wedge test, as in Fig. 2.4, affected by a rapid crack growth event due to the action of an external transient load (high loading rate), and assuming a material with an elastic mechanical behaviour. Considering the representation of crack tip zone for a DCB specimen under dynamic loading from Fig. 2.12, the boundary contour Γ subjected to an energy input increment $\mathrm{d}U$ due to an external loading (load P for a mode I loading condition) can be defined. The shaded region in Fig. 2.12 represents a small process zone in an elastic continuum to assume the elastic behaviour of the body, and S_c and S_c^+ represent the existing and the new crack surface, respectively. The energy change in the enclosed body takes place because

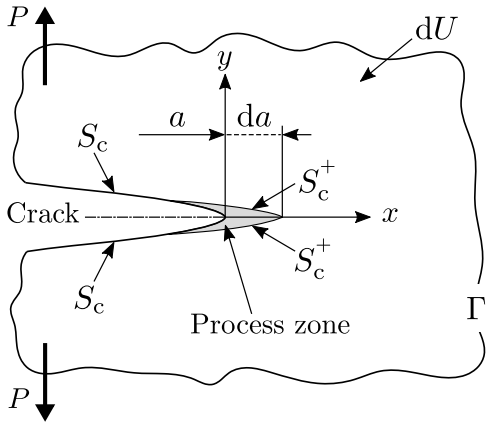

Fig. 2.12: Representation of the crack tip zone for a DCB specimen (Image adapted from: Perez [72]).

of the arising change of the fracture area dA for a constant thickness and a variable crack length. Since all changes with respect to time t are caused by changes in crack size, it can be defined that:

$$\frac{\partial}{\partial t} = \frac{\partial}{\partial A}\frac{\partial A}{\partial t} = \frac{\partial A}{\partial t}\frac{\partial}{\partial A} \; ; \qquad A \geq 0 \tag{2.9}$$

A way to define the energy balance for a dynamic event according to the law of conservation of energy can be expressed as:

$$\frac{\partial W}{\partial A} = \left(\frac{\partial Q}{\partial A} + \frac{\partial U_\mathrm{p}}{\partial A} + \frac{\partial U_\gamma}{\partial A}\right) + \frac{\partial U_\mathrm{e}}{\partial A} + \frac{\partial U_\mathrm{k}}{\partial A} \tag{2.10}$$

where W is the work performed by the applied loads, Q is taken here as the heat due to the dynamic loading or plastic flow in the crack tip. For an isothermal case ∂Q is transferred across the contour Γ of the system, and for an adiabatic case ∂Q is not transferred and the system temperature rises. U_p is the plastic work, U_e is the elastic strain energy, U_k is the kinetic energy and U_γ the energy spent in increasing the crack area. In the wedge configuration, there is an extra input source of energy due to the friction between the wedge and the cracked surfaces.

Eq. (2.10) is the base for the analysis from now on, since it considers all the

energies involved in a fracture event, and it is used for the development of the fracture toughness analysis of the test proposed in this thesis. Likewise, a review about the extra energies involved in a dynamic fracture event in quasi-brittle materials, in comparison with a quasi-static event, is done next.

2.3.1 Heat

An approach of the problem of heating in a fracture event can be described using the Classical Theory of Irreversible Thermodynamics (CTIT). The thermodynamics of irreversible processes is a general framework that can be used to formulate constitutive equations. The work of Rice [73] presents a thermodynamic analysis of Griffith's approach for quasi-static crack growth. He assumed that all crack motion to be considered is sufficiently slow so the body has negligible kinetic energy. In this sense, the body, during crack motion, can be regarded as traversing a "sequence of constrained equilibrium states" corresponding to the sequence of instantaneous crack lengths. In his study, Rice did not consider the thermodynamic restrictions on faster crack motion processes, e.g. with significant temperature non-uniformities and/or with inertial effects.

The second law of thermodynamics asserts that an entropy state function $S = S(\delta, a, T)$ exists for the body and that, in the given circumstances of heat delivery at a uniform surface temperature with equality characterising 'reversible' alterations of state and with Λ as the entropy production rate, an expression for the entropy gradient may be written as:

$$\frac{\partial S}{\partial t} = \Lambda + \frac{\partial Q}{\partial t} \Big/ T \; ; \qquad A \geq 0 \tag{2.11}$$

The entropy production rate can be defined as:

$$\Lambda = -\left[\frac{\partial \Phi(\delta, a, T)}{\partial a}\right] \frac{\partial a}{\partial t} \Big/ T = (G - 2\gamma) \frac{\partial a}{\partial t} \Big/ T \tag{2.12}$$

where Φ is the Helmholtz free energy (per unit thickness) and the presumed constancy of temperature is recalled, γ is the surface energy per length of the crack face, and G is the energy release rate. Then, since $T > 0$, the

requirement of non-negative entropy production rate is:

$$(G - 2\gamma)\frac{\partial a}{\partial t} \geq 0 \tag{2.13}$$

This approach only takes into account an isothermal quasi-static crack growth, which is not valid for some dynamic events where an adiabatic analysis is required.

In the work of Christensen [74], in order to consider the heat energy in a viscoelastic material in an isothermal case, an energy conservation analysis was used. Starting from the fundamental form of the energy conservation equation, the basic energy balance equation takes the form:

$$\frac{\partial U_{\mathrm{k}}}{\partial t} + \frac{\partial U_{\mathrm{e}}}{\partial t} = \frac{\partial W}{\partial t} + \frac{\partial Q}{\partial t} + \frac{\partial U_{\gamma}}{\partial t} \tag{2.14}$$

Using the local conservation of energy equation and the entropy production inequality yields the final form of the energy balance under isothermal conditions:

$$\frac{\partial U_{\mathrm{k}}}{\partial t} + \frac{\partial U_{\mathrm{e}}}{\partial t} = \frac{\partial W}{\partial t} - \int_{v} \Upsilon dv - c\frac{\partial U_{\gamma}}{\partial t} \tag{2.15}$$

where Υ is the rate of energy dissipation of the material by heat and c is the steady-state crack velocity. If the material was perfectly elastic, there would be no dissipation of heat energy ($\Upsilon = 0$) and the criterion above would simply reduce to the corresponding Griffith criterion.

The central problem in this method involves the rigorous determination of the energy dissipation term Υ, besides the fact that it is an isothermal analysis not intended for dynamic events of crack propagation.

Blackman et al. [55] considered the effect of the temperature in the fracture energy decrement with the increase of the crack velocity $\dot{a}$, for mode I loading in adhesives. In their study, the fracture energy changes because of the localised adiabatic heating that may appear in regions of the material in the vicinity of the crack tip. Thus, an isothermal to adiabatic transition may occur in the vicinity of the crack tip due to the heat generated by the plastic

deformation around the crack tip, having no sufficient time to diffuse through the polymer. The temperature rise may affect in significant values the local modulus and yield stress of the material, and finally may affect the toughness. That phenomenon is important when relative short loading times, t_i, are expected. t_i is defined as the time between the onset of loading the material and the moment where crack propagation starts.

Their model for the isothermal-adiabatic transition effect is developed based on three assumptions: firstly, that fracture occurs when a constant crack opening displacement at the crack tip is attained where:

$$\delta = \frac{G_{\mathrm{Ic}}}{\sigma_y} \tag{2.16}$$

Secondly, that the yield stress of the adhesive, σ_y, is linearly dependent upon the temperature, T, and the reference temperature, T_o, by the relationship:

$$\sigma_y = \sigma_o \left(1 - \frac{\Delta T}{\Delta T_{\mathrm{o}}}\right) \tag{2.17}$$

Thirdly, the highest temperature rise, ΔT, in the centre of a zone of the adhesive immediately ahead of the crack tip at the initiation of crack growth is given by:

$$\Delta T = \frac{G_{\mathrm{Ic}}}{Z\rho c_{\mathrm{m}}} \left(1 - 4i^2 erfc(\xi)\right) \tag{2.18}$$

where Z is the thickness of the thermally-heated zone of material at the crack tip, and ρ and c_{m} are the density and the specific heat capacity of the adhesive, respectively. $i^2 erfc(\xi)$ is the second integral of the error function where the dimensionless quantity ξ is defined by:

$$\xi = Z\sqrt{\frac{\rho c_{\mathrm{m}}}{16kt_i}} \tag{2.19}$$

where k is the thermal conductivity of the adhesive and t_i is the time available to dissipate the heat away from the test affected zone, i.e. the loading time defined previously. The final relationship is:

$$G_{\mathrm{Ic}} = \frac{G_{\mathrm{Ico}}}{\left[1 + \dfrac{G_{\mathrm{Ico}}}{\Delta T_{\mathrm{o}} Z\rho c_{\mathrm{m}}} \left(1 - 4i^2 erfc(\xi)\right)\right]} \tag{2.20}$$

where G_{Ico} is the fracture energy at the reference temperature, T_{o}.

For tests at very slow rates, the above equation can be reduced to:

$$G_{\mathrm{Ic}} = G_{\mathrm{Ico}}\left[1 - \frac{G_{\mathrm{Ico}}}{\Delta T_{\mathrm{o}}\sqrt{\pi\rho c_{\mathrm{m}} k t_i}}\right] \tag{2.21}$$

At high rates of test the main expression can be approximated to:

$$G_{\mathrm{Ic}} \approx \frac{G_{\mathrm{Ico}}}{\left[1 + \frac{G_{\mathrm{Ico}}}{\Delta T_{\mathrm{o}} Z \rho c_{\mathrm{m}}}\right]} \tag{2.22}$$

However, the value of the adhesive thickness ahead of the crack tip affected during the test, Z, cannot be easily determined. For this reason, appropriate upper and lower limits need to be defined.

The work of Haslach [75] presents a thermodynamic analysis for a crack propagation. His model for dynamic crack propagation under dynamic loading is based on non-equilibrium thermodynamics foundations. It includes a high-rate crack propagation analysis in terms of a generalised energy function that allows a simpler analysis in contrast to the classical energies for the stress intensity factor. The effect of temperature at crack tip in this work is presented for the crack driving force in terms of the temperature at the crack tip θ, following the energy balance:

$$\left(G_{\mathrm{I}} - 2\gamma\right)\dot{a} + c_{\mathrm{v}}\frac{d\theta}{dx}\dot{a} = \sigma\dot{\epsilon}^{p} + k_f\frac{d^2\theta}{dx^2} \tag{2.23}$$

where G_{I} is the crack driving force, γ is the surface energy per length of the crack face, c_{v} is the specific heat, $\dot{\epsilon}^{p}$ is the plastic strain rate at the crack tip, $\dot{a}$ is the crack propagation rate and k_f is the thermal conductivity.

Finally, from the works reviewed it can be outlined that the heat during dynamic crack propagation events is complex to assess. Most of the time, measurements of the temperature at the crack tip are required, which in the experimental work implies complex set-ups, making difficult to get the proper values. Besides, the effect of heat takes more prominence when relatively short loading times are considered.

2.3.2 Transient loading

In the cases where the load is rapidly applied (transient loading) and there is a considerable change in the load in a short time, the behaviour of the body could experiment a big effect of the inertia forces and reflecting stress waves. That effect is linked with the linear elastic behaviour of the structure and the equilibrium through the equation of motion. General solutions for cleavage fracture, such as the DCB and the WDT tests, are uncommon due to the nature of the equation of motion [76]. Therefore, approximations are obtained assuming displacement profiles from elastic theories [76, 77]. The static displacement profile of one arm of a DCB beam specimen, owing to symmetry, is defined as:

$$\delta = \frac{\delta_o}{2}\left(2 - \frac{3x}{a} + \frac{x^3}{a^3}\right) \tag{2.24}$$

where δ is the transverse deflection, δ_o the transverse deflection at the loading point end, x the distance along the beam and a the crack length. Then, $\delta = \delta_o$ when $x = a$.

For a transient crack growth problem for a DCB configuration, where the tracking of discrete waves pulses is important, elastic theories such as the Euler-Bernoulli are deficient, and a higher order idealisation for the model is required. Freund [78] proposed an analysis using a modal approach, based on the equations of motion. The general differential motion equation, associated with the boundary conditions may be written as:

$$EI\frac{\partial^4\delta}{\partial x^4} = \rho A\frac{\partial^2\delta}{\partial t^2} \tag{2.25}$$

$$\begin{aligned}
\delta(0,t) &= \delta_o \\
\frac{\partial^2\delta}{\partial x^2}(0,t) &= 0 \\
\delta(a,t) &= 0 \\
\frac{\partial\delta}{\partial x}(a,t) &= 0
\end{aligned}$$

where E is the elastic modulus, I is the area moment of inertia of the beam

cross section, A is the area of the beam cross section, ρ is the mass density of the material and $\delta(x,t)$ is the transverse deflection. For the transient crack growth problem in a DCB configuration, the equation governing the transverse deflection at any time t is given by:

$$\delta(x,t) = \frac{\delta_o}{2}\left(2 - 3\frac{x}{a(t)} + \frac{x^3}{a(t)^3}\right) + \sum_{n=1}^{\infty} A_n(t)\phi_n\left(\frac{x}{a(t)}\right) \tag{2.26}$$

where $a(t)$ is the instantaneous crack length, $A_n(t)$ is an unknown amplitude, and $\phi_n(x/a)$ is the n^{th} normal mode shape for free vibration of a beam subjected to homogeneous boundary conditions, for this case they are $\phi_n(0) = \phi''_n(0) = \phi_n(1) = \phi'_n(1) = 0$ for any n. Moreover, when $A_n = 0$ for all n, the transverse deflection is the same as in Eq. (2.24). From the deflection equation and the equation of motion, the velocities can be derived, and hence the kinetic energy.

In the works of Chen et al. [79, 80] and Kotsinis and Loutas [81], the dynamic strain energy release rate was calculated as a function of the beam's vibrational modes and natural frequencies. However, considering the effect of vibration on the fracture toughness is complex for the crack propagation. Besides, capturing accurately the displacement profile of the arms for a transient loading in order to use the description of Eq. (2.24) is a challenging task.

2.3.3 Kinetic energy

The kinetic energy contribution in dynamic events may be analysed in different scenarios. In the case of rapid loading events, reflecting stress waves influence the local crack-tip stress and strain fields, affecting the initiation or propagation of fracture [71]. In situations where stress waves reflect back to the crack tip, the stress intensity must be determined for each particular case. Kalthoff et al. [82] studied the effect stress waves have on the stress intensity factor at the crack arrest, using internal wedge-loaded DCB specimens. The geometry design of the common DCB specimen is such that stress waves can reach the specimen boundaries and return back to the crack tip in a very short time. Thus, if the fracture event takes place after the elastic waves have

made several reflections within the specimen length, the stress wave effect might be ignored and static equilibrium can be assumed.

When the structure is loaded in short-time, but the stress wave effect can be ignored, inertia effects can be relevant due to accelerations in the system. The load tends to increase with time, but oscillates at a particular frequency, which depends on the specimen material and geometry. The amplitude of these oscillations decreases with time, as kinetic energy is damped by the specimen material, as shown in Fig. 2.13. In the cases where a dynamic analysis is required, different approaches may be used such as the one proposed by Chen et al. [79, 80], who performed a mode I DCB analysis using a dynamic and vibration analysis of Euler-Bernoulli beams, or the one from Kotsinis and Loutas [81], who performed a dynamic vibrational analysis of the mode I DCB but using Timoshenko beam theory.

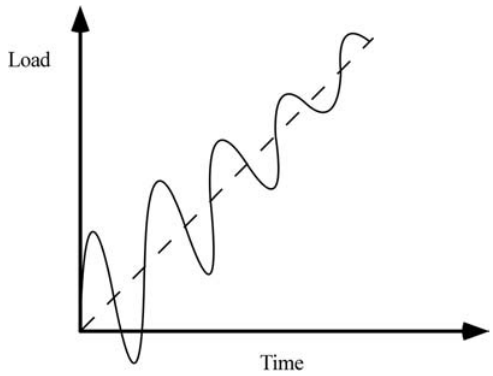

Fig. 2.13: Schematic load-time response of a rapidly loaded structure (source: Anderson [71]).

For sufficiently long-time loading events, where the behaviour is essentially quasi-static, the inertia effects are minimal [71]. Therefore, in these cases the quasi-static approach is valid. To assess the inertia effects in a dynamic test, Nakamura et al. [83, 84] defined a time criterion that provides an estimate when inertia effects can be neglected in a Three-Point Bend (3PB) metallic specimen. The criterion uses a transition time, defined as the time when the

kinetic energy equals the internal energy, which represents the period where inertia effects are still present in the system. This time is compared against the time for the initiation of fracture propagation (or time to fracture), ensuring that the fracture event takes place at a longer time than the transition time. In that way, a quasi-static analysis can be used to calculate the fracture toughness at a given high loading rate. The transition time concept was firstly introduced in bending and impact tests for metals (Three-Point Bend test [85], Four-Point Bend test [86] and Charpy V-Notch test [87]). Ireland [88] and Böhme [89] proposed an experimental approach to determine the transition time, whereas Nakamura et al. [83, 84] defined it based on numerical studies.

For cases where inertia effects are considered, different authors [55, 76, 77] have adopted the kinetic energy from a simple energy balance as the difference between the work done on the system and the increase in potential energy.

2.4 Dynamic fracture analysis using a transition time

The transition-time approach allows material rate effects to be quantified independently of inertia effects. Therefore, if the effects of inertia and reflected stress waves can be suppressed from the analysis, only the rate-dependent material response is left, which in the case of this thesis is the main goal, being preferable to apply the criterion for transition time whenever possible. In this section three different models available in the literature for the determination of the transition time, t_τ, and their associated threshold criterion are summarised. For all three cases, the aim is to determine a characteristic time after which inertia effects can be neglected and a dynamic event can be accurately described by means of a quasi-static model.

2.4.1 Theoretical background of the transition time

Nakamura et al. [83] defined a transition time (t_{τ_N}) as the time at which the kinetic energy and the internal energy are equal in a high loading rate test. However, measuring kinetic and internal energies separately during a

fracture mechanics test is a difficult task. For this reason, Nakamura et al. proposed to estimate the kinetic energy and the elastic energy through an analytical model based on the Euler-Bernoulli beam theory. In order to use this approach, it is necessary to measure the opening displacement and its rate at the loading point. The resulting equation to determine the transition time (t_{τ_N}) for a Single Edge Notched Bend (SENB) steel specimen in a 3PB impact test is:

$$t_{\tau_\mathrm{N}} = DS\frac{H}{c_\mathrm{o}} \tag{2.27}$$

$$S = \left(\frac{LBEC_\mathrm{s}}{H}\right)^{1/2} \tag{2.28}$$

where c_o is the sound speed in the material, E is the material Young's modulus, C_s is the specimen compliance that accounts for the crack length, H is the specimen width, B is the thickness and L is half of the span between supports. D is a dimensionless coefficient that depends on the velocity profile during the test.

Ireland [88] analysed the transition time for a 3PB Charpy impact test on metallic specimens for a wide range of cases: from a rapid loading response (dominated by stress waves) to a long-time loading response (dominated by the fundamental structural elastic deformation mode). Ireland introduced the transition time (t_{τ_I}) as an effective specimen inertial oscillation period and cited numerous experimental data to show that inertial effects are dominant for loading times smaller than $2t_{\tau_\mathrm{I}}$. The empirical expression can be expressed in the form:

$$t_{\tau_\mathrm{I}} = \left(1.68\sqrt{2}\right) S\frac{H}{c_\mathrm{o}} \tag{2.29}$$

Despite being an empirical model, the criterion proposed by Ireland has been widely accepted for the analysis of the dynamic response of 3PB fracture toughness tests using Charpy and drop-weight impact [90, 91], and Hopkinson pressure bar apparatus [92]. Jiang and Vecchio [39] explained how Eq. (2.29) can be derived based on the inertial modelling of a classic Charpy impact

test in terms of the natural frequency of the testing system (Charpy impact machine + bending specimen system), obtaining similar results.

Böhme [89] proposed a transition time t_{τ_B} to quantify the dynamic effects in impact tests with SENB specimens. The transition time was obtained based on the definition of a time-dependent function, identified as dynamic correction function $k^{dyn}(t)$. This function is defined as the ratio between the dynamic stress intensity factor $K_I^{dyn}(t)$ (Böhme measured it experimentally using the optical method of caustics) and the quasi-static stress intensity factor $K_I^{qs}(t)$ (analytically calculated). The transition time was defined as the time from which the variation of the dynamic correction function $k^{dyn}(t)$ differs from 1 (the quasi-static value) by less than 10%. The expression for a 3PB specimen in an impact test can be expressed as follows:

$$t_{\tau_B} = k^{dyn}(t)\frac{H}{c_o} \qquad \text{for} \qquad 0.9 \leqslant k^{dyn}(t) \leqslant 1.1 \tag{2.30}$$

Sunny et al. [93], Shazly et al. [94], Martins et al. [95], and Jones and Davies [96] applied the expression in Eq. (2.27) from Nakamura's approach to determine the transition time in standard ASTM E23-18 [97] SENB specimens, obtaining that $t_{\tau_N} = 23.3H/c_o$ when the ratio between the crack length and the specimen width is $a/H = 0.5$.

On the other hand, other authors such as Henschel and Krüger [98], used similar approaches to obtain the transition time in a four-point split Hopkinson bending test. However, Eq. (2.27) depends on geometric parameters that are not always clearly specified or that cannot be directly translated from a ASTM E23-18 specimen to another type of test, leading to incorrect results. Besides, Koppenhoefer and Dodds [99], and Takashima and Minami [100] reported a dependency of the transition time on the loading velocity for Charpy specimens that was not considered by Nakamura et al. [83, 84]. Consequently, further analysis is required to generalise the determination of the transition time for different types of tests, including DCB, and test conditions.

2.4.2 Transition time threshold criterion

The models reviewed previously in this section aim at establishing a criterion to determine when a quasi-static-based data reduction method can be used to calculate the fracture toughness under high loading rates. In order to neglect the inertia effects, the criterion defines a limit between a rapid loading (dominated by discrete elastic waves and inertia effects), and a long-time loading (dominated by the elastic energy). Basically, it needs to be ensured that the time when the fracture starts to propagate, referred as time to fracture t_f, is well after the transition time so the response of the system is dominated by the fundamental structural elastic deformation. The criteria proposed by the previously mentioned authors can be summarised as:

$$\begin{aligned} t_\mathrm{f} &> 2t_{\tau_\mathrm{N}} && \text{Nakamura et al. [83]} \\ t_\mathrm{f} &> 3t_{\tau_\mathrm{I}} && \text{Ireland [88]} \\ t_\mathrm{f} &> t_{\tau_\mathrm{B}} && \text{Böhme [89]} \end{aligned} \tag{2.31}$$

Böhme [89] compared the transition time of the three different methods for the same particular case. From this, it can be considered that the transition time proposed by Böhme is about two times the one considered by Nakamura et al. Thus, these two criteria can be taken as equivalent. On the other hand, as the transition time suggested by Ireland is almost coincident to that proposed by Nakamura et al., the time to fracture according to Ireland's criterion should be 1.5 times higher. Additionally, Ireland's criterion is the most conservative because it quantifies the hammerload oscillations (dynamic effects at the impacting hammer), instead of the dynamic effects at the crack tip as Nakamura et al. and Böhme. Following Ireland's approach, Dutton and Mines [101] modified the criterion to be used in a Hopkinson bar loaded fracture test as $t_\mathrm{f} > 1.1t_{\tau_\mathrm{I}}$.

Part II

Towards a methodology for mode I dynamic testing

3 Quasi-static analysis for mode I dynamic testing

In the present chapter the transition time defined by Nakamura et al. [83, 84] and described in Section 2.4 is reformulated and a time-based threshold criterion is defined in order to characterise the pure mode I interlaminar fracture toughness under high loading rates in composite materials using the DCB test. Using a geometrical scalability analysis with three different materials, this chapter assesses different methods to obtain the transition time. In addition, the influence of the velocity profile and its maximum value over the transition time are analysed. The approach is validated through a numerical analysis implemented as a three-dimensional dynamic Finite Element (FE) model.

The objective of this chapter is not only to assess the value of the coefficient α from Section 3.1, and the threshold time, but also to clearly determine the time to fracture for different configurations of the DCB test and different loading velocity conditions, ensuring that the dynamic effects on the fracture event are minimal. The time to fracture is obtained through FE simulations. Regarding the transition time, three different approaches are considered to determine it, allowing sound determination of the coefficient α and the threshold time.

The three approaches to determine the transition time are based on the assumption of the transition time as the time when $U_{\mathrm{k}}/U_{\mathrm{e}} = 1$, as assumed by Nakamura et al. [83]. The first approach consists on an analytical analysis of the energies. The second approach is based on the deduction of a numerically-based expression using the Buckingham Pi theorem [102] and FE simulations. In the third approach, the transition time is determined analysing the evolution of the energy ratio versus a dimensionless time parameter based on FE

simulations. The last two methods are based on FE simulations since they can take into account the neglected effects of the analytical approach of first method.

3.1 Definition of the time-based threshold criterion

Based on the analysis done by Nakamura et al. [83] and Böhme [89], in the present section a time-based threshold criterion is defined to calculate the mode I fracture toughness under high loading rates for a DCB test [9]. As explained in Section 2.4, the contribution of the kinetic energy can be considered as minimal when t_f is certain times larger than t_τ. For this thesis, it is considered that the dynamic effects on the initiation of fracture propagation can be neglected once the ratio of kinetic energy to elastic energy (U_k/U_e) is below 20%. Thus, for times to fracture t_f larger than a threshold time t_c, the contribution of the kinetic energy is lower than 0.2 times of that of the elastic one. Consequently, it can be considered that the dynamic event is close to a quasi-static event and a quasi-static data reduction method can be used. This energy threshold is less conservative than others from literature (such as the typically considered for Explicit FE simulations [103]), but giving sufficient margin to neglect the dynamic effects. Even so, the user may define a different percentage of energy ratio lower than the 20% to have more conservative analysis. The criterion proposed is formulated in Eq. (3.1), where the threshold time t_c is expressed in function of the transition time.

$$t_f > t_c = \alpha t_\tau \tag{3.1}$$

3.2 Analytical determination of the transition time

Considering the DCB specimen shown in Fig. 3.1, the kinetic energy generated during the test can be obtained by integrating one half of the product of the mass by the displacement rate $\dot{u}(x)$ over the initial crack length a_o. Assuming a symmetric opening of the arms, the kinetic energy for the whole specimen

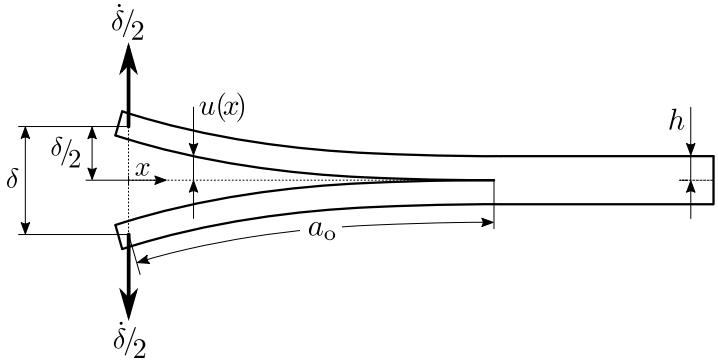

Fig. 3.1: Parameters for the analysis of a DCB test.

is:

$$U_k = 2\left(\frac{1}{2}\rho bh\int_0^a \left[\dot{u}\left(x\right)\right]^2 dx\right) \tag{3.2}$$

where the mass is defined in terms of the density ρ, the specimen width b and the thickness h of one specimen arm, and a is the crack length, which is equal to a_o before the crack starts to propagate.

According to the Euler-Bernoulli beam theory and considering no crack propagation, the opening displacement $u(x)$ can be obtained as a function of the opening displacement at the loading point of a single arm ($\delta/2$):

$$u\left(x\right) = \frac{\delta}{2}\left(1 - \frac{3x}{2a_o} + \frac{x^3}{2{a_o}^3}\right) \tag{3.3}$$

Deriving Eq. (3.3) and replacing in Eq. (3.2), the kinetic energy in a DCB test can be expressed as:

$$U_k = \frac{33}{560}\rho bha_o\dot{\delta}^{\,2} \tag{3.4}$$

where $\dot{\delta}$ is the applied load-line opening rate. This result coincides with the kinetic energy proposed by Hug et al. [56].

On the other hand, the elastic energy of the specimen under bending can be defined in terms of the opening displacement δ and the specimen compliance

C as:

$$U_{\mathrm{e}} = \frac{1}{2}\frac{\delta^2}{C} \tag{3.5}$$

Using the Euler-Bernoulli beam theory, the previous equation can be rewritten as:

$$U_{\mathrm{e}} = \frac{Ebh^3\delta^2}{16{a_{\mathrm{o}}}^3} \tag{3.6}$$

Eqs. (3.2) to (3.6) are equivalent to the ones proposed by Blackman et al. [54]. Then, using the longitudinal wave propagation velocity in the specimen $c_{\mathrm{o}} = (E/\rho)^{1/2}$, the energy ratio from Eqs. (3.4) and (3.6) can be expressed as:

$$\frac{U_{\mathrm{k}}}{U_{\mathrm{e}}} = \frac{33}{35}\frac{{a_{\mathrm{o}}}^4\dot{\delta}^2}{c_{\mathrm{o}}^2h^2\delta^2} \tag{3.7}$$

In order to obtain an explicit expression for the transition time t_τ, it is convenient to introduce the dimensionless displacement coefficient D defined by Nakamura et al. [83] as:

$$D = \left.\frac{t\dot{\delta}}{\delta}\right|_{t_\tau} \tag{3.8}$$

$$\frac{\dot{\delta}}{\delta} = \frac{D}{t_\tau} \tag{3.9}$$

Combining Eqs. (3.7) and (3.9), the transition time can be expressed as:

$$t_\tau = \left(\frac{33D^2}{35}\frac{{a_{\mathrm{o}}}^4}{{c_{\mathrm{o}}}^2h^2}\right)^{0.5} = \left(\frac{33D^2}{35}\right)^{0.5}\frac{{a_{\mathrm{o}}}^2}{c_{\mathrm{o}}h} \tag{3.10}$$

If the displacement is expressed as a power law such as $\delta = \beta t^{\varsigma}$, the value of the parameter D is equal to the power factor ς. When applying a constant velocity, i.e., step acceleration, D is equal to one. For a linear increment of velocity respect to time, i.e., linear acceleration, D is equal to two.

3.3 FE analysis of the DCB

In this section two different methods are presented to determine the transition time in a DCB test, a numerically-based method and a graphical method.

The FE model used in the simulations to numerically determine and validate the transition time is presented next. At an initial stage, the model is used for the determination of a numerically-based expression of the transition time t_τ using the Buckingham Pi theorem [102] in a dimensional analysis. Then, a geometrical scalability analysis using different materials is performed for the validation of the graphical method. Both methods are based on FE simulations since they allow to obtain an accurate transition time that accounts for the effects neglected in the analytical approach.

3.3.1 FE model description

A three-dimensional model accounting for geometric non-linearity of the DCB specimen is defined using the commercial software Abaqus/Explicit [103]. Solid elements with incompatible modes (C3D8I) are used to capture the bending response due to large displacements, avoiding the shear-locking and hourglass phenomena. Since the studies focus on the global bending behaviour and not on the stress distribution in the material, only two elements in the through-the-thickness direction are used for each of the arms of the specimen to reduce the computational time. As only the initial stage of loading is considered and the crack propagation is ruled out (constant a_o), the initial pre-crack is modelled merging nodes of the two arms ahead of the crack tip.

One of the main problems of using the classical DCB test under high loading rates is that the specimen deforms unsymmetrically when the load is applied to one of the arms while the other one is fixed to the test rig [48, 50]. In order to simulate the ideal situation with symmetrical opening, a prescribed velocity is applied to each of the specimen arms while all the displacements at the other end are constrained. The boundary conditions and meshing of the model are shown in Fig. 3.2. To reduce the computational time of the simulations, the specimen is meshed with regular hexahedral elements using different mesh densities along its length. Near the crack tip a refined mesh is used with an element size of 1 mm, while away from the crack tip, a coarse mesh with an element size of 3 mm is employed. A progressive mesh is defined

in between. The width of the elements is set to 1 mm in all areas.

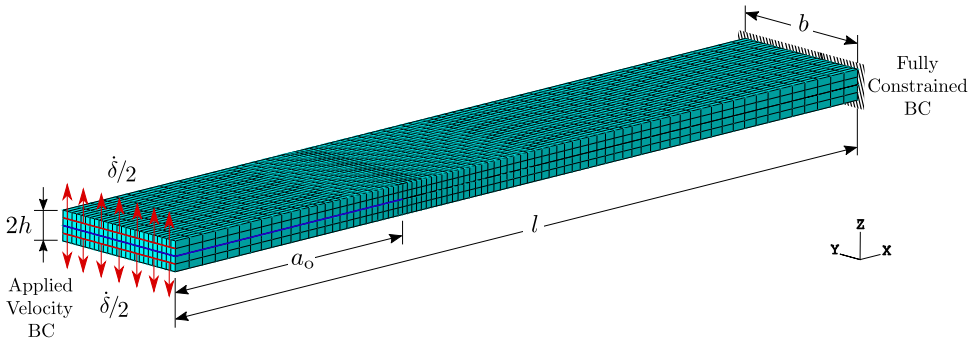

Fig. 3.2: Geometry, mesh and boundary conditions considered for the numerical analysis of the DCB test.

3.3.2 Numerically-based determination of the transition time

A dimensionless framework based on the Buckingham Pi theorem [102] combined with an inverse analysis is used for the numerical determination of the transition time. The use of FE simulations allows to obtain an accurate transition time that accounts for the effects neglected in the approach reported in Section 3.2. Moreover, the dimensionless framework allows studying the scalability of results between different geometries and/or materials in DCB specimens.

The dimensional analysis relies on the proper selection of the variables that influence the problem. For the determination of the transition time, the ratio between the kinetic and elastic energies can be expressed as a function of all the involved variables as:

$$\frac{U_\mathrm{k}}{U_\mathrm{e}} = f\left(t, \delta, \dot{\delta}, c_\mathrm{o}, a_\mathrm{o}, h, b, l\right) \tag{3.11}$$

For clarity, the involved parameters are specified again, being $U_\mathrm{k}/U_\mathrm{e}$ the energy ratio. The variable t is the time of the test, δ is the displacement and $\dot{\delta}$ is the maximum applied velocity (applied loading rate). The variable c_o is the sound propagation velocity. The geometrical parameters of the specimen are the initial crack length a_o, the thickness of one arm h, the width b and

the length l.

Taking into account that not all the variables affect the problem in the same way, a preliminary analysis is carried out to assess the effect of the overall variables over the problem, and reduce these variables using the Buckingham Pi theorem. Hence, first all the possible variables from Eq. (3.11) involved in the problem are considered, studying their effects and thereby choosing the critical ones for the final analysis. U_k/U_e is the dependent variable, while δ and t are selected as the repeatable variables in order to obtain a π-parameter equivalent to the dimensionless displacement coefficient D introduced by Nakamura et al. [83] (see Eq. (3.8)).

According to the Buckingham Pi theorem, the relation can be described in function of the dimensionless π-parameters as follows:

$$\frac{U_k}{U_e} = f\left(\pi_{1p} = \frac{tc_o}{\delta}, \pi_{2p} = \frac{t\dot{\delta}}{\delta}, \pi_{3p} = \frac{a_o}{\delta}, \pi_{4p} = \frac{h}{\delta}, \pi_{5p} = \frac{b}{\delta}, \pi_{6p} = \frac{l}{\delta}\right) \quad (3.12)$$

To analyse the effect of each preliminary π-parameter, different FE simulations are carried out using the FE model described in Section 3.3.1. For the parametric study, the geometrical reference values for the models are: $l = 200$ mm, $b = 20$ mm, $h = 1.5$ mm and $a_o = 50$ mm. The material used in the study is Hexply AS4/8552 CFRP, whose properties are listed in Tab. 3.3. Besides, a linear acceleration ($D = 2$) is considered as the reference condition with a maximum velocity of 2 m/s for a time of 0.5 ms.

The parametric study is carried out by varying the variables that define the π-parameters according to the ranges and increments defined in Tab. 3.1. It is worth noting that while one of the π-parameters is varied, the rest of the π-parameters remain constant. The variable c_o accounts for the change of the material properties, while the dimensionless parameter D takes the effect from the velocity $\dot{\delta}$.

Fig. 3.3 shows the results of the preliminary parametric study. As it can be observed, there is no effect of the π_{6p}-parameter, that accounts for the length

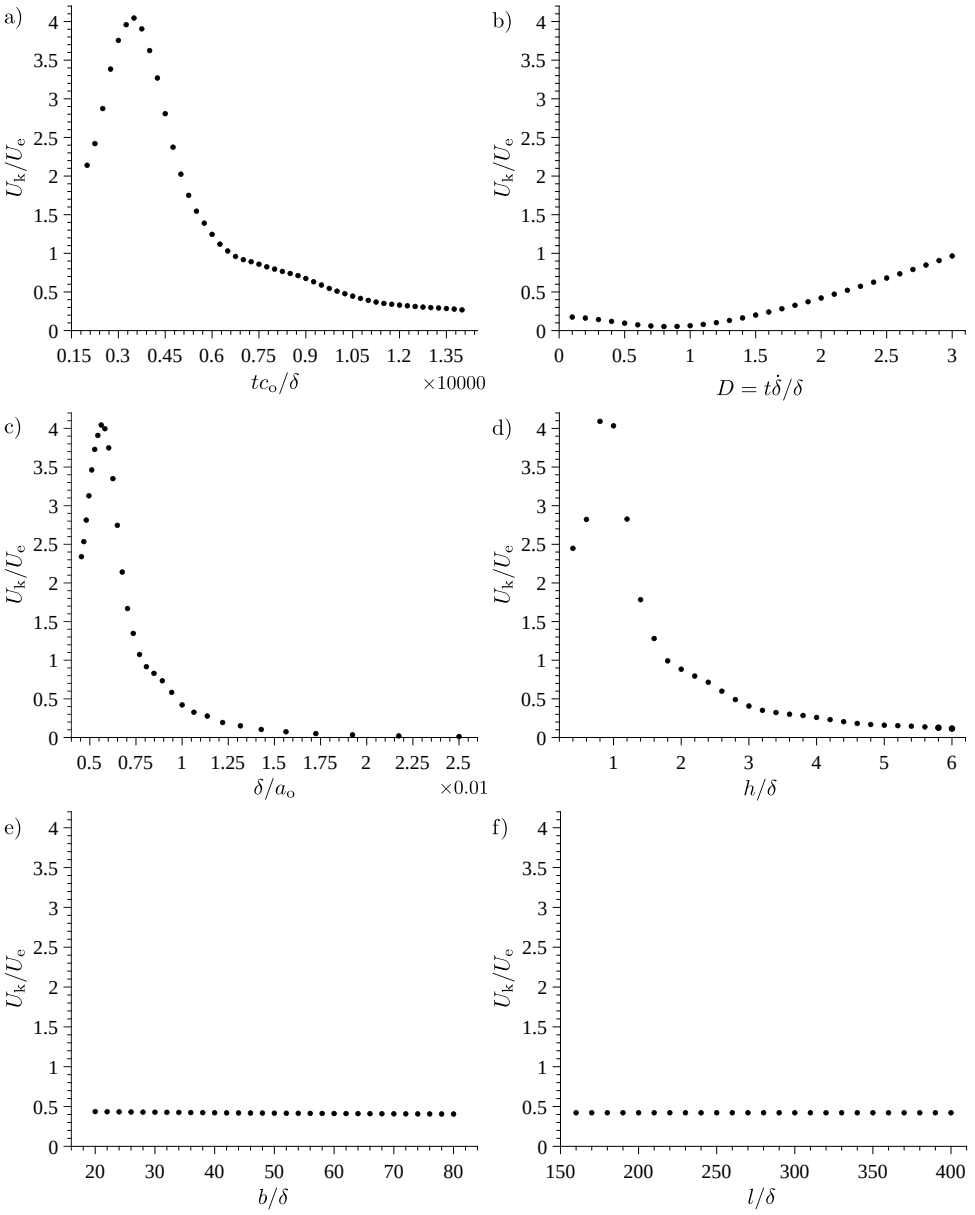

Fig. 3.3: Curves of the energy ratio in terms of the preliminary π-parameters for a) π_{1p}, b) π_{2p}, c) π_{3p}, d) π_{4p}, e) π_{5p} and f) π_{6p}.

Tab. 3.1: Range of variation of the variables for the different preliminary π-parameters.

π-parameter	Variable to modify	Min. value	Max. value	Increment
π_{1p}	c_o [m/s]	2000	14000	250
π_{2p}	$\dot{\delta}$ [m/s]	0.1	3	0.1
π_{3p}	a_o [mm]	20	110	3
π_{4p}	h [mm]	0.4	3	0.1
π_{5p}	b [mm]	10	40	1
π_{6p}	l [mm]	80	200	5

of the specimen (see Fig. 3.3f). Besides, the effect of the π_{5p}-parameter, that accounts for the specimen width, is negligible, as it can be seen in Fig. 3.3e. Accordingly, it is possible to discard these variables for the final dimensional analysis. On the other hand, the rest of variables have an effect on the energy ratio and hence they are retained for the reduced dimensional analysis.

An additional remark is that when using the displacement δ as a repeating variable, it is not possible to vary the π_{1p}-parameter for a given material without varying t and δ and, thus, also vary parameter π_{2p}, which also depends on t and δ. This would require several simulations to obtain the curve of energy ratio. However, if the crack length is used instead as the repeating variable, it is possible to obtain the energy ratio curve with the information of only one FE simulation through the change of t but keeping constant a_o and the ratio t/δ. This is why, for the final reduced dimensional analysis performed next, it is better to use a_o as a repeating variable instead of δ. Therefore, the repeating variables for this analysis are t and a_o. With the change of the repeating variables, the dimensionless displacement coefficient D defined by Nakamura et al. [83] is not longer obtained. However, it is possible to introduce it as a combination of two π-parameters: $t\dot{\delta}/a_o$ and a_o/δ. This allows to simplify the analysis in one π-parameter less and consider the coefficient D in order to analyse the effect of the applied velocity (see Sections 3.5.2 and 3.5.3). Thus, according to the Buckingham Pi theorem [102], the

energy ratio can be defined as a function of three π-parameters:

$$\frac{U_\mathrm{k}}{U_\mathrm{e}} = f\left(\pi_1 = \frac{tc_\mathrm{o}}{a_\mathrm{o}}, \pi_2 = D = \frac{t\dot{\delta}}{\delta}, \pi_3 = \frac{h}{a_\mathrm{o}}\right) \tag{3.13}$$

To obtain the function that describes the relation from Eq. (3.13), a final parametric study using FE simulations is carried out. For this parametric analysis, the results of the FE simulations for the variables c_o, D and h from Fig. 3.3 are used. In order to obtain the energy ratio curves, the variables are set to the dimensionless form of the particular π-parameter associated, knowing that a_o and t are the repeating variables. A curve for each π parameter versus the energy ratio is obtained as shown in Fig. 3.4.

First, an expression that defines the complete variation of the energy ratio is adjusted using the least squares regression method for each π-parameter. The fitting analysis describes the full behaviour of the π-parameters curves, which means including the initial stage of growth of the energy ratio where the kinetic energy is increasing in the system, similar to the ones shown in Fig. 3.3 for the preliminary analysis curves. The expressions obtained for each π-parameter can be expressed as:

$$\begin{aligned}
&\text{for } \pi_1: \quad \frac{U_\mathrm{k}}{U_\mathrm{e}} = \frac{\pi_1}{(42.9244 - 2.362\pi_1 + 0.0395{\pi_1}^2)} \\
&\text{for } \pi_2: \quad \frac{U_\mathrm{k}}{U_\mathrm{e}} = 0.253792 - 0.543916\pi_2 + 0.417791{\pi_2}^2 - 0.052619{\pi_2}^3 \\
&\text{for } \pi_3: \quad \frac{U_\mathrm{k}}{U_\mathrm{e}} = \frac{1}{(0.8867 - 145.8592\pi_3 + 8345.633{\pi_3}^2)}
\end{aligned} \tag{3.14}$$

With these expressions, the equation that describes the behaviour of the energy ratio in function of the different variables is obtained as the product of the expressions of Eq. (3.14) for the π-parameters. The resulting general expression for the energy ratio is:

$$\frac{U_\mathrm{k}}{U_\mathrm{e}} = 0.0525\left(\frac{\psi}{\xi}\right){a_\mathrm{o}}^3 c_\mathrm{o} t \tag{3.15}$$

where ψ is a polynomial function that accounts for the effects of the dimen-

sionless parameter D and it is described as follows:

$$\psi = -0.3876D^3 + 3.0778D^2 - 4.0069D + 1.8696 \tag{3.16}$$

On the other hand, ξ is a function that accounts for the interaction of a_o, h, c_o and t. The function can be expressed as follows:

$$\xi = \left(\lambda_1 {a_o}^2 + \lambda_2 a_o h + \lambda_3 h^2\right)\left(\lambda_4 {a_o}^2 + \lambda_5 a_o c_o t + \lambda_6 {c_o}^2 t^2\right) \tag{3.17}$$

where $\lambda_1 = 0.076$; $\lambda_2 = -12.529$; $\lambda_3 = 716.884$; $\lambda_4 = 193.314$; $\lambda_5 = -10.638$ and $\lambda_6 = 0.178$.

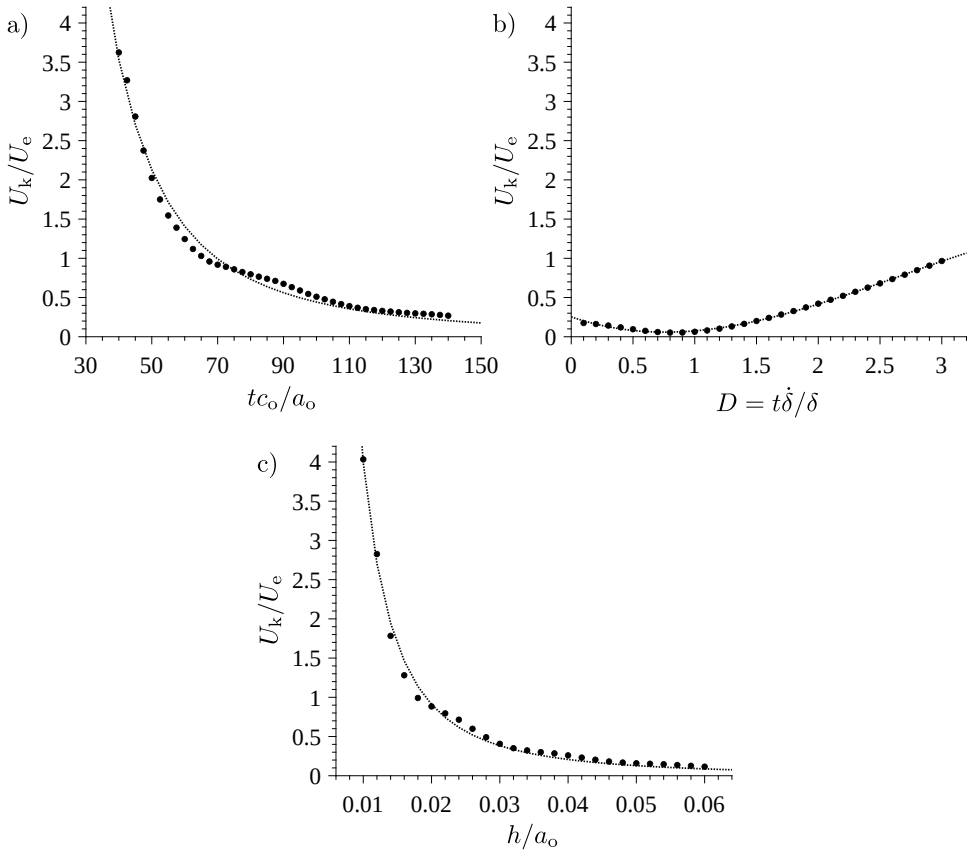

Fig. 3.4: Fitting of the energy ratio curves in terms of the π-parameters for the reduced analysis a) π_1, b) π_2 and c) π_3.

The use of Eq. (3.15) to obtain the transition time derives in a complex solution, being impractical to use. Taking into account that the analysis is focused on the time solution at which the energy ratio is one, the initial evolution of the energy ratio curve may be avoided. For this reason, a new fitting analysis is carried out only taking into account the part of the curves relevant for the determination of the transition time, i.e. once the energy ratio starts to decrease, as shown in Fig. 3.4. Following the same procedure as for the full behaviour of the energy ratio, the fitting expressions adjusted using the least squares regression method are:

$$\begin{aligned} &\text{for } \pi_1: && \frac{U_\mathrm{k}}{U_\mathrm{e}} = 1.5237 \times 10^4 {\pi_1}^{-2.269} \\ &\text{for } \pi_2: && \frac{U_\mathrm{k}}{U_\mathrm{e}} = -0.0526{\pi_2}^3 + 0.4178{\pi_2}^2 - 0.5439\pi_2 + 0.2538 \\ &\text{for } \pi_3: && \frac{U_\mathrm{k}}{U_\mathrm{e}} = 2.1632 \times 10^{-4} {\pi_3}^{-2.133} \end{aligned} \tag{3.18}$$

The equation that describes the behaviour of the energy ratio is obtained once again as the product of the π-parameters. From this analysis, a simpler master expression that involves the DCB test parameters can be obtained as:

$$\frac{U_\mathrm{k}}{U_\mathrm{e}} = \psi \frac{a_\mathrm{o}^{4.402}}{c_\mathrm{o}^{2.269}\ h^{2.133}\ t^{2.269}} \tag{3.19}$$

where ψ is the polynomial function described in Eq. (3.16) that accounts for the effects of the dimensionless parameter D.

Equalling $U_\mathrm{k}/U_\mathrm{e} = 1$, a new expression for the transition time can be obtained:

$$t_\tau = \left(\psi \frac{a_\mathrm{o}^{4.402}}{c_\mathrm{o}^{2.269}\ h^{2.133}} \right)^{0.44} = \psi^{0.44} \frac{a_\mathrm{o}^{1.937}}{c_\mathrm{o}^{0.998}\ h^{0.938}} \tag{3.20}$$

Comparing Eq. (3.10), analytical approach, and Eq. (3.20), numerically-based approach, it can be observed that both equations follow the same pattern but with certain differences in the coefficients affecting D and the exponents affecting a_o, c_o and h. For the case of a step acceleration, $D = 1$, the coefficients for the analytical (taken in front of $a_\mathrm{o}^2/c_\mathrm{o}h$) and the numerically-based expressions (taken in front of $a_\mathrm{o}^{1.937}/c_\mathrm{o}^{0.998}h^{0.938}$) are 0.971 and 0.770,

respectively. For the case of a linear acceleration, $D = 2$, these coefficients for the analytical and the numerically-based expressions are 1.942 and 1.637, respectively. The indexes of the power for the analytical expression for a_o, c_o and h are 2, 1 and 1, respectively. While for the numerically-based expression are 1.937, 0.998 and 0.938, respectively. Therefore, despite the similitude of the expressions, relatively different predictions of the transition time may be expected with both methods and a further analysis is required to elucidate which of the two is more accurate (see Section 3.4).

3.3.3 Graphical determination of the transition time

A third approach is based on the graphical representation of the evolution of the energy ratio obtained through FE simulation versus time or the dimensionless time parameter tc_o/a_o (for each FE simulation, a_o and c_o remain constant and only t varies). Following the same concept of Nakamura et al. [83], the values of the transition time t_τ or the dimensionless time parameter $t_\tau c_o/a_o$ are obtained when the energy ratio is equal to one ($U_k/U_e = 1$).

This graphical method, as a dimensionless approach using tc_o/a_o, can be used not only for the particular simulation, but also for scalable similar problems. Thus, the results obtained with this method are valid for any DCB specimen where the combination of parameters results in the same values of π_2 and π_3, independently of the material or initial crack length. The use of this method is shown in the following section for a geometrical scalability analysis.

3.3.4 Geometrical scalability analysis for different materials

A parametric FE analysis is carried out to validate the capabilities of the Buckingham Pi theorem approach and the expression for the determination of the transition time proposed in Eq. (3.20) in terms of geometrical scalability and dynamic similarity.

The parametric study considers a wide range of scenarios, varying the geometrical and material variables while keeping the other π-parameters introduced in Eq. (3.13) constant, as indicated in Tab. 3.2. The resulting energy ratio

versus time and the dimensionless time parameter (π_1-parameter) curves allow to illustrate the graphical method proposed in Section 3.3.3. Although as shown in Section 3.2, the length and the width of the specimen do not affect the results, they are defined accordingly to the size of the crack length to maintain the value of the corresponding π-parameters as constant.

Tab. 3.2: Values for the dimensionless π-parameters for the scalability analysis.

$\frac{U_k}{U_e}$	$\frac{tc_o}{a_o}$	$D = \frac{t\dot{\delta}}{\delta}$	$\frac{h}{a_o}$	$\frac{b}{a_o}$	$\frac{l}{a_o}$
response variable	response variable	1 and 2	0.05	0.5	3

All the simulations are carried out considering a maximum velocity of 2 m/s for the applied load. However, two different scenarios are taken into account: i) step acceleration ($D = 1$) and ii) linear acceleration ($D = 2$). Three different materials are considered: steel and two different Carbon Fibre Reinforced Polymers (CFRPs), Hexply AS4/8552 and TeXtreme®, whose properties are summarised in Tab. 3.3. For each material, three different cases are considered based on the different values of the geometrical variables. These three cases are reported in Tab. 3.4. For each case, the values of the dimensionless π-parameters listed in Tab. 3.2 are respected.

Tab. 3.3: Material properties for the scalability analysis.

	ρ [kg/m^3]	E_1 [GPa]	ν_{12}	$c_o = (E/\rho)^{1/2}$ [m/s]
Steel	7850	210.0	0.3	5421.9
AS4/8552 [104]	1590	128.0	0.35	9578.2
TeXtreme® [105]	1500	61.4	0.042	6405.3

During the parametric analysis, the geometry and mesh of the FE model reported in Section 3.3.1 are adapted to the corresponding configuration. The mesh for Case 1 has 1 mm elements in the refined mesh zone (near the crack tip), while 3 mm mesh size is used in the region away from the crack tip (the opposite ends). The mesh size is scaled up proportionally for Case 2 and

Tab. 3.4: Values of the geometrical variables for each material configuration in the geometrical scalability analysis.

Geom. variables	Case 1	Case 2	Case 3
a_o [mm]	50	25	70
h [mm]	2.5	1.25	3.5
b [mm]	25	12.5	35
l [mm]	150	75	210

Case 3. The kinetic energy U_k and the elastic energy U_e of the specimens are directly obtained from the simulation.

Fig. 3.5 presents the results of the scalability analysis. The scalability is assessed for each of the three different materials by means of the evolution of the energy ratio. The charts in the left column of Fig. 3.5 show the energy ratio versus time curves for the three different materials (steel, AS4/8552 and TeXtreme®), the three geometrical cases and the two velocity profiles considered. As it can be observed for each velocity condition, the energy ratio evolution is equal for the three geometrical cases but with a certain time delay or offset. As seen in the figures, the energy ratio increases from zero in an unsteady manner until a maximum value is reached. Further, the energy ratio decreases rapidly below 1, which corresponds to the transition time defined by Nakamura et al. [83, 84], and with a global tendency towards 0. It can also be seen that for the same geometrical case, the evolution of the energy ratio is steadier when $D = 2$ but the maximum energy ratio and the transition time occur later.

On the other hand, the charts in the right column of Fig. 3.5 show the curves of the variation of the energy ratio versus the dimensionless time parameter. It can be observed that for each material and for each velocity condition, the energy ratio profile is the same for the three geometrical cases. Accordingly, one value of $t_\tau c_o/a_o$ determines the transition time for the three different scalable cases. In addition, thanks to the scalability analysis carried out, the obtained transition time is valid for any DCB test, independently of the corresponding material and initial crack length, provided that the values of

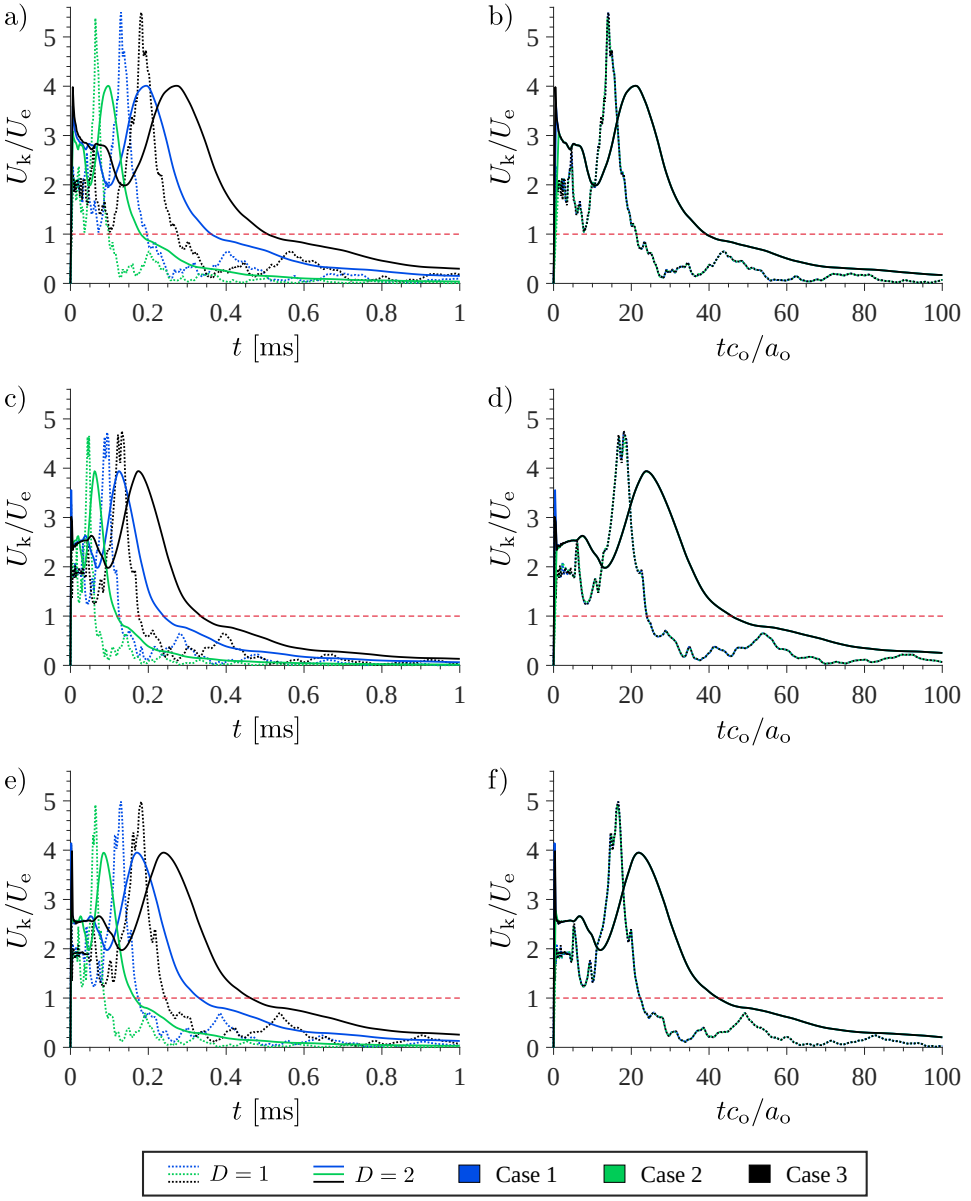

Fig. 3.5: Variation of the energy ratio versus time (a,c,e) and the dimensionless time parameter (b,d,f). Curves a) and b) for steel, curves c) and d) for AS4/8552, and curves e) and f) for TeXtreme®.

π_2 and π_3 are the same.

3.4 Assessment of the proposed methods to determine the transition time

The different methods to determine the transition time can be assessed using the FE simulations of the scalability analysis. First, the evolution of the energy ratio versus time obtained from the FE simulations is plotted versus time, as shown in Fig. 3.6a for $D = 1$ and Fig. 3.6b for $D = 2$, which corresponds to the graphical method. It is worth remarking that the results for the three configurations or cases considered in Section 3.3.4 are very similar. Thus, for conciseness, only the results for Case 1 are represented in Fig. 3.6. In addition, for the sake of clarity, the figure only presents the time range after which the maximum value of the energy ratio is achieved. Then, the variations of the energy ratio predicted using the analytical (Eq. (3.7)) and the numerically-based (Eq. (3.19)) methods are included for comparison. In this way, it is not only possible to assess the accuracy of the analytical and the numerically-based methods in predicting the transition time but also the

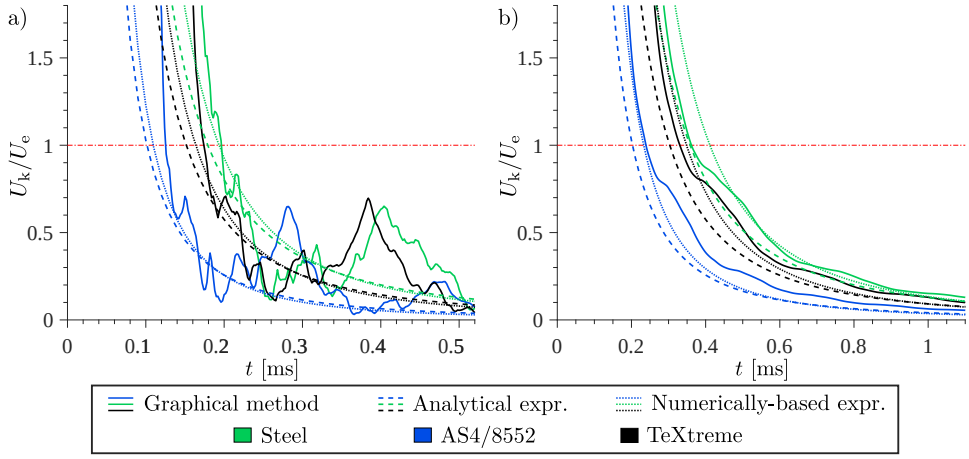

Fig. 3.6: Comparison of curves of energy ratio for Case 1 from the graphical method, the analytical method and the numerically-based method for a) step acceleration ($D = 1$) and b) linear acceleration ($D = 2$).

good approximation in capturing the evolution of the energy ratio.

From Fig. 3.6, a general agreement is seen between the different methods, particularly around the transition time region ($U_k/U_e = 1$). However, after the transition time, the analytical and numerically-based expressions show a different tendency than the graphical method from the FE simulation, especially for the case with $D = 1$. This might be due to the effect of the infinite acceleration profile at $t = 0$ which cause vibrations in the arms of the specimen adding kinetic energy from the wave propagation and other effects that are not taken into account in Eq. (3.7) and Eq. (3.19).

Focusing on the transition time, an assessment of the analytical and numerical expressions, Eqs. (3.10) and (3.20) respectively, can be done. The obtained transition time values are compared with respect to the values from the graphical method, which can be considered as the reference values, as shown in Tab. 3.5.

Analysing the results summarised in Tab. 3.5, it can be concluded that there is a good global agreement between the three approaches. The numerically-based approach shows a slightly better accuracy (the maximum difference is of 14.8%), than the analytical method (the maximum difference is of 19.2%). Only in one case (steel and linear acceleration ($D = 2$)) the difference is lower for the analytical approach. On the other hand, the differences are lower for linear acceleration than for step acceleration ($D = 1$), except for the numerically-based approach and steel. The global tendency observed can be explained by the fact that the analytical method is based on the assumptions of the Euler-Bernoulli beam theory, and the numerically based equation is obtained using non-linear FE simulations. Also a linear acceleration is less abrupt than a step acceleration case, which cannot be so accurately predicted by general approximations. Finally, the numerically-based approach comes from a global fitting of different configurations, loosing accuracy in some of the cases but minimizing the difference in a global response.

Tab. 3.5: Results of the transition time for Case 1 using the graphical approach, the analytical expression and the numerically-based expression, showing the percentage of difference (%DIFR) versus the graphical method. All values of t_τ are in [ms].

Material	D	Graphic t_τ (FE Sim.)	Analytical t_τ (Eq. (3.10))	% DIFR	Numerically-based t_τ (Eq. (3.20))	% DIFR
Steel	1	0.196	0.179	8.7	0.195	0.4
	2	0.362	0.358	1.1	0.415	14.8
AS4/8552	1	0.125	0.101	19.2	0.113	9.9
	2	0.239	0.203	15.1	0.239	0.2
TeXtreme®	1	0.174	0.152	12.6	0.158	9.3
	2	0.330	0.303	8.2	0.336	1.8

From the assessment of the different approaches, it is recommended to use the numerically-based method to obtain the transition time. Even so, performing FE simulations to use the graphical method will allow to get not only the transition time but also the general behaviour of the energy ratio.

3.5 Loading rate effect on the time to fracture

In order to develop the time-based threshold criterion of Eq. (3.1) for a DCB specimen, in addition to the analysis of the transition time carried out in the previous section, it is also necessary to take into account how the time to fracture behaves. Therefore, in this section, a numerical investigation is carried out to study the effects of the velocity profile and its maximum value on the transition time behaviour in presence of a fracture event, i.e., when the initiation of the crack propagation is considered. The FE model presented in Section 3.3.1 is used here with some modifications.

3.5.1 FE model for crack propagation

Since the simulations in this section consider the time for the initiation of crack propagation, t_f, a new numerical model based on the FE model of Section 3.3.1 is defined. The mesh is refined and zero-thickness cohesive elements COH3D8 are added to capture the onset of delamination. The modelling strategy is described in Fig. 3.7. The cohesive constitutive behaviour considered is from

Abaqus' library, where the onset of delamination is defined by a quadratic stress-based criterion, whereas delamination propagation is characterised by the mixed mode energy-based propagation criterion proposed by Benzeggagh and Kenane [106].

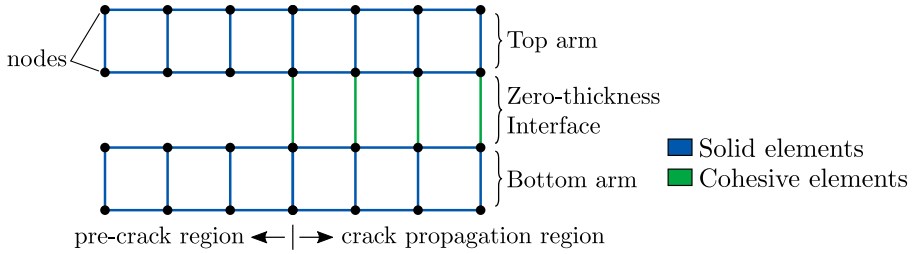

Fig. 3.7: Sketch of modelling strategy using solid elements with incompatible modes (C3D8I) linked with zero-thickness cohesive elements (COH3D8) to capture the initiation of fracture propagation.

A refined mesh of the model is used to account for the interface delamination with biased transition from coarse mesh to fine mesh (see Fig. 3.2). The Fracture Process Zone (FPZ) and the element size in the direction of crack propagation are defined based on the approach proposed by Soto et al. [107]. The corresponding length of the FPZ is 1.21 mm and the element size selected around the crack tip is 0.3 mm, thus, ensuring a minimum of three cohesive elements to model the interlaminar FPZ. A maximum size of 0.6 mm is used at the ends of the specimen. An element size of 0.625 mm is defined in the width direction of the whole specimen.

The DCB specimen modelled has an initial crack length of 50 mm, an arm thickness of 1.5 mm, a length of 150 mm, and a width of 25 mm. The material used is Hexply AS4/8552 CFRP composite, with the following elastic properties [104]: $E_1 = 128000$ MPa; $E_2 = E_3 = 7630$ MPa; $G_{12} = G_{13} = 4358$ MPa; $G_{23} = 2631$ MPa; $\nu_{12} = \nu_{13} = 0.35$ and $\nu_{23} = 0.45$. The interface material properties used are [104]: $G_{\mathrm{Ic}} = 0.28$ N/mm; $G_{\mathrm{IIc}} = 0.79$ N/mm; $\tau_{\mathrm{I}} = 26$ MPa; $\tau_{\mathrm{II}} = 78.4$ MPa and $\eta = 1.45$.

3.5.2 Analysis of the velocity profile

A study of the effect of the velocity profile over the transition time is performed considering different profiles of acceleration, from step acceleration ($D = 1$) to linear acceleration ($D = 2$) for a maximum value of velocity of 6 m/s. The intermediate profiles have a ramp acceleration behaviour, presenting an initial stage of linear acceleration until reaching a state of constant velocity until a final time of 1.8 ms. The description of the different velocity profiles is shown in Tab. 3.6 and illustrated in Fig. 3.8.

Tab. 3.6: Profiles of acceleration for the velocity profile analysis.

Profile	Acceleration value [m/s^2]	Time to constant velocity [ms]
P_1	∞	0 ($D = 1$)
P_2	60×10^3	0.1
P_3	40×10^3	0.15
P_4	20×10^3	0.3
P_5	12×10^3	0.5
P_6	6×10^3	1
P_7	0.33×10^3	1.8 ($D = 2$)

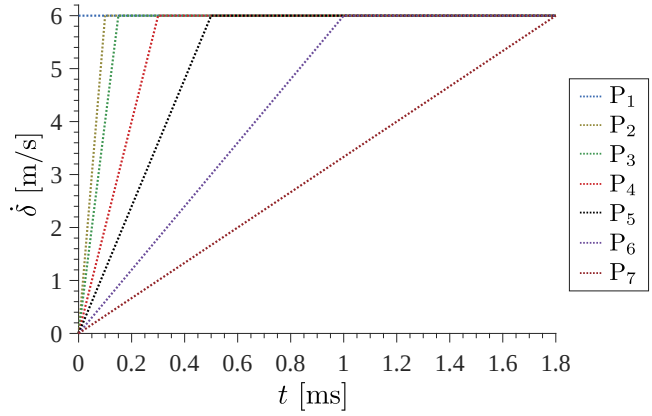

Fig. 3.8: Velocity profiles of the loading rates response analysis.

Fig. 3.9 shows the numerical results from the velocity profile analysis. For simplicity and better understanding of the global behaviour around the transition time zone, the initial part of the curves is omitted and, log-log axes

are used to represent the evolution of the energy ratio versus the dimensionless time parameter. In the figure, the vertical dashed lines indicate the time when the first row of cohesive elements located at the pre-crack are fully degraded, which can be considered as the time to fracture, t_f. The horizontal lines corresponding to an energy ratio equal to 1 (transition time t_τ) and to 0.2 (threshold criterion t_c) are also included in the figure for reference. If the 20% energy ratio limit is crossed in several times for a particular case, in general, the threshold time t_c should be taken as the last time when the energy ratio overpasses the defined limit value.

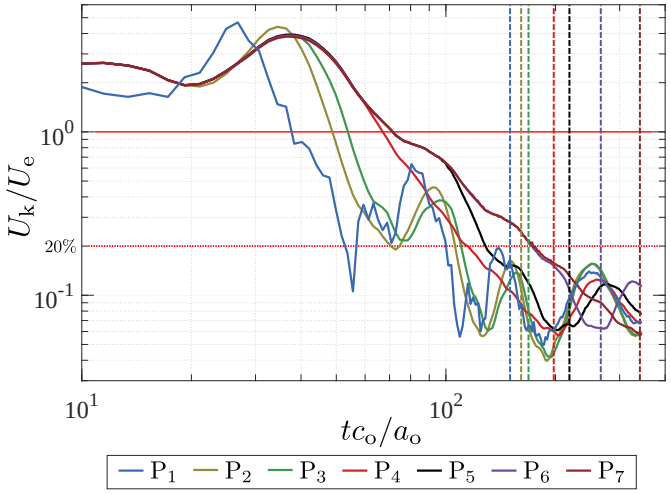

Fig. 3.9: Variation of the energy ratio versus the dimensionless time parameter for the AS4/8552 composite material with a maximum velocity of 6 m/s and different velocity profiles. The t_f is indicated in each case with vertical dashed lines.

The curves in Fig. 3.9 show a different response depending on the velocity profile. There is a gradual change in the behaviour of the maximum energy ratio, as well as the waviness of the curves, from profile P_1 to profile P_7. When decreasing the acceleration, both the transition time and the time to fracture increase. This could be reasoned as when the acceleration decreases, a shorter displacement is achieved in a longer time. On the contrary, as D gets closer to one the acceleration is higher, reaching an infinite acceleration when $D = 1$.

Additionally, it can be noticed that there is no virtual change in the energy ratio behaviour close to the transition time when moving from profile P_5 to P_7. This means that there is a critical value of acceleration in the velocity profiles below which the energy ratio behaves equal to the case of linear acceleration $D = 2$. Even so, it is worth noting that the relative difference in fracture time from case to case is different to the relative difference in transition time. Still, in all the cases, the fracture time is sufficiently larger than the transition time to consider that for this value of maximum velocity, the effect of the velocity profile can be neglected. This is important for the analysis of the effect of the maximum value of the applied velocity, Section 3.5.3, and the analysis of the proportionality of the threshold criterion, Section 3.6. In fact, after the results shown in Fig. 3.9, it can be considered that the case of linear acceleration, $D = 2$, is representative for a wide range of practical cases and it is only necessary to consider the situations where D is equal to 1 or 2.

3.5.3 Analysis of the maximum value of velocity

A study of the effect of the maximum value of applied velocity on the transition time is carried out considering a step acceleration ($D = 1$) and a linear acceleration ($D = 2$). Seven maximum velocities (1, 2, 4, 6, 10, 16 and 20 m/s) are considered to get a wide range of loading rates and to determine the limits of using the transition time for a quasi-static analysis in DCB tests. The simulation time is adjusted to reach the initiation of fracture propagation in each case without extending them unnecessarily. The resulting evolutions of the energy ratio for all the considered velocity values when $D = 1$ and $D = 2$ are reported in Fig. 3.10. Similar to what is observed in Fig. 3.5, Fig. 3.10 presents a different pattern in the variation of the energy ratio when D is equal to 1 (Fig. 3.10a) or when it is equal to 2 (Fig. 3.10b). In both cases, the energy ratio shows a high amount of kinetic energy at the beginning, in the early load stage. For the step acceleration case, $D = 1$, the curves have a wavy behaviour independent of the velocity applied, even for low energy ratios (below 0.1). If an infinite acceleration is applied to reach the constant velocity, stress waves are generated and propagated through the specimen.

Even so, there is a similar tendency in the global behaviour of the curves.

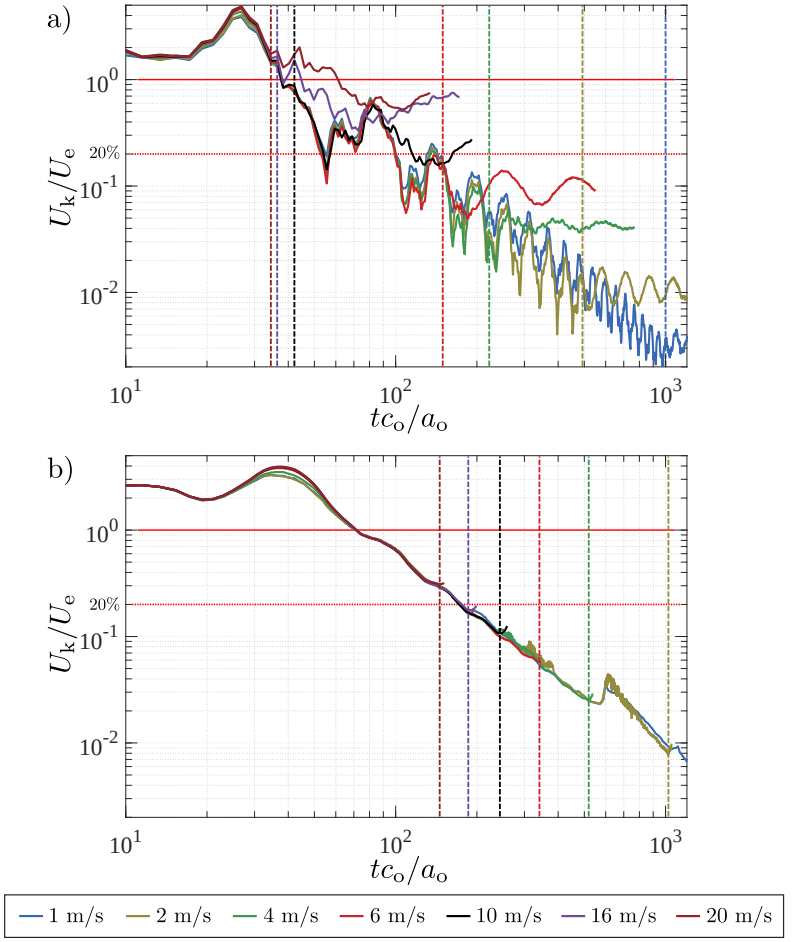

Fig. 3.10: Variation of the energy ratio versus the dimensionless time parameter with different maximum values of the applied velocity for a) step acceleration ($D = 1$) and b) linear acceleration ($D = 2$). The t_f is indicated in each case with vertical dashed lines.

It can be observed in Fig. 3.10a that the value of the transition time is the same for all the cases except for 16 and 20 m/s, where the propagation of the crack starts before the transition time. For these cases, the variation in the evolution of the energy ratio due to the increase of the internal energy during

the crack propagation event, affects the determination of the transition time.

As it can be seen in Fig. 3.10b, the evolution of the energy ratio is practically the same for all the considered velocities when a linear acceleration is used, $D = 2$. The wavy behaviour is not as prominent as in Fig. 3.10a since the kinetic energy is becoming less relevant with the evolution of time during the test. The transition time remains practically the same for all the cases since the linear acceleration allows to reach the maximum value of velocity incrementally, and in turn, increasing the kinetic energy progressively.

Takashima and Minami [100] demonstrated that for impact velocities higher than 1 m/s (step acceleration assumed), the transition time decreases when increasing the velocity in a Charpy test configuration. However, the current study exhibits that the transition time is practically independent of the maximum value of the applied velocity for a DCB test, as seen in Fig. 3.10. In fact, the transition time is exactly the same for all the considered values of the maximum velocity when $D = 2$ and it is only different for the two highest values of velocity when $D = 1$, where it may have been affected by the starting of crack propagation.

3.6 Assessment of the time-based threshold criterion

The transition times obtained in the previous analysis are compared with the time to fracture to determine the proportionality of the time-based threshold criterion of Eq. (3.1). In all the cases considered in the study of the velocity profile carried out in Section 3.5.2 for a maximum velocity of 6 m/s (see Fig. 3.9), the initiation of the fracture propagation takes place when the energy ratio is below 1. In all the profiles the fracture propagation takes place in a time larger than twice the corresponding transition time, fulfilling the time criterion proposed by Nakamura et al. [83, 84]. It can be also observed that for all the cases the initiation of the fracture propagation is predicted when the energy ratio is below 20%, in agreement with the limit established in

Section 3.1. However, although the transition time is the same for profiles P_5 to P_7 and almost the same for P_4, the time to fracture in these four cases varies considerably. Even so, imposing that the initiation of fracture propagation must take place once the energy ratio is below 20% ensures that the dynamic effects can be neglected. This is why it is important to carefully assess the transition time and the threshold criterion for each combination of parameters.

Analysing the results of the maximum value of the velocity carried out in Section 3.5.3, for the case of step acceleration, $D = 1$ (Fig. 3.10a), it is observed that for values of the maximum velocity equal to 16 and 20 m/s, the time to fracture is lower than the transition time. For the case of a maximum velocity of 10 m/s, the fracture event takes place shortly after the transition time. Therefore, in all these three cases, the time criterion of the fracture time being at least twice the transition time is not fulfilled nor the criterion of an energy ratio below 20%. This implies that for the considered conditions, a quasi-static approach can be used only for velocities below 6 m/s. For a linear acceleration, $D = 2$ (Fig. 3.10b), the fracture event is reached in all the cases after the transition time, which results to be the same for all. In fact, in all the cases except for a velocity of 20 m/s, the time-based threshold criterion of an energy ratio lower than 20% is accomplished. For the case of a maximum velocity of 20 m/s, and taking into account that the fracture event is predicted for an energy ratio of about 30%, thus above the limit established, dynamic effects cannot be neglected and a dynamic analysis must be considered.

After the analysis of the evolution of the energy ratio for all the cases considered in the previous sections and taking into account the effect of the different parameters on the time to fracture, it can be concluded that to rule out any dynamic effect on the initiation of fracture propagation, the contribution of the kinetic energy should be less than 20%. Additionally, a criterion only based on the proportionality between the time to fracture with respect to the

transition time might not be always enough to neglect the contribution of this kinetic energy. Nevertheless, a criterion based on the comparison between the level of energy ratio may be impractical and difficult to implement and assess because of the need of FE simulations to obtain the energy ratio. For this reason, a time-based criterion based on the assumption of an energy ratio below 20% is derived. From Eq. (3.19) and imposing $U_{\mathrm{k}}/U_{\mathrm{e}} = 0.2$, it is possible to obtain a value for the threshold time t_{c} through the coefficient α as in Eq. (3.1). The threshold criterion for the numerically-based approach can be now defined as:

$$t_{\mathrm{f}} > t_{\mathrm{c}} = 2.03 t_{\tau} \tag{3.21}$$

After applying and comparing the threshold time criterion proposed by Nakamura et al. [83, 84] and the criterion based on the level of the energy ratio proposed in this work on the results of the evolution of the energy ratio of the previous sections (Eq. (3.21)), it can be concluded that both criteria are almost equivalent. However, the criterion proposed in this work is based on an energy analysis, which has a direct relation with the test rather than imposing an arbitrary proportionality of time (in fact, the criterion proposed by Nakamura et al. considers a coefficient between 2 and 3, without further clarification on how to select these values).

In order to summarise the previous discussion, Fig. 3.11 represents the variation of the transition time and the time to fracture with respect the value of maximum velocity. Fig. 3.11a corresponds to the case of a step acceleration, while a linear acceleration is considered in Fig. 3.11b. In both cases, the threshold criterion with $\alpha = 2.03$ in Eq. (3.21), is included for better visualisation.

It is worth noting that the results in Fig. 3.11 correspond to the case of a DCB specimen made of unidirectional AS4/8552 carbon epoxy composite with $a_{\mathrm{o}} = 50$ mm, $h = 1.5$ mm, $l = 150$ mm and $b = 25$ mm. Thanks to the scalability analysis carried out, these curves are valid for any DCB specimen made of any possible material provided that h/a_{o} is equal to 0.03. This makes

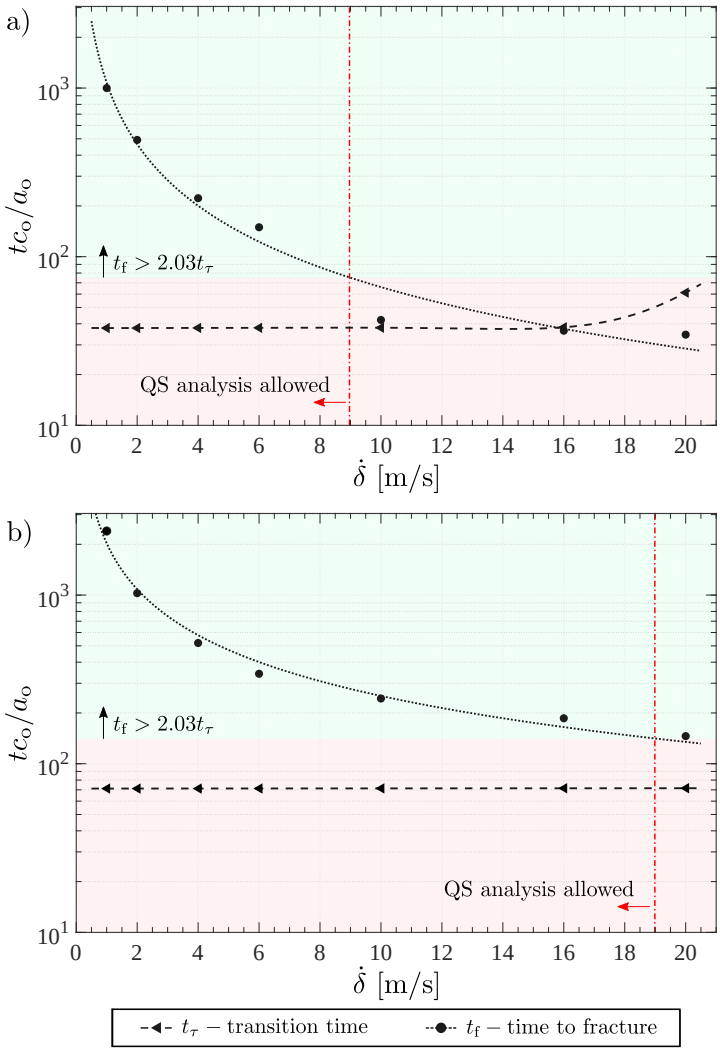

Fig. 3.11: Dimensionless time parameter for transition time and the time to fracture in a DCB specimen of AS4/8552 composite material versus the maximum value of velocity applied using a) step acceleration ($D = 1$) and b) linear acceleration ($D = 2$). The vertical line represents the velocity until which a quasi-static analysis can be performed. The green section represents the cases that fulfil the threshold criterion proposed.

these results very useful for composite materials because the ASTM D5528-13 [10] standard considers an initial crack length of 50 mm and 3 mm thick specimens ($h = 1.5$ mm).

There is currently few experimental data on dynamic delamination tests available in the literature [1, 48, 54] that can be used to validate the proposed method. Using the data from the work of Blackman et al. [48, 54] for the case of epoxy/carbon-fibre composite at test rates from 0.65 m/s up to 20.50 m/s. Applying the numerically-based approach to fulfil the threshold criterion (Eq. (3.21)), it can be determined that a quasi-static scheme analysis can be safely used for all the considered test rates. Although in their work Blackman et al. applied the dynamic analysis approach they proposed, they verified that at 8 m/s the contribution of the kinetic energy is negligible. Thus, confirming the predictions of the numerically-based approach proposed in this thesis.

4 Guided Double Cantilever Beam test method

This chapter presents a test method, the Guided Double Cantilever Beam (GDCB), to measure the mode I interlaminar fracture toughness in composites laminates under intermediate/high loading rates using a novel device. The proposed tool is based on a modified DCB test method with a guided tensile configuration. One of the main characteristics of the device, in contrast to other methods reported in the literature (Section 2.2.1), is that it allows symmetric opening of the specimen arms and reaches a constant opening velocity at the loading points. The tool presents a system of grips for clamping the specimen and allowing the load/displacement transmission from the main part of the tool. It includes a simple, fast and reliable design avoiding adhesive joints and overcomes the problems associated to end blocks and piano hinges. A validation of the test method is conducted by comparing the quasi-static mode I fracture toughness obtained with the GDCB method and the standardised quasi-static mode I fracture toughness ISO 15024:2001 [9]. A test campaign under intermediate and high loading rates is also carried out, showing a good performance of the tool at these velocities.

4.1 Proposed test method

The test method proposed in this chapter is designed for applying symmetric opening to a DCB type specimen under controlled displacement rate to determine the dynamic interlaminar fracture toughness of composites under pure mode I loading. The system is thought to apply intermediate and high loading rates using a high-speed testing machine. Fig. 4.1 shows the tool designed for the GDCB test method. The tool drives the opening of a DCB specimen using guiding plates and applying a tensile load. Additionally, it offers the possibility to reach higher opening velocities than the ones applied by

the machine with an increment around two and a half times the displacement rate of the tester.

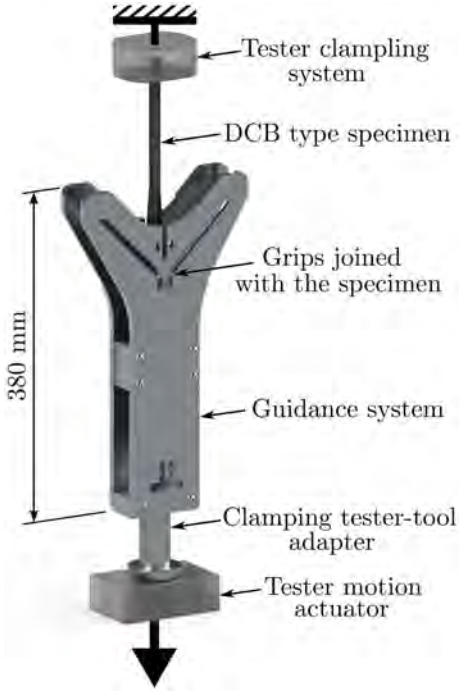

Fig. 4.1: GDCB tool for the intermediate/high loading rates testing.

The device has been designed to be used preferably in hydraulic high strain-rate testing machines allowing to control the test velocity to get a constant opening velocity. To keep the configuration of the machine's inertia, and other related settings, the proposed tool has a similar mass than the manufacturer's tool commonly used in the Instron VHS servo-hydraulic high loading rate machine for the tensile testing. The tool can be used in other testing machines such as the drop tower apparatus with an adapter for the tool clamping. However, in order to achieve constant velocity during propagation, the use in hydraulic high strain-rate testing machines is preferred.

4.1.1 Tool parts

The GDCB testing device is composed of two separated parts. The first one is the guidance system as seen in Fig. 4.2 and it includes: a set of two plates with a guidance profile, a support that joins the guidance profile plates and keeps them parallel to each other, two plates that join the two guidance plates and offer stiffness to the set, a cylindrical adapter for clamping the device to the testing machine (external to the testing tool) and the corresponding required screws and pins.

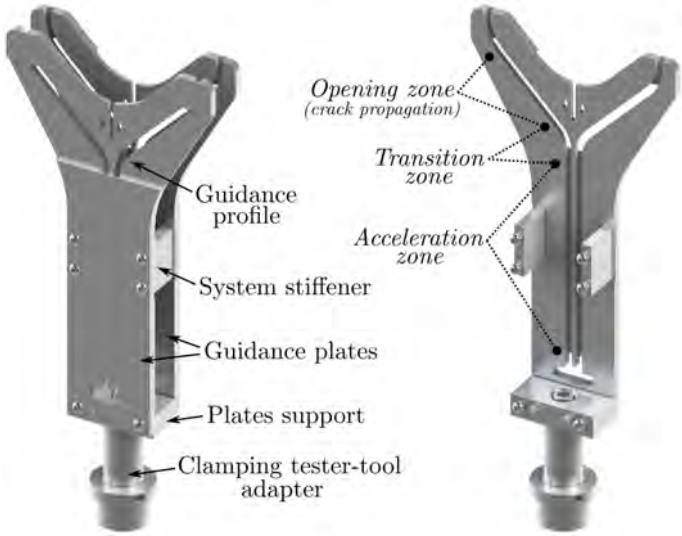

Fig. 4.2: Guidance system of the GDCB tool.

The second part of the device corresponds to the one that transfers the load from the guidance system to the specimen (see Fig. 4.3). It is composed by a set of two grips clamped to the end of each of the symmetrical arms of the test specimen. Each grip consists of a main metallic body with a prismatic centre-slot where one of the arms of the specimen is clamped using a metallic plate or thickness shoehorn and using two tightening bolts. Two round and stiff ends are machined in the main body of the grip to act as loading pins at the opposite ends. As all the interconnections of the different parts of the

device are mechanical, there is no need for gluing clamps, allowing an easy reuse of the system to test DCB specimens with common thickness.

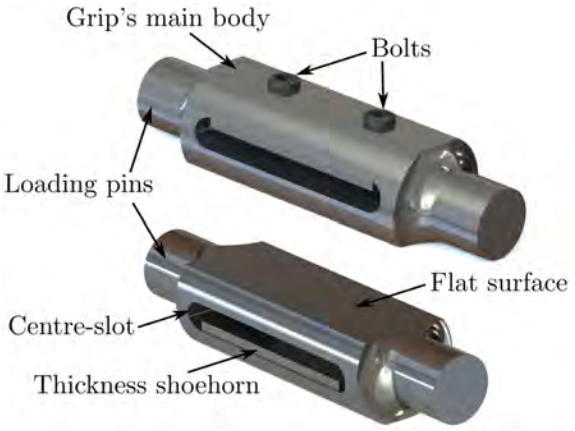

Fig. 4.3: Grip of the GDCB tool.

The design of the tool has been done in such a way that allows to measure the displacements and crack propagation by means of image analysis using optical tracking, performing a data reduction method only based in displacements. Even so, the tool allows to have the measurement of the load if desired, through the load cell or other techniques.

4.1.2 Tool operation

As shown in Fig. 4.1 for a vertical configuration of the system (it can be also mounted in other directions depending on the testing machine), the specimen is hold by the clamping grips of the machine and loaded by applying a single tensile displacement to the cylindrical clamping tester-tool adapter of the guidance system. The transfer of the opening load to the specimen involves friction in the contact between the guides and the pins of the grips. However, this friction can be minimised by means of smooth surfaces and bearing like movement, ensured by tight tolerances and good lubrication. For this aim, a thin layer of Molybdenum-Disulphide (MoS_2) paste lubricant was used to reduce the friction coefficient. In any case, the friction coefficient between the load pins and the guides can be considered as small and constant, contrary

to what can happen in the case of the internal wedge driven test, where the coefficient of friction changes from the initial crack zone to newly generated surface.

When the guidance system is pulled away in the tensile direction of the specimen, the guidance profiles in the guidance plates guide the pins of the grips resulting in an opening displacement of the specimen arms. The guidance profiles contain an acceleration zone where no opening displacement of the specimen arms is achieved to allow for the acceleration of the system without opening in the arms until reaching a desired constant speed value, as shown in Fig. 4.4. After, the pins are driven to a transition zone to change from the acceleration movement with no opening displacement to the opening

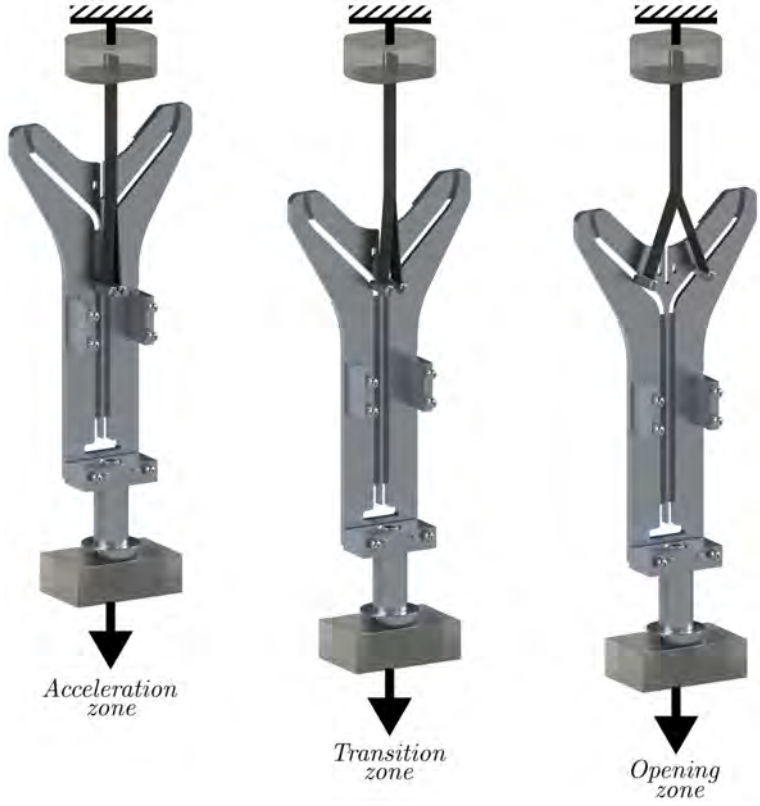

Fig. 4.4: Opening process of the specimen during a test (from left to right).

zone where the constant opening displacement is applied. The transition zone is designed in order to avoid sudden changes in the acceleration of the grip pins. In that way, the initiation of the crack propagation starts only when the constant velocity of the machine is reached and after the transition zone, where the opening velocity is constant (see Fig. 4.4). The guidance profile angle in the opening zone can be varied. In this study a guiding angle of 45° with respect to the machine movement was chosen so that the opening and axial loading on the pin are of equal magnitude. The test device is complemented with an extra mounting tool to put together and correctly align the grips on the specimen before testing. In this way, when the specimen is clamped to the testing machine, the correct alignment between the machine, the guiding-plates and the specimen is guaranteed and, consequently, a symmetrical opening is achieved.

The system has been designed in such a way that the specimens to be used are similar to the ones defined for the characterisation of the mode I interlaminar fracture toughness in laminated materials, i.e., the DCB test [9]. However, some changes regarding the initial crack length and the length of the specimen are recommended to ensure the propagation of the crack within the opening zone (see Section 4.2.1).

As mentioned before, besides the opening force, the GDCB method involves an additional axial force in the specimen arms that will load both arms in tension and, in turn, will generate a flexural moment that will induce bending energy. Although the contribution of this axial force is smaller than that of the opening forces, it is necessary to take it into account for the correct determination of the material fracture toughness (see Section 4.1.3). The developed tool uses a set of external guiding profiles in a tensile configuration since the composite materials commonly have a better behaviour under tension than in compression. In this way, this design avoids impacts in the specimen as the ones present when using the falling external wedge method [52, 60–62]. In addition, the device also solves the friction issues of the wedge-insert inside

the DCB specimen reported in the literature [47, 53, 57, 58].

4.1.3 Data reduction method

Based on the deductions of the first order beam theory described by Williams [108] andHashemi et al. [109], it is possible to determine the energy release rate based on the applied moments at the end of a crack, as shown in Fig. 4.5. For this case, the crack is located in the mid-plane between the upper and lower sections of the beam. The load is considered to be applied centred with the mid-plane of the beam arms of the specimen. In this way, the non-linear effects due to large displacements are minimised during the analysis. Fig. 4.5 shows how the crack grows from point O (XW) to point O' (YZ), with an increment of delamination length Δa with respect to the initial crack length a. The upper arm is loaded with a moment M_1 and the lower arm with a moment M_2, and the uncracked portion has a bending moment $(M_1 + M_2)$.

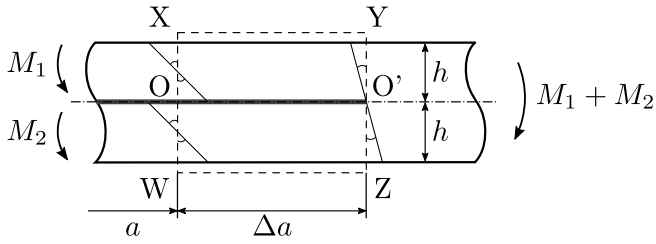

Fig. 4.5: Delamination geometry and loaded crack tip contour.

The total energy release rate may be expressed as:

$$G_{\mathrm{I}} = \frac{3}{4Eb^2h^3}\left[8{M_1}^2 + 8{M_2}^2 - (M_1 + M_2)^2\right] \tag{4.1}$$

where b is the width, h is half of the specimen thickness and E is the flexural modulus of the laminate for an arbitrary stacking laminate or the axial modulus of the laminate for the case of unidirectional material. Since the total energy release rate of Eq. (4.1) is the sum of mode I and mode II, it must be partitioned to obtain the mode I component [108]. Pure mode I implies that the moment applied in both arms is the same but in opposite

direction. Therefore, Eq. (4.1) yields to:

$$G_{\mathrm{I}} = \frac{6\left(M_2^2 + M_1^2\right)}{Eb^2h^3} \tag{4.2}$$

In the DCB mode I test configuration of Fig. 4.6, the bending moments are $M_2 = -M_1 = Pa$, so the expression obtained is:

$$G_{\mathrm{I}} = \frac{12P^2a^2}{Eb^2h^3} \tag{4.3}$$

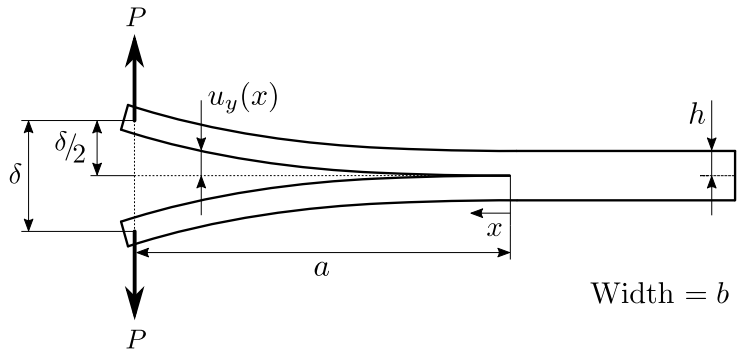

Fig. 4.6: Mode I double cantilever beam (DCB) configuration.

For the case of the GDCB mode I test of Fig. 4.7, the bending moments are defined by the contribution of the opening load and the axial-tensile load

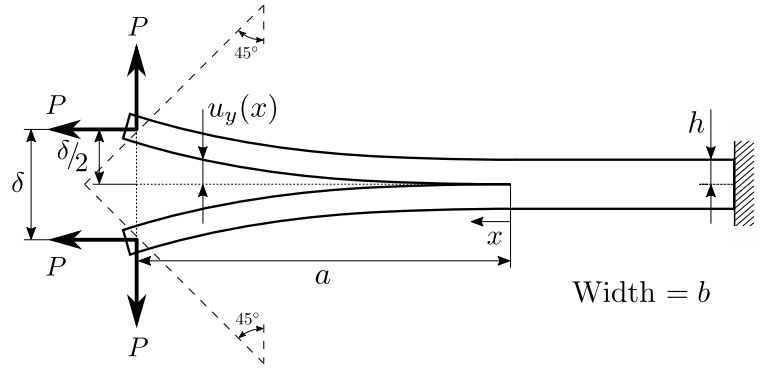

Fig. 4.7: Mode I guided double cantilever beam (GDCB) configuration.

$M_2 = -M_1 = Pa - P(\delta/2)$, so the expression obtained is:

$$G_{\mathrm{I}} = \frac{6}{Eb^2h^3}\left[\left(Pa - P\frac{\delta}{2}\right)^2 + \left(Pa - P\frac{\delta}{2}\right)^2\right] = \frac{12P^2a^2}{Eb^2h^3}\left(1 - \frac{\delta}{2a}\right)^2 \quad (4.4)$$

In the previous equations, the effect of the involved shear deformation is considered negligible for the calculation of the energy release rate. This assumption applies for sufficiently long cracks.

Eqs. (4.3) and (4.4) are valid for cases where the load can be measured, i.e., for quasi-static testing. Nevertheless, taking into account that the signal of the load cell is not recommendable in high loading rate tests, an alternative analysis based on displacements is required. For this, it is necessary to obtain the compliance of the system, which for the case of the DCB may be deduced from the energy release rate equation in terms of the derivative of the compliance respect to the crack length and the Eq. (4.3), obtaining that:

$$C = \frac{\delta}{P} = \frac{8a^3}{Ebh^3} \quad (4.5)$$

In the GDCB configuration, due to the axial-tensile load, it is not easy to obtain the compliance in such a way because the opening displacement due to the opening load is affected by the axial force and vice versa. One way to determine the compliance of the GDCB method is by studying the deflection of a cantilever beam subjected to a combined end force as shown in Fig. 4.8. Therefore, assuming Euler-Bernoulli beam theory, the flexural moment can be approached as:

$$M(x) = EI\frac{\mathrm{d}\theta}{\mathrm{d}s} = EI\frac{\mathrm{d}^2y}{\mathrm{d}x^2} \quad (4.6)$$

$$M(x) = P\left(a + u_x - x\right) - P\left(u_y - y\right) \quad (4.7)$$

where $M(x)$ is the equivalent bending moment applied at the arbitrary cross section, with a transverse load equal to the axial-tensile load P; x is the direction along the undeflected beam axis; y the transverse direction; a is the crack length (assumed as the length of the beam); θ is the angular deflection and $\mathrm{d}\theta/\mathrm{d}s$ is the change rate of the angular deflection along the beam. E is

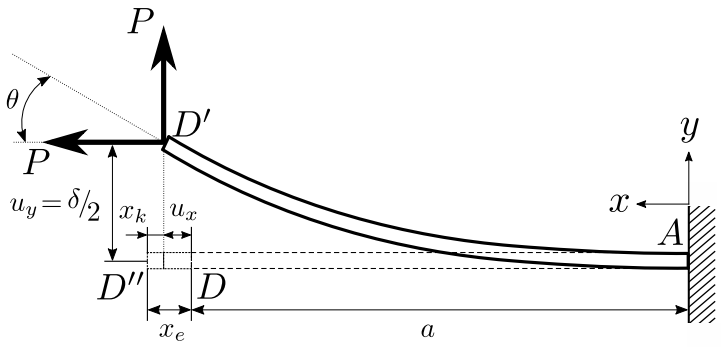

Fig. 4.8: Cantilever beam configuration subjected to an opening load and a tensile axial load.

the flexural modulus, I is the inertia moment, and u_x and u_y are the axial and the transverse deformations at the end-edge of the arm.

The solution for Eqs. (4.6) and (4.7) was defined by Awtar et al. [110] as approximations by inverse linear expressions to the hyperbolic functions solution. This solution captures the effects of load-stiffening and elastokinematic non-linearities in a simple beam subjected to end forces. The force equilibrium condition is applied in the deformed configuration of the beam, where the axial-tensile load contributes to the bending moments. The axial displacement u_x is comprised of two components: a purely elastic component x_e resulting from the elastic stretching of the beam, and a bending component x_k that results from the conservation of beam arc-length, as represented in Fig. 4.8. Liu and Yan [111] summarised the solution for displacements of a simple beam subjected to end forces from [110], and the resulting displacement relationship in terms of the load and the flexural stiffness for the beam analysis is:

$$\frac{u_y}{a} = \frac{\delta}{2a} \approx \frac{5Pa^2}{15EI + 6Pa^2} \tag{4.8}$$

Thus, reorganising the terms in Eq. (4.8), the compliance of the GDCB method can be described as:

$$C = \frac{\delta}{P} \approx \frac{8a^3}{Ebh^3}\left(1 - \frac{3\delta}{5a}\right) \tag{4.9}$$

Using the expression of the compliance in Eq. (4.9), which is a function of δ and a, to obtain the value of the force P in function of the other parameters and substituting in Eq. (4.4), a displacement-based equation for the energy release rate can be found.

$$G_{\mathrm{I}} = \frac{3Eh^3\delta^2}{16a^4}\left[\frac{\left(1-\frac{\delta}{2a}\right)^2}{\left(1-\frac{3\delta}{5a}\right)^2}\right] \tag{4.10}$$

The previous analysis of the simple beam theory equations assumes that at the crack tip the compliance is zero (Eqs. (4.5) and (4.9)). However, it has been proved the existence of some deflection and rotation at the crack tip [109]. Then, the rotation of the arms at the crack tip is modelled by adding a length χh to the crack length, defining an effective crack length $a_{\mathrm{e}} = a + \chi h$, where χ is a constant given by the elastic properties of the material as described in [109]. Then, the corrected expression for the mode I energy release rate using the GDCB method is:

$$G_{\mathrm{I}} = \frac{3Eh^3\delta^2}{16\left(a_{\mathrm{e}}\right)^4}\left[\frac{\left(1-\frac{\delta}{2a_{\mathrm{e}}}\right)^2}{\left(1-\frac{3\delta}{5a_{\mathrm{e}}}\right)^2}\right] \tag{4.11}$$

Furthermore, corrections for large displacements and/or end block corrections might be necessary in accordance to ISO 15024:2001 [9], and as reported by Williams [112].

4.1.4 Correction for high loading rates

When the GDCB test is performed under high loading rates, the kinetic energy of the system might play an important role during the analysis. The transition time threshold criterion proposed in Chapter 3 [113], based on the relation between the kinetic and elastic energies, can be used to determine if the contribution of the kinetic energy is relevant for the analysis of the mode I interlaminar fracture toughness or not. For the cases where the kinetic energy plays a relevant role, its contribution to G_{I} can be calculated from the

kinetic energy of a cantilever beam with a lumped mass m at the free end. Due to the complex solutions and the need of numerical methods to compute the real contribution of the kinetic energy, a simplified approximate solution can be used instead. Based on the work done by Blackman et al. [54], using the simple beam theory and assuming the static displacement profile of a cantilever beam with a transverse loading, the kinetic energy can be expressed as:

$$U_{\mathrm{k}} = 2\left[\frac{1}{2}\int_0^a \rho b h\left[\dot{u_y}\left(\frac{3ax^2 - x^3}{2a^3}\right)\right]^2 \mathrm{d}x\right] + 2\left[\frac{1}{2}m\left(\dot{\delta}/2\right)^2\right] \tag{4.12}$$

$$\frac{\mathrm{d}U_{\mathrm{k}}}{\mathrm{d}a} = \frac{33\rho b h\dot{\delta}^2}{560} = \frac{33Ebh}{560}\left(\frac{\dot{\delta}}{c_{\mathrm{o}}}\right)^2 \tag{4.13}$$

where $c_{\mathrm{o}} = (E/\rho)^{1/2}$ is the longitudinal wave propagation velocity in the material. Finally, the displacement-based expression for the G_{I} of the GDCB method at high loading rates can be expressed as:

$$G_{\mathrm{I}} = \frac{3Eh^3\delta^2}{16\left(a_{\mathrm{e}}\right)^4}\left[\frac{\left(1 - \frac{\delta}{2a_{\mathrm{e}}}\right)^2}{\left(1 - \frac{3\delta}{5a_{\mathrm{e}}}\right)^2}\right] - \frac{33Ebh}{560}\left(\frac{\dot{\delta}}{c_{\mathrm{o}}}\right)^2 \tag{4.14}$$

4.1.5 Finite Element model for design and validation

The aim of the simulations was to study the accelerations and stresses of the tool when submitted to high loading rates and to use the results for the design process. The simulations were mainly focused on the grips, especially the pins, since they are the weakest but the most loaded parts of the test system. They transfer all the load from the actuator to a small contact area with the guidance plates, and finally, to the specimen. The grips are of small size to reduce the inertia effects on the end-edges of the specimen arms and to avoid inducing non-linear effects when introducing the load in the specimen.

A three-dimensional model of the GDCB specimen was defined using the commercial software Abaqus™/Explicit [103]. The composite specimen was

modelled using solid elements with incompatible modes (C3D8I) to capture the bending response due to the large displacements, avoiding the shear-locking phenomena. Since the delamination must be modelled, zero-thickness cohesive elements COH3D8 were added to capture the onset of delamination and the propagation. The cohesive constitutive behaviour considered was the Traction-Separation law available in Abaqus, where the delamination onset is captured based on a quadratic stress criterion, and the mixed-mode energy-based approach proposed by Benzeggagh and Kenane [106] is used for propagation.

The GDCB specimen modelled had an initial crack length $a_o = 92.5$ mm, an arm thickness $h = 1.5$ mm, a length $l = 250$ mm, and a width $b = 20$ mm. The specimen was assumed as unidirectional with all fibres parallel to the direction of the crack growth. The material used for the simulations was a unidirectional Hexply AS4/8552 CFRP composite, with the following elastic properties [104]: $E_1 = 128$ GPa; $E_2 = E_3 = 7.63$ GPa; $G_{12} = G_{13} = 4.358$ GPa; $\nu_{12} = \nu_{13} = 0.35$ and $\nu_{23} = 0.45$. The interface material properties used are [104]: $G_{Ic} = 0.28$ N/mm; $G_{IIc} = 0.79$ N/mm; $\tau_I = 26$ MPa; $\tau_{II} = 78.4$ MPa and $\eta = 1.45$.

A refined mesh of the model was used in the delamination propagation zone with biased transition from fine to coarse mesh away from the crack tip, as shown in Fig. 4.9. The Fracture Process Zone (FPZ) and the appropriate element size in the direction of crack propagation were defined based on the approach proposed by Soto et al. [107]. The corresponding length of the FPZ for pure mode I propagation was 1.21 mm and the element size selected was 0.3 mm from the crack tip until the end of a propagation length, ensuring a minimum of three cohesive elements used to discretise the interlaminar FPZ. A maximum element size of 1.5 mm was used at the fixed end of the specimen. An element size of 0.375 mm was defined in the width and the through-thickness directions of the whole specimen.

The grips were modelled using hexahedron solid elements C3D8R for the pins

and the central body of the grip, and tetrahedron solid elements C3D4 for the curved transition region between the pins and the central body, as shown in Fig. 4.10.

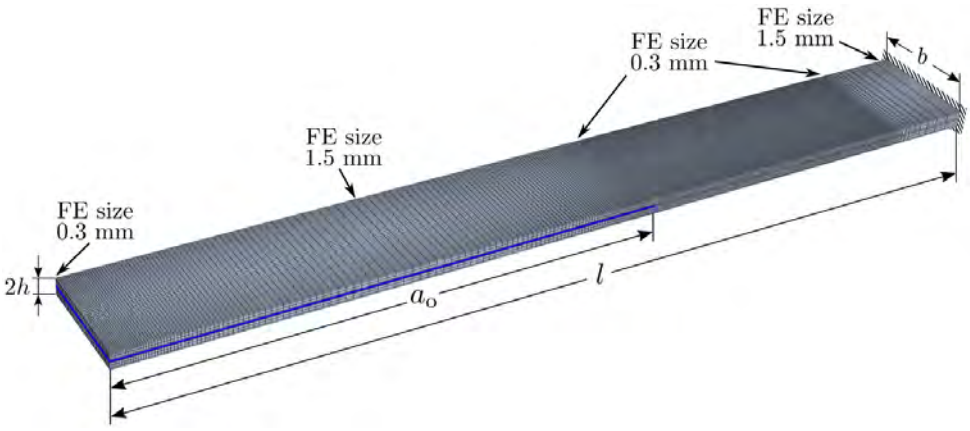

Fig. 4.9: Mesh of the specimen.

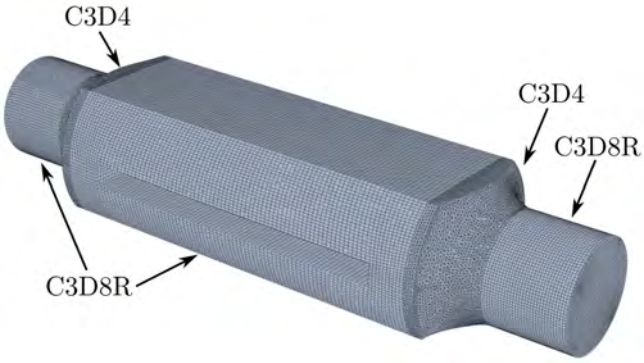

Fig. 4.10: Mesh of the grip and element types used.

For the main body of the GDCB tool, the two plates with guidance profiles were modelled through surface profiles and rigid elements type R3D4 with an element size of 0.3 mm. Then, using a rigid body motion, the three zones identified previously were simulated: acceleration zone, transition zone and opening zone (constant velocity zone). A first step was used to perform the acceleration stage until reaching the desired velocity, i.e., the acceleration

zone. A second step was done applying constant velocity for the transition zone and the opening zone. Velocities up to 15 m/s of the actuator were considered in different simulations to check all the possible loading rates that the servo-hydraulic tester can achieve. All the displacements at the end of the specimen were constrained, while the arms were linked to the grips by a tie constrain definition. Contact constrains between the rigid bodies of the guidance surfaces and the pins of the grips were defined. Fig. 4.11 shows the boundary conditions of the FE model.

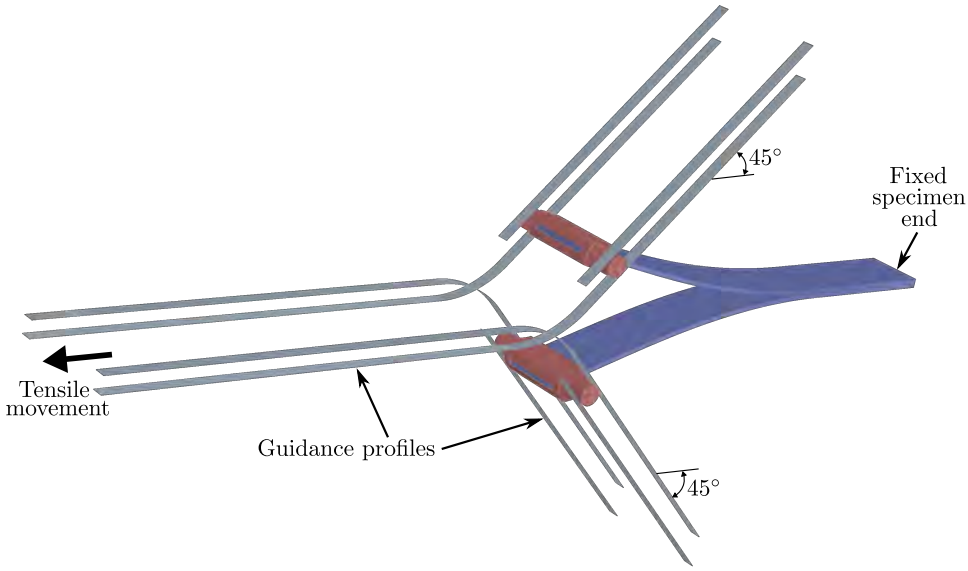

Fig. 4.11: FE model of the GDCB guides, specimen and grips with the applied boundary conditions.

4.1.6 Results of the FE modelling

The results of the simulations showed that the critical moment of the test is when the grips pass through the transition zone from the acceleration zone, with no opening, to the constant velocity opening zone. In this transition zone is when the opening force starts to appear, subjected to a change in direction. It is also in this zone when contact between loading pins and guide is intensified and even small impacts occur (Fig. 4.12). In order to achieve

tolerant stresses in the grips, their design suffered several transformations. In fact, the final design of the grips uses titanium for its low density (titanium is around 1.8 times lighter than steel) to reduce inertial effects while ensuring a sufficiently high yield strength (1100 MPa for titanium and 1300 MPa for steel).

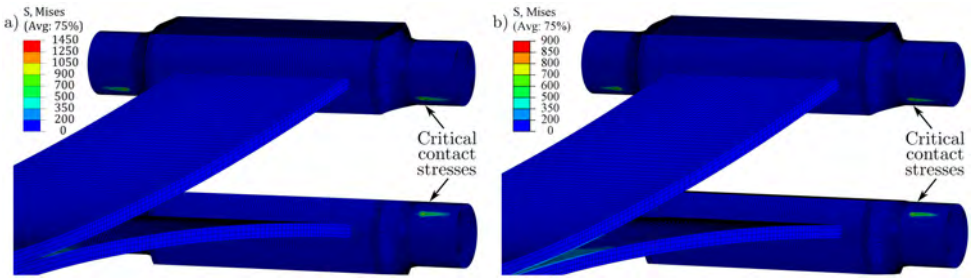

Fig. 4.12: Stress field in the grips in the transition zone at 15 m/s tester velocity for a) steel grips and b) titanium grips (stress values in MPa).

Apart from the analysis of stress in the pins of the grips as the most critical parts, it was also necessary to assess the performance of the guidance profiles and the specimen. In the profiles, the stresses were equal to the ones reported for the case of titanium pins (Fig. 4.12b). However, since the inertia effects are not problematic for the guidance plates, these are made of tool steel with a higher strength than that of the titanium. Thus, contact stresses should not cause any problem in the guiding profiles. For the specimen, there was a concern about the bending behaviour of the arms and the stresses in the region of the connection with the grips, since it is possible to overload the arms causing their premature failure. After the analysis, it was observed that even for the critical loading rate of 15 m/s, the stresses in the specimen arms were low and handleable by typical composite materials.

Fig. 4.13 shows the opening velocity from a simulation with a tester velocity of 15 m/s. This graph validates the method and its expected behaviour, presenting an increase of the opening velocity due to the acceleration in the transition zone and reaching a constant velocity at the opening zone. However, the opening velocity increases when the crack propagation begins due to the

inertia effect. Although the opening velocity has a small increase, it may be considered as a constant value. In addition, according with the design, the crack propagation starts once the opening zone is reached.

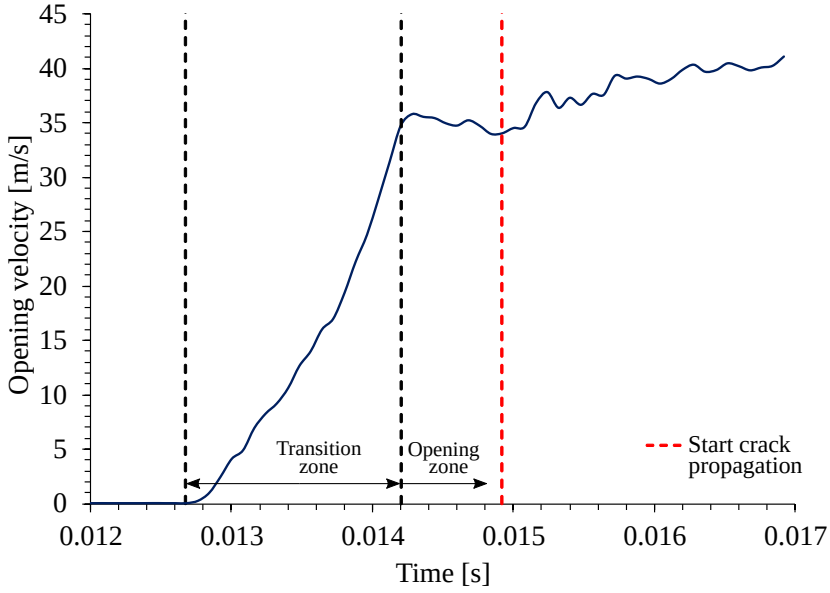

Fig. 4.13: Opening velocity vs time from the simulation at 15 m/s tester velocity.

4.2 Experimental campaign for validation and characterisation

In this section an experimental testing campaign is performed. Initially, the results of quasi-static DCB and GDCB tests with woven CFRP specimens are compared to assess and validate the proposed test method. After, additional tests with the GDCB tool using the same material are carried out to assess the performance under high loading rate conditions.

4.2.1 Material and specimen geometry

The woven composite material used in this study combined the carbon fabric type G0926 (5HS, 6 K, 370 gsm) produced by Hexcel® with the HexFlow® RTM6 mono-component epoxy system using the Resin Transfer Moulding

(RTM) process. The composite material has the following elastic properties [114]: $E_{11} = 59.54$ GPa; $E_{22} = 54.95$ GPa; $G_{12} = 5.21$ GPa; and $\nu_{12} = 0.03$.

An 8-ply 400×300 m^2 plate with all layers oriented in the same direction was manufactured with a 400×120 mm Teflon film placed at the mid-plane of one end to generate the starter crack. The laminate had a ply stacking sequence of $[0_4/\text{Teflon}/0_4]$. The specimens were cut from the plate using a diamond blade. The longitudinal edges of the specimens were polished with sandpaper of different grain sizes and coated with white spray paint to facilitate the optical tracking of the crack propagation. The resulting average specimen thickness was 2.925 mm. This thickness corresponds to the mean value of cured specimens, counting six measures per specimen at different locations with a thickness variation within the limits established by the DCB standard [9]. The specimen's dimensions and preparation were kept the same for the two test configurations, DCB and GDCB. The in-plane dimensions of the final samples were 270×20 mm^2.

The specimen length has been selected to ensure the initiation of propagation once the transition zone is finished and a constant opening velocity is reached. For this aim, two steps are required to obtain the crack length and the opening displacement that fulfil the requested conditions. First, using the analytical expression from Eq. 4.11 and assuming an expected value of the fracture toughness, an initial value of the crack length is obtained when the crack propagation starts for a defined opening displacement (value selected to be in the opening zone). Then, a trial GDCB test is performed to check if the selected crack length fulfils the condition of only crack propagation in the constant opening velocity zone. Moreover, this trial test allows to assess if any form of failure in the arms of the specimens due to excessive bending or low stiffness is occurring. In this case, based on an estimation of the expected fracture toughness, it was determined that the initial crack length should be of 105 mm from the edge of the specimens. Before clamping the specimens to the testing machine, the cracked regions were manually opened carefully

and the Teflon sheet was removed. As recommended by the DCB standard [9], all pre-cracks were extended a few millimetres using the DCB set-up to avoid any influence of resin-rich pockets originated at the edge of the Teflon tape. Once the specimens were placed into the grips, the initial crack length was around 115 mm for the DCB and 105 mm for the GDCB. Although this crack length is longer than the one specified in the DCB standard [9], this length was chosen to obtain load-displacement curves in the same order of magnitude and similar crack lengths during propagation for both tests.

4.2.2 Set-up for the quasi-static test validation

The quasi-static tests were performed under laboratory conditions. An electromechanical screw-driven MTS machine equipped with a 5 kN load cell was employed to load the specimens for both DCB and GDCB tests, with a constant cross-head velocity of 5 mm/min. In addition to the own data acquisition system of the testing machine to record load and displacement, a set of two cameras was used to track the displacement at the load-application

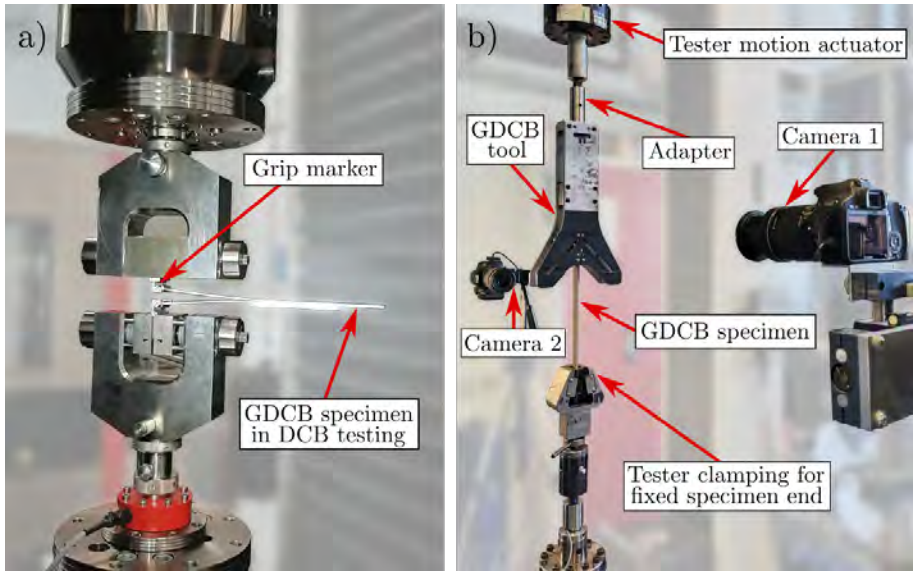

Fig. 4.14: Set-ups for the quasi-static testing of a) the DCB and b) the GDCB (rotated 180° with respect to usual orientation).

point, and to monitor the crack propagation, as shown in Fig. 4.14 (not included in the picture for the DCB test, Fig. 4.14a). Camera 1 was used for the tracking of the grip pins and Camera 2 for the crack tip location. The displacement at the load-application point was tracked optically by means of markers placed at the pins in the specimen grips. For the DCB tests, the cameras recorded images at 1 fps with a resolution of 2200×2200 pixels. For the GDCB tests, the cameras recorded images at 3 fps with a resolution of 2048 pixels along the loading direction, and 328 pixels along the transverse direction for Camera 1 and 2048×2048 pixels for Camera 2. The lighting conditions during testing were set in such a way that sharp contrast between the white specimen surface and the background was obtained. Fig. 4.15 shows a photo frame for the set of two cameras used in the GDCB test.

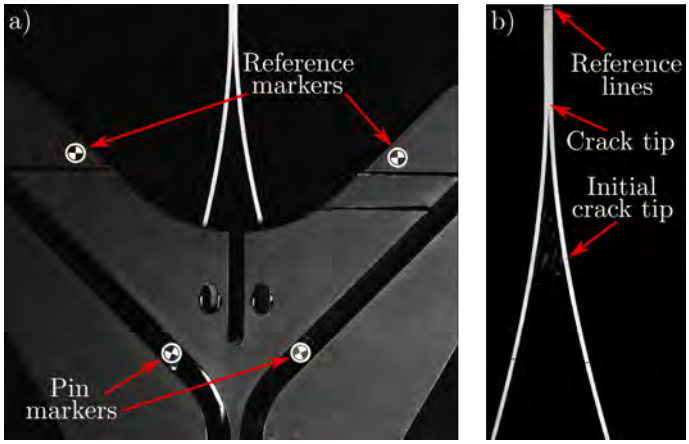

Fig. 4.15: Photo frames from a) Camera 1 and b) Camera 2 for the image post-processing of the GDCB.

Although the DCB quasi-static tests were performed based on the standard ISO 15024:2001 [9], some modifications as the initial crack length and the length of the specimen were done. Additionally, the same data reduction process with the image post-processing was used in the DCB to validate the data acquisition and the data reduction methods for the GDCB. The grip markers and the two cameras were also used for the DCB tests, requiring the

use of the same grip system of the GDCB and using an additional part to obtain the hinge behaviour over the pins of the grips.

All the images taken with the two cameras were post-processed using in-house Matlab scripts/algorithms. The script for Camera 1 analyses all the image frames of this camera to determine the current position of the grip pins and the reference markers. Then, the opening displacement is obtained as the distance between the two loading pins, as seen in Fig. 4.16a. The reference markers are used as set points for the pin markers and as a control for the conversion from pixels to millimetres. Finally, the opening velocity can be calculated using the testing time. A second Matlab script is used to determine the current position of the crack tip along the test by processing the images taken with Camera 2. First, the longitudinal inner edge of each specimen arm is detected, as shown in Fig. 4.16b. Then, a polynomial expression is adjusted to each inner arm edge by a curve fitting process. Finally, the crack tip is detected by the intersection of the two polynomial curves, as shown in Fig. 4.16c. In Fig. 4.16c, two different crack tips are shown: the crack tip from the image post-processing, which is the one detected by the pixel analysis, and the predicted crack tip, which is the one from the curve fitting process.

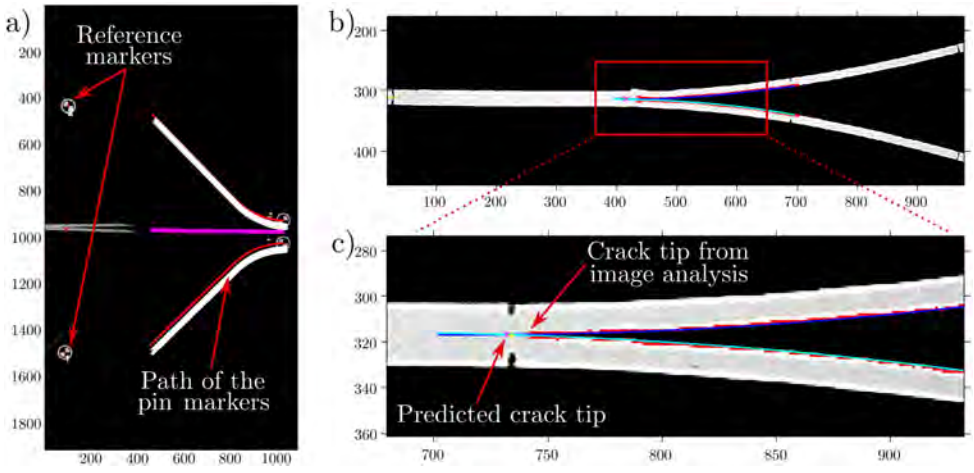

Fig. 4.16: Matlab script images for the analysis of the GDCB from a) Camera 1, b) Camera 2 and c) zoom of the Camera 2 analysis (axes units in pixels).

Being the pixel analysis underestimated and inaccurate since it relies on the optical resolution of the system, without considering the nearby deflection of the arms, the useful crack tip is the one defined by the curve fitting process.

4.2.3 Results and discussion for the quasi-static validation

Fig. 4.17 shows the experimental and analytical load-displacement curves for both the DCB and the GDCB tests. From this figure, it can be noticed that there is a clear stick-slip behaviour present in the experimental DCB curves, while the experimental GDCB curves have a noisy behaviour that may conceal the stick-slip drops. The noise in these curves can be explained by the contact between the pins and the guidance plates of the GDCB method. As it will be commented later, the effect of this noise on the GDCB test is more important for quasi-static and low-velocity conditions. Due to stick-slip, the pre-cracking process of the DCB and GDCB specimens resulted in a

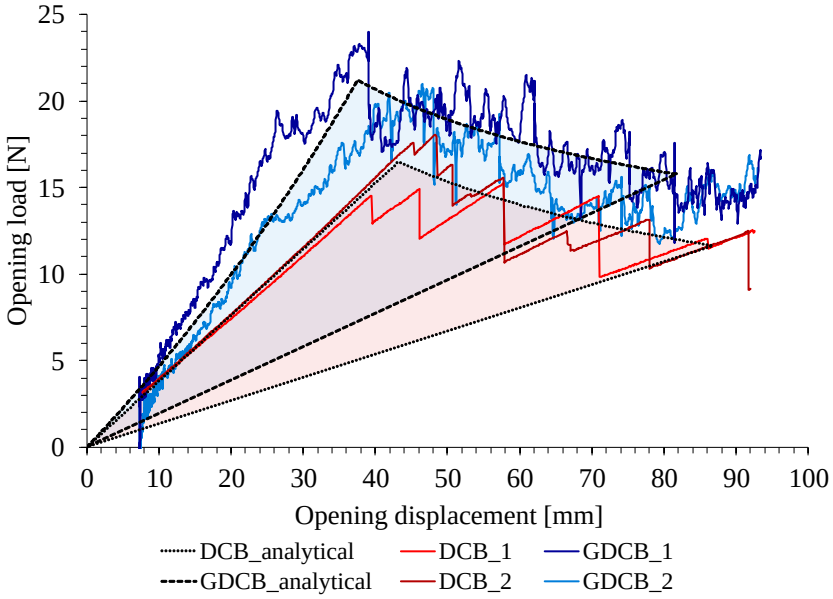

Fig. 4.17: Load-displacement curves for DCB and GDCB tests. The coloured areas correspond to the theoretical dissipated energy in each case for comparison purposes.

crack propagation greater than the 3 to 5 mm defined by the standard, with a remarkable difference between the initial crack length of the specimens used for the GDCB test. This is why, the elastic stiffness of both GDCB curves shown in Fig. 4.17 differ considerably between them. The analytical curves were obtained from a mean value of the initial crack length for both cases. In both cases, the experimental curves show a high dispersion during propagation mainly due to the stick-slip behaviour. Even so, the experimental curves follow the same trend of the analytical ones from Eqs. (4.3) and (4.4).

Additionally, in Fig. 4.17 it can also be seen that the effect of the axial load involved in the GDCB method when compared to the DCB. This axial load affects the compliance, as seen by comparing Eqs. (4.5) and (4.9), resulting in a non-linear increment in the elastic curve of the chart, increasing the maximum load and shifting the crack propagation curve. The figure shows the analytical curves with the loading, propagation up to the same crack length for both methods and unloading stages. It is worth mentioning that although both curves show different trends in stiffness, maximum load and propagation curve, the areas between the three curves for each specimen type (shaded/coloured areas in Fig. 4.17) are exactly the same and correspond to the dissipated energy during the crack growth process, i.e. the same fracture toughness.

Fig. 4.18 shows the variation of the mode I interlaminar fracture toughness vs the crack length for the DCB and the GDCB tests. While for the GDCB a higher number of data reduction points can be used and a more continuous evolution of G_{I} can be determined, only the discreet propagation and arrest points are obtained for the DCB case. Even though, it can be clearly noticed that the fracture behaviour of the material has a large scatter in both cases. This is due to the stick-slip crack propagation behaviour (see Fig. 4.17). Although the fracture behaviour observed and the large scatter associated, the values of the fracture toughness are in the same range for both test methods, validating the GDCB method for mode I delamination testing.

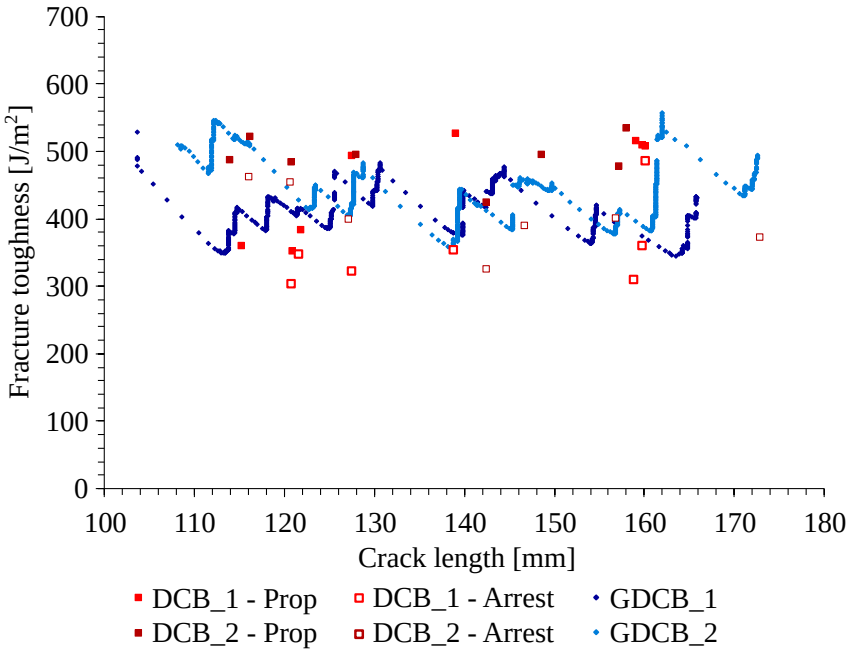

Fig. 4.18: Quasi-static mode I fracture toughness for quasi-static DCB and GDCB tests.

4.2.4 Testing set-up at intermediate/high loading rates

The aim of this testing campaign was to show the performance of the tool when submitted to intermediate/high testing velocities. The objective of these tests was to verify if a symmetrical opening of the specimen arms was obtained under dynamic conditions and if there was any effect of the loading rate on the fracture toughness of the material tested. Accordingly, a series of experimental GDCB tests have been carried out, using the same material and specimen dimensions as in the quasi-static validation.

The tests were performed under laboratory conditions using an Instron VHS servo-hydraulic high loading rate machine. As commented in Section 4.1.2, during the tests special care was taken to ensure that crack propagation took place after the transition zone of the guiding profiles.

As explained before, measuring the force in high-velocity experiments is not recommended. This is why the test set-up was prepared for a data reduction process based on image analysis. The set-up, as shown in Fig. 4.19, consists of a set of two cameras: Camera 1 to track the displacement at the grip pins, and Camera 2 to monitor the crack length growth. The cameras used were two Photron Fastcam SA-Z high-speed cameras with macro lenses Tokina 100 mm f/2.8. A selected position signal of the machine was used as the trigger for activating the high-speed cameras system. The lighting conditions during testing were set in such a way that sharp contrast between the white specimen surface and the background was obtained using an in house lighting system of more than 70000 lumens [115]. In addition, the images taken during the tests were post-processed using the Matlab scripts/algorithms explained in Section 4.2.2.

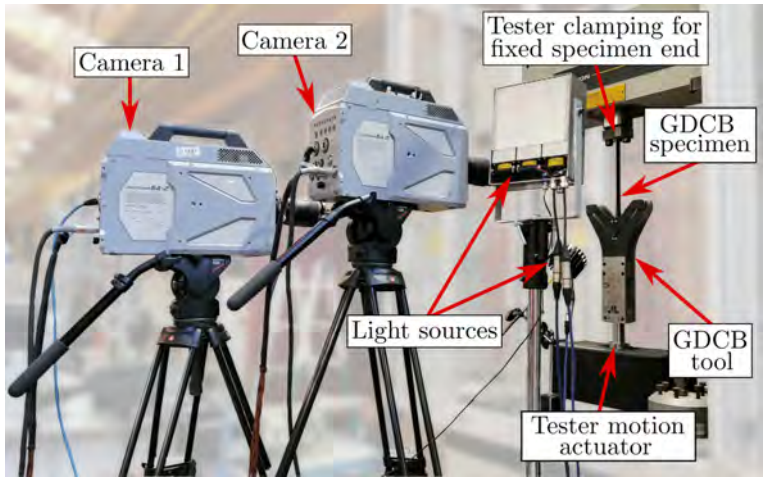

Fig. 4.19: GDCB set-up for high loading rate testing.

The tests were conducted at four different loading velocities of the tester's actuator: 0.1, 1, 3, and 10 m/s (tester loading rates from now on). Three specimens per loading rate were tested. The frame rates and resolution of the cameras used for the different velocities are shown in Tab. 4.1. Camera 1 used a shutter of 1/80000 s, and Camera 2 used a shutter of 1/50000 s. The

resolution of the cameras was adjusted with the increase of the test loading velocity to obtain higher fps and be able to capture the crack propagation, by modifying the required window for each camera.

Tab. 4.1: Frame rates and resolution of the high-speed cameras for the intermediate/high loading rates testing.

Tester loading rate [m/s]	Data acquisition rate [fps]	Resolution Cam 1 [pixels]	Resolution Cam 2 [pixels]
0.1	2000	1024×1024	1024×1024
1	15000	1024×1024	1024×1024
3	30000	896×736	640×1024
10	30000	896×736	640×1024

4.2.5 Results and discussion of the intermediate/high loading rate tests

The results of the mode I interlaminar fracture toughness for intermediate/high loading rates are shown in Fig. 4.20 using Eq. (4.14). The same stick-slip fracture behaviour of the material observed for the quasi-static cases can be

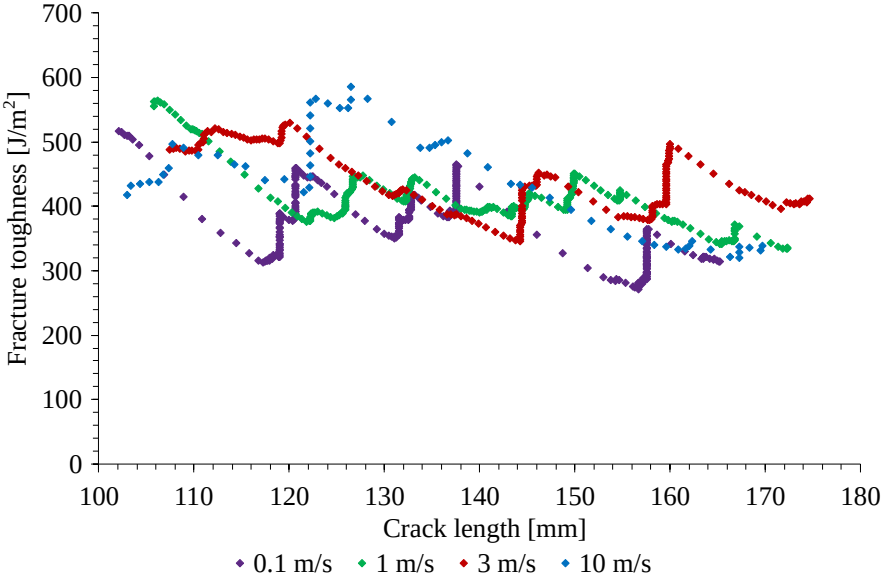

Fig. 4.20: Mode I fracture toughness for the intermediate/high loading rate GDCB tests.

noticed. However, when increasing the loading rate, the stick-slip events are reduced, both in number and amplitude. Although there is significant scatter in the data, similar trends can be observed for all cases.

To assess the effect of taking into account the kinetic energy on the determination of the interlaminar fracture toughness energy, a comparison between the data reduction using Eq. (4.11) (without kinetic energy effects) and Eq. (4.14) (with kinetic energy effects) can be established. Fig. 4.21 shows this comparison for the cases of 3 and 10 m/s. It is noticed that at 3 m/s or smaller, the contribution of the kinetic energy in the dynamic fracture toughness is relatively low, being negligible for the cases of 0.1 and 1 m/s (not included in the figure for simplicity). However, for a loading rate of 10 m/s this contribution cannot be neglected. In fact, the value of G_{I} without taking into account the kinetic term is around 15% higher. This might explain why studies available in the literature report an inaccurate value of the interlaminar fracture toughness at medium/high loading rates.

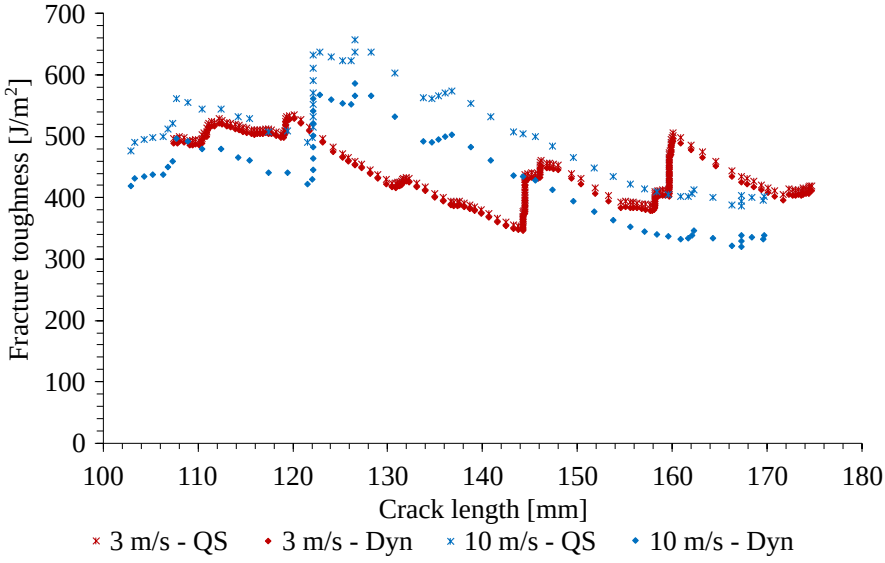

Fig. 4.21: Effect of the kinetic energy for the GDCB tests (QS corresponds to Eq. (4.11), without kinetic energy effects and Dyn corresponds to Eq. (4.14), with kinetic energy effects).

It is possible to use the numerically-based expression for the transition time proposed in Chapter 3 to assess which tester loading rates fulfil the time-based threshold criterion ($t_f > 2.03\ t_\tau$) so a quasi-static data reduction scheme can be used. Being t_τ the transition time, and t_f the time to fracture, i.e., the time of the crack propagation start, for the specimen dimensions and material used in these tests, a transition time of 1.8 ms is obtained. Thus, the time to fracture should be $t_f > 3.6$ ms. For the tester loading rates considered in this case, 0.1, 1, 3 and 10 m/s, the corresponding times to fracture are 200, 24, 7.3 and 2 ms, respectively. Therefore, according to this criterion, only the tests at 10 m/s cannot be treated using a quasi-static data reduction scheme. Besides, even in the case of tester loading rate of 3 m/s, where the kinetic energy contribution over the fracture toughness is perceptible as shown in Fig. 4.21, the effect is minimum and it can be neglected.

Tab. 4.2 summarises the mean values of the interlaminar fracture toughness for the quasi-static, DCB and GDCB, and intermediate/high loading rates, GDCB. No clear effect of the loading rate can be seen up to 3 m/s tester velocities. As previously explained, there is a high scatter in all the cases, as indicated by the large standard deviation values for each case.

Tab. 4.2: Mode I fracture toughness results for the quasi-static testing of the DCB and the GDCB, and for intermediate/high loading rates testing using the GDCB method.

			G_{Ic} [J/mm^2]
DCB	–	quasi-static	422 ± 57
GDCB	–	quasi-static	430 ± 45
GDCB	–	0.1 m/s	402 ± 70
GDCB	–	1 m/s	420 ± 88
GDCB	–	3 m/s	388 ± 92
GDCB	–	10 m/s	489 ± 105

The variation of the opening velocities of the arms with respect to the loading velocities for the GDCB device are shown in Fig. 4.22. The results of the three specimens per loading rate are shown. All the curves present the same overall behaviour: initial velocity increase with constant slope/acceleration, short

transition zone and horizontal/plateau in the constant opening velocity. Once the specimen has reached the velocity plateau, the curve remains smooth until the crack propagation begins, noticing a variation due to the propagation and the stick-slip effect. As it can be observed in the figure, the value of the crack opening velocity in the opening zone is fairly constant and equal to 2.5 times the corresponding tester loading rate. From Fig. 4.22, it is important to remark the smooth velocity plateau at high loading rates, i.e., 10 m/s of the tester or around 25 m/s for the opening velocity of the arms. The oscillations in the crack opening velocity, especially in the opening zone, are due to the stick-slip fracture behaviour of the material. These oscillations are less evident as the loading rate is increased.

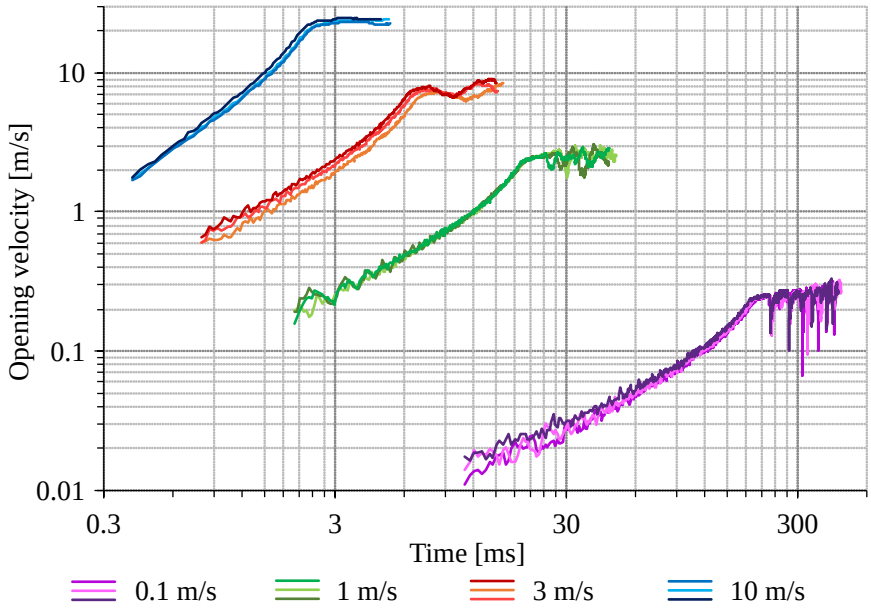

Fig. 4.22: Opening velocities vs time for the loading velocities of the GDCB tests.

Fig. 4.23 summarises the results of the fracture toughness for each of the four tested velocities in terms of the crack propagation velocities. This figure is obtained by considering the mean value of the fracture toughness and the associated standard deviation for different values of crack propagation

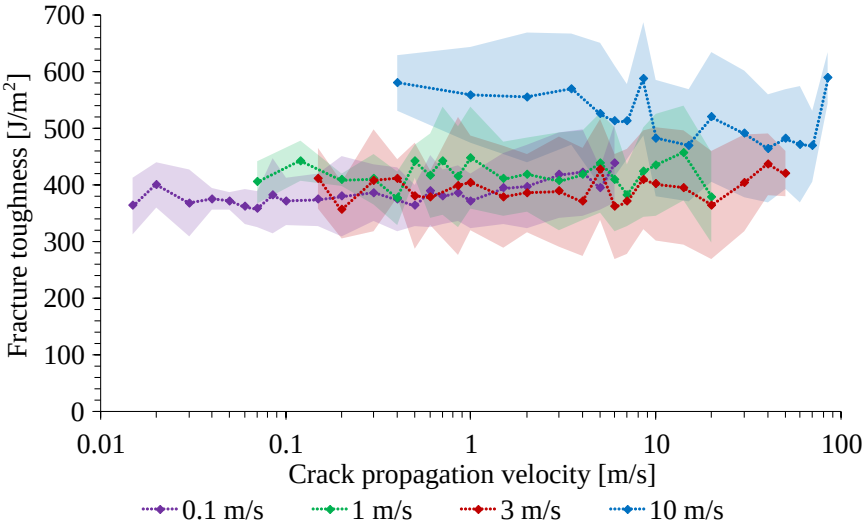

Fig. 4.23: Fracture toughness in terms of the crack propagation velocities.

velocities for each tester loading rate. The results present an important scatter, increasing with the increase of the loading rate. Due to the stick-slip behaviour present in the tests, a wide range of crack propagation velocities can be achieved for each one of the tester loading rates. For the tester loading rate of 0.1 m/s, crack propagation velocities up to 65 times the tester velocity were reached; for 1 and 3 m/s up to 20 times; and for 10 m/s almost 10 times. Therefore, the higher the tester loading rate, the lesser the stick-slip events, and the lesser the crack propagation velocity reached. Despite the scatter, the mean values of the fracture toughness for the tester loading rates of 0.1, 1 and 3 m/s are similar, being possible to conclude that for these loading rates and material used there is no effect over the interlaminar fracture toughness. However, for the tests at 10 m/s, the fracture toughness values are significantly higher, as seen in Fig. 4.23. Although these results seem to indicate that there is an effect of the loading velocity on the interlaminar fracture toughness of the material, there are some considerations to take into account. The dynamic correction of Eq. (4.14) is based on beam theory of a DCB specimen and it does not account for the axial load effect. Besides, non-linear effects can be important enough at these velocities for not being

discarded. Therefore, the contribution to the energy release rate may be over-estimated, being necessary to improve the data reduction method for high loading rates.

Data reduction methods for the dynamic GDCB

5

This chapter presents a study of different data reduction strategies for the Guided Double Cantilever Beam (GDCB) test method proposed and described in Chapter 4, to measure the mode I interlaminar fracture toughness in composites and adhesive joints under different loading rates. Three different data reduction methods have been assessed: a displacement-based formulation taking into account the dynamic contribution through the kinetic energy, a near-crack-tip displacement formulation, and, a numerical assessment based on the experimental specimen arms displacements and using the Virtual Crack-Closure Technique (VCCT) method. A validation of the data reduction strategies was conducted by comparing the quasi-static mode I fracture toughness obtained with the GDCB method and the standardised ISO 15024:2001 [9] and ISO 25217:2009 [68] methods. A test campaign from quasi-static up to high loading rates, 30 m/s, was carried out to show the performance of the data reduction methods at these loading rates.

5.1 Method 1: Displacement-based method with kinetic energy contribution

The first method formulation is based on the deductions of the first order beam theory described by Williams [108] and Hashemi et al. [109], and assuming the postulates of linear elastic fracture mechanics (LEFM). The detailed development of this method is described in Section 4.1.3. Here, a brief summary of the method is presented. For the case of the GDCB configuration of Fig. 5.1, where δ is the opening displacement at the loading point, P is the load with a transverse load equal to the axial-tensile load, $\dot{\delta}$ is the opening displacement rate, b is the width of the specimen, h is half of the specimen

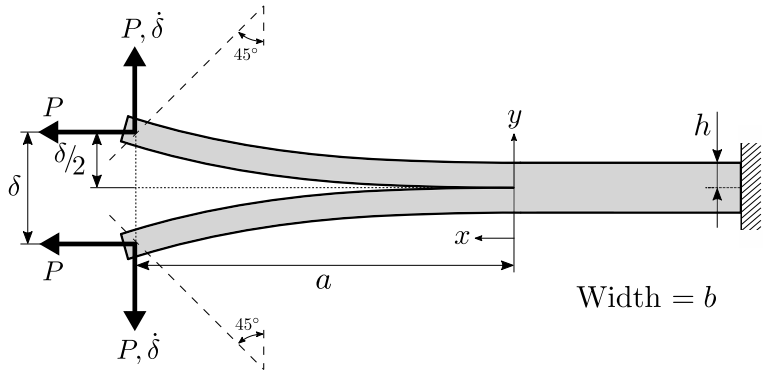

Fig. 5.1: Mode I guided double cantilever beam (GDCB) configuration.

thickness, and a is the crack length; and making use of its compliance from Eq. (4.9), a displacement-based equation for the energy release rate can be obtained as in Eq. (4.11).

Eq. (4.11) is useful when the contribution of the kinetic energy for the analysis of the mode I interlaminar fracture toughness is not relevant. This may occur at quasi-static cases and high-rate cases when the transition time threshold criterion proposed in Chapter 3 is fulfilled. However, in a high-rate scenario where the kinetic energy of the system might play an important role, its contribution to G_{I} can be calculated from the kinetic energy of a cantilever beam with a lumped mass m at the free end as explained in Section 4.1.4. Using simple beam theory and assuming the static displacement profile of a cantilever beam with a transverse loading, the kinetic energy contribution can be expressed as in Eq. (4.13). Finally, the displacement-based expression for the G_{I} of the GDCB method at high loading rates can be expressed as in Eq. (4.14).

The displacement-based method has some limitations since it is based on a beam theory and LEFM. One of its limitations is that it depends on elastic properties that can be rate-sensitive for some materials. Moreover, the measure of the crack length, which can be a complex task, has a huge effect on the accuracy of the method. In fact, this parameter appears to

the forth power in the expression and small measurement errors can lead to completely wrong values of G_{Ic}. In addition, considering the contribution of the axial-loading present in the GDCB test method to the kinetic energy can be complex. Therefore, the dynamic contribution for the GDCB test, which corresponds to the last term in Eq. (4.14), has been assumed the same as for the DCB test. This simplification may not be completely correct and can lead to inaccurate predictions, especially at high-rates.

5.2 Method 2: Crack tip local displacement method

For the second method, a data reduction method based on a near-crack-tip displacement formulation is proposed to obtain the mode I fracture toughness. This method considers the moment equilibrium close to the crack tip of the specimen, carrying out a local analysis to determine the moments through the deformation of the arms. Hence, the analysis must be focused as close as possible to the crack tip, as shown in Fig. 5.2. In this near-crack-tip region, the formulation assumes a linear elastic behaviour of the specimen, thus, the inertia effects can be considered as negligible since the closer to the crack tip

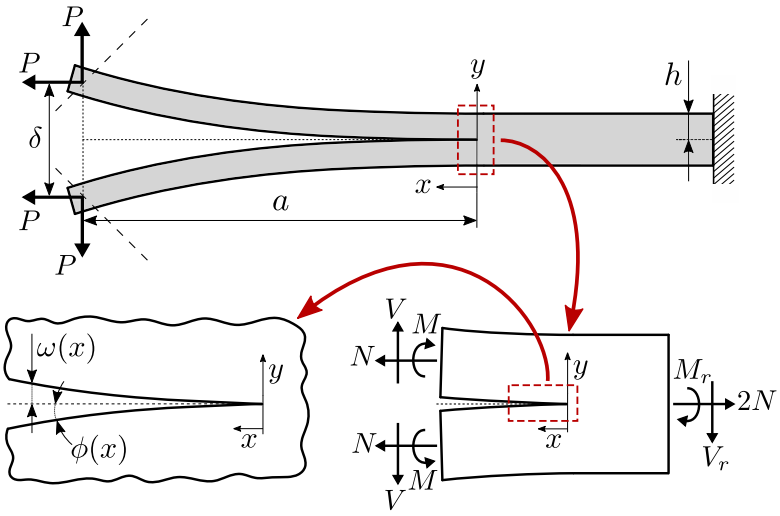

Fig. 5.2: GDCB configuration highlighting the near-crack-tip displacement profile $\omega(x)$ and rotation profile $\phi(x)$.

the lower the mass considered and lower the deformation of the arms due to dynamic effects, allowing to assume that the GDCB problem is treated as a quasi-static case close to the crack tip.

Performing the analysis in a near-crack-tip region as illustrated in Fig. 5.2, from Eq. (4.2) and using the compliance of the DCB, the energy release rate can be described in terms of an equivalent moment M as:

$$G_{\mathrm{I}} = \frac{3M\delta}{2ba^2} \tag{5.1}$$

Using again the compliance of the DCB, a crack-independent expression of the energy release rate can be defined as:

$$G_{\mathrm{I}} = \frac{\varphi}{b}M^2 \tag{5.2}$$

where $\varphi^{-1} = EI = Ebh^3/12$, being I the second moment of area of the cross section.

In the expressions in Eqs. (5.1) and (5.2) the contribution of the axial-load of the GDCB is implicitly considered because it is based on a moment analysis and the equivalent moment is based on the experimental deformation of the arms near the crack tip, thus, only an equivalent vertical load is used for compliance.

Then, the equation for the energy release rate can be obtained using the Euler-Bernoulli theory where $M = \varphi^{-1}\mathrm{d}\phi/\mathrm{d}x$ and $\mathrm{d}\omega/\mathrm{d}x + \phi = 0$, being $\omega(x)$ the opening displacement of the arms near the crack tip and $\phi(x)$ the rotation of the arms near the crack tip, defined by the n-grade polynomial expressions:

$$\omega(x) = \omega_0 + \omega_1 x + \omega_2 x^2 + \omega_3 x^3 + ... + \omega_n x^n \tag{5.3}$$

$$\phi(x) = \phi_0 + \phi_1 x + \phi_2 x^2 + \phi_3 x^3 + ... + \phi_n x^n$$

For the case where the analysis is carried out sufficiently close to the crack tip, i.e., when $x \to 0$, the equivalent moment can be expressed as:

$$M = \varphi^{-1}\frac{\mathrm{d}\phi}{\mathrm{d}x} = \varphi^{-1}\phi_1 \tag{5.4}$$

This solution implies measuring the rotations close to the crack tip, which can require a complex set-up. However, measuring the near-crack-tip displacement profile can be performed in an easier way. Then, using the second derivative of the displacements of the arms, the equivalent moment can be expressed in terms only of the near-crack-tip displacement parameters as:

$$M = -\varphi^{-1}\frac{\mathrm{d}^2\omega}{\mathrm{d}x^2} = \varphi^{-1}(2\omega_2) \tag{5.5}$$

With this solution, it does not matter the degree of the polynomial expression used for the description of the experimental displacement ($n \geq 2$). However, when determining the opening displacement of the arms, for instance using an image analysis, it is important to define a correct grade of the polynomial fitting expression, since the coefficients can change drastically and the results may vary considerably. A third grade expression ($n = 3$) is chosen for this study since the quasi-static deformation of a cantilever beam is described by a third grade expression in beam theory [76].

The energy release rate in the GDCB can be determined substituting the equivalent near-crack-tip moment from Eq. (5.5) in Eq. (5.1), resulting in what from now on will be referred to as the expression for Method 2a:

$$G_{\mathrm{I}} = \frac{3Eh^3\delta\omega_2}{12a^2} \tag{5.6}$$

Use of Eq. (5.6) for the determination of the energy release rate has the advantage of reducing the fourth power of the crack length in Method 1 (Eq. (4.14)) to half of it (second power in (Eq. (5.6)). Thus, the possible errors associated to the measure of the crack length should be reduced. However, the use of the second derivative of the near-crack-tip displacements represents a new source of errors.

Combining the displacement profile parameter in Eq. (5.5) with the alternative equation for the energy release rate in Eq. (5.2) results in the energy release rate expression for what from now on will be referred to Method 2b:

$$G_{\mathrm{I}} = \frac{Eh^3{\omega_2}^2}{3} \tag{5.7}$$

The use of Eq. (5.7) avoids the difficult task of physically measure the crack length during the test. However, it still depends on the second derivative of the near-crack-tip displacements, being the critical source of error.

This crack tip local displacement method depends still on the elastic properties that can be rate-sensitive for some materials. Moreover, the accuracy of the method relies on the accuracy of capturing the displacement profile close to the crack tip, being necessary to have a high resolution optical method (high speed cameras in this case). Finally, the advantage of this method is that it can include the dynamic effects by using a quasi-static frame analysis. Since the method uses an equivalent cross section internal moment around the crack tip in order to equilibrate the near-crack-tip displacements of the arms, this near-crack-tip loading state considers all the possible dynamic effects.

5.3 Method 3: Numerical-based method

The third method consists on a numerical assessment using the experimental displacement profiles of the arms in conjunction with the Virtual Crack-Closure Technique (VCCT) method [116] in a Finite Element (FE) model. In this method, the high-rate effects are captured by means of the displacement profile of the arms. However, in contrast to Method 2, the displacement profile for Method 3 considers a longer segment of the crack length.

In fact, the deformed shapes of most of the length of the specimen arm is monitored or measured during the tests. In this way, not only the quasi-static deformation is captured but also the deformation due to the dynamic and inertial effects. Although the deformed shapes of the two arms of the specimen should be symmetric, both arms are analysed to take into account that because of the inertial effects, small differences in the specimen arms can generate slightly different displacement profiles in each arm of the specimen during the test. Finally, a mean of the displacement profiles of both arms is obtained to be used as input for the FE analysis. Then, a FE simulation of the GDCB test is carried out imposing the mean experimental displacement

profile. Applying the one evaluation step VCCT method (Fig. 5.3), the energy release rate can be obtained as:

$$G_{\mathrm{I}} = -\frac{1}{2\Delta a} R_y \Delta u_y \tag{5.8}$$

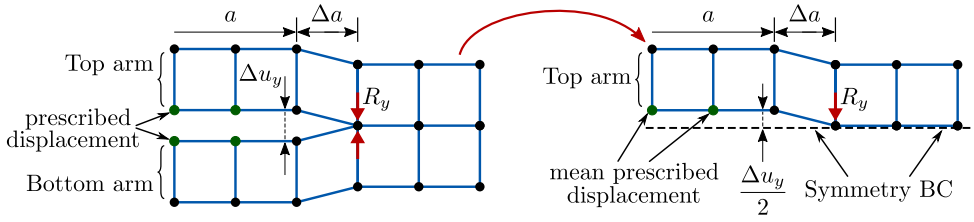

Fig. 5.3: Reaction force R_y and separation displacement Δu_y applied in VCCT analysis based on one evaluation step. Model considering both arms of the specimen in the left image and model considering symmetry of one arm in the right image.

This method is a combination of experimental test data and numerical modelling, having the advantages of no-dependency on a beam theory, and less need of accuracy of the images to obtain the displacement profile as in comparison with the data required for Method 2. However, as limitations of the method, the analysis is still based on LEFM and it needs several FE simulations. Even though, the computational cost and time of the simulations are relatively low.

For this study, a 2D linear elastic model using the commercial software Abaqus™/Standard [103] was developed. One half of the GDCB specimen (upper arm) was modelled and symmetric conditions were assumed, as shown in Fig. 5.4. The specimen was assumed as unidirectional with all fibres parallel to the direction of the crack growth. The composite specimen was modelled using continuum elements with incompatible modes (CPS4I) which eliminate the shear locking phenomenon, properly capturing the bending behaviour [103]. The final mesh of the model was selected by carrying out a study with different mesh sizes looking for a good compromise between processing time and accuracy of the results. A unitary width size was used. A refined mesh of the model was used near the crack tip, as shown in Fig. 5.4, with an element

size of 0.0385 mm in both directions. An element size of 0.95 mm was used along the length of the specimen for the coarse mesh region. An element size of 0.36 mm was defined in the through-thickness directions of the coarse mesh region.

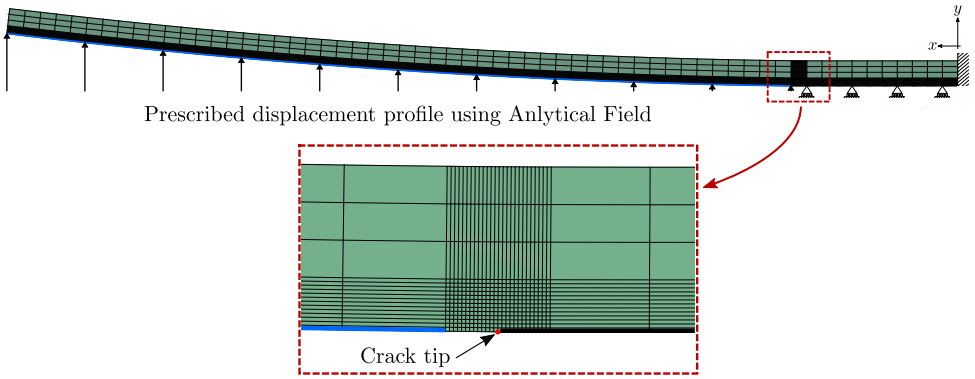

Fig. 5.4: Mesh and boundary conditions of the final model considering a segment of the full specimen length.

The model of the segment of the GDCB had a crack length $a_o = 50$ mm, an arm thickness $h = 1.58$ mm, and a length $l = 60$ mm. The arm of the specimen was loaded imposing a prescribed displacement profile in a segment of the crack length. This segment corresponds to the initial cracked length of 50 mm since it was the length used experimentally by the image post-processing to obtain the displacement profile of the arms. The displacement profile was obtained using a polynomial curve fitting of the images recorded during the tests. Then, the VCCT method was applied to obtain the value of the fracture toughness of the crack propagation for each prescribed displacement profile.

It is important to remark that this model using a segment of the full GDCB specimen was selected to reduce the computational time and the number of elements of the model. However, a comparison with a full GDCB specimen length model was performed to validate the results obtained with the reduced-length model. The full length model was a 2D linear elastic model as represented in Fig. 5.5. In this case, one half of the GDCB specimen (upper

arm) was modelled and symmetric conditions were assumed, as for the model of the segment. The results of the fracture toughness obtained with the VCCT method were equal in both cases with less than 1% of difference, supporting the use of the segmented model.

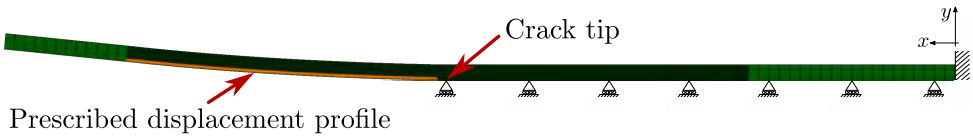

Fig. 5.5: Initial model for the full specimen length simulation.

A summary of the different methods proposed in this chapter for the data reduction of the GDCB test method is presented in Tab. 5.1.

Tab. 5.1: Summary of the data reduction method proposed for the GDCB test method.

Method	Expression for high-rates	Data inputs
1	$G_{\mathrm{I}} = \frac{3Eh^3\delta^2}{16\,(a)^4}\left[\frac{\left(1-\frac{\delta}{2a}\right)^2}{\left(1-\frac{3\delta}{5a}\right)^2}\right] - \frac{33Ebh}{560}\left(\frac{\dot{\delta}}{c_{\mathrm{o}}}\right)^2$	$\delta, \dot{\delta}, a$
2a	$G_{\mathrm{I}} = \frac{3Eh^3\delta\omega_2}{12a^2}$	δ, a, ω_2
2b	$G_{\mathrm{I}} = \frac{Eh^3{\omega_2}^2}{3}$	ω_2
3	$G_{\mathrm{I}} = -\frac{1}{2\Delta a}R_y\Delta u_y$	$\omega(x)$

5.4 Materials and specimens

Two different materials were used in this study: a unidirectional Hexply® M21EV/34%/UD200/IMA/150ATL thermoset-matrix carbon fibre prepreg composite and an adhesively bonded joint made of an epoxy adhesive film FM® 300M with the previous carbon/epoxy composite as adherents. The properties of the used materials cannot be made public due to confidentiality.

However, the elastic, strength and fracture properties of the materials are within the range of the commonly used materials in aeronautic applications.

A 16-ply plate with all layers oriented in the same direction was manufactured. The starter crack was introduced in the mid-plane with a non-adhesive polytetrafluoroethylene (Teflon) film. The laminate had a ply stacking sequence of $[0_8/\text{Teflon}/0_8]$. The specimens preparation were kept the same for the two test configurations, DCB and GDCB. The average specimen thickness was 3.165 mm for the carbon/epoxy composite material and 3.272 mm for the adhesively bonded joint with an adhesive thickness of around 0.1 mm. These thicknesses correspond to the mean value of cured specimens, counting six measures per specimen at different locations with a thickness variation within the limits established by the standard. The longitudinal edges of the specimens were polished with sandpaper of different grain sizes and coated with white spray paint to facilitate the optical tracking of the crack propagation.

The specimen geometry used for the GDCB test method is similar to the one defined for the DCB test ISO 15024:2001 [9] for the characterisation of the mode I interlaminar fracture toughness in laminated materials under quasi-static loading. However, the initial crack length and the total length of the specimen for the GDCB test are larger than the standard DCB specimen. These dimensions have been determined to ensure the initiation of propagation only once the constant opening velocity is reached during the propagation zone of the GDCB, as described in Section 4.1.2, without plastic deformation or failure in the arms of the specimen due to excessive bending or low stiffness. The in-plane dimensions of the GDCB samples were 350×20 mm^2. The pre-crack was 150 mm for both materials, the composite laminate and the adhesively bonded joint. As recommended by the DCB standard [9], all pre-cracks were extended a few millimetres using the DCB set-up to avoid any influence of resin-rich pockets originated at the edge of the Teflon tape. Once the specimens were placed into the grips, the initial crack length was around 60 mm for the DCB and 146 mm for the GDCB. Four opening displacement

rates were tested: quasi-static (QS), 1, 6 and 30 m/s. Four specimens per loading rate configuration were tested.

5.5 Testing set-up

The set-up was thought in such a way that the different parameters needed for the data reduction methods can be obtained. As the different reduction methods require different input parameters (see Tab. 5.1), a set of two cameras was used to obtain all of them at the same time for each test in order to assess the different method in each test. In this way, Method 1 and Method 2b require two cameras to obtain the different parameters, while Method 2b and Method 3 only require one camera to obtain their respective input parameters. For Method 1 the input parameters are the opening displacement at the loading point δ, the displacement rate at the loading point $\dot{\delta}$, and the crack length a. Method 2a requires the opening displacement at the loading point δ, the crack length a, and the near-crack-tip deformation parameter ω_2. Method 2b only needs the near-crack-tip deformation parameter, ω_2. Method 3 requires the deformation profile of the arms along a relatively long segment from the crack length $\omega(x)$. All of them were obtained during the tests using common reflex cameras for quasi-static tests and high-speed cameras for the high-rate tests as it will be described next.

5.5.1 Quasi-static tests

The quasi-static tests were performed under controlled laboratory conditions using an electromechanical screw-driven MTS machine equipped with a 10 kN load cell for both the DCB and the GDCB tests, with a constant cross-head velocity of 5 mm/min. The DCB quasi-static tests were carried out according to the test method ISO 15024:2001 [9] for the composite laminate and the test method ISO 25217:2009 [68] for the adhesively bonded joint. The exception from the test standards was to use a side-clamped beam (SCB) test fixture [117], and only four specimens were tested. According to the standards ISO 15024 and ISO 25217, the data reduction methods of the test were based on the Corrected beam theory (CBT).

In addition to the own data acquisition system of the testing machine to record load and displacement, a set of two cameras was used for the GDCB QS tests. Camera 1 was used for the tracking of the grip pins. Depending on the data reduction method to be used, the second camera needs to track different locations. Thus, Camera 2 is used to track the crack tip location for Method 1, the near-crack-tip displacement profile for Method 2, and the long range displacement profile for Method 3. The set-up for the quasi-static GDCB tests follows the same configuration as the one shown in Fig. 4.14b of Chapter 4. The displacement at the load-application point was tracked optically by means of markers placed at the pins in the specimen grips. For the GDCB tests, the cameras recorded images at 0.2 Hz with a resolution of 2048 pixels along the loading direction and 328 pixels along the perpendicular direction for Camera 1, and 2048 × 2048 pixels for Camera 2. The lighting conditions during testing were set in such a way that sharp contrast between the white specimen surface and the background was obtained.

5.5.2 Intermediate/high-rate tests

The intermediate/high displacement rate tests were carried out using the GDCB test method described in Chapter 4, using an Instron VSH dynamic servo-hydraulic testing machine. The combination of this testing machine and the GDCB test rig allows obtaining a constant and symmetric opening displacement independently of the loading rate of the test. For the reduction of the experimental data and determination of the energy release rate, the tests were monitored with a high-speed video system. The set-up consisted of a set of two cameras as previously described for the QS tests and using the same configuration as the one presented in Fig. 4.19 of Chapter 4. Two Photron Fastcam SA-Z high-speed cameras were used: Camera 1 with a macro lens Tokina 100 mm f/2.8, a resolution of 896×544 pixels and a shutter of 1/61538 s; Camera 2 with a macro lens Pentax 100 mm f/4, a resolution of 384×1024 and a shutter of 1/66667 s. Both cameras used a data acquisition rate of 42000 fps for all the loading rates. A selected position signal of the machine was used as the trigger for activating the high-speed cameras system. The

lighting conditions during testing were set in such a way that sharp contrast between the white specimen surface and the background was obtained using an in house lighting system of more than 70000 lumens [115].

5.5.3 Image post-processing

The image frames obtained from the quasi-static tests and the high-rate tests were post-processed using in-house Matlab scripts/algorithms to obtain the required data for each of the data reduction methods. The post-processing is the same for the quasi-static and the high-rate GDCB tests. Fig. 5.6 shows a photo frame for the set of two cameras used in the GDCB test. The photo frames of Camera 2 in Fig. 5.6b were rotated 90° anti-clockwise for the post-processing.

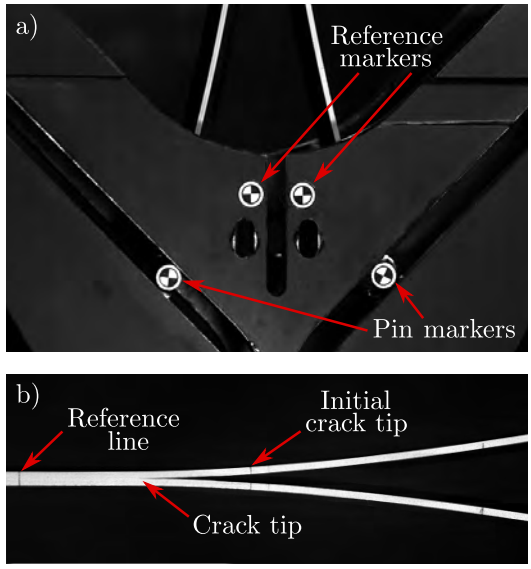

Fig. 5.6: Photo frames from a) Camera 1 and b) Camera 2 for the image post-processing of the GDCB.

The script for Camera 1 analyses all the image frames to determine the current position of the grip pins and the reference markers. Then, the opening displacement is obtained as the distance between the two loading pins, as seen in Fig. 5.7. The reference markers are used as set points for the pin

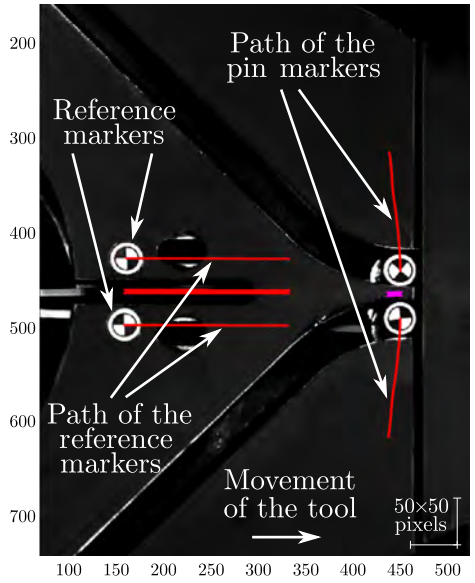

Fig. 5.7: Matlab script image from Camera 1 for the analysis of the GDCB (axes units in pixels).

markers, and as a control for the conversion from pixels to millimetres. Using the opening displacement and the test time, the opening loading rate can be calculated.

A second Matlab script was used to determine the current position of the crack tip and the arm displacement profiles during the test by post-processing the images taken with Camera 2. First, the displacement of the longitudinal outer edge of each specimen arm is detected and a polynomial expression is adjusted to each outer arm edge by a curve fitting process, as shown in Fig. 5.8a. Then, to obtain the crack length required as input data in Method 1 and Method 2a, the detected edge points and the fitted curves are translated to the middle of the specimen where the crack is actually located, as shown in Fig. 5.8b. Finally, the crack tip is detected by the intersection of the two polynomial curves. It is important to mention that in contrast to the image post-processing previously performed in Section 4.2.2 of Chapter 4 (see Fig. 4.16), in this case, the outer edges of the specimen are used instead of the

Fig. 5.8: Matlab script images from Camera 2 for the analysis of the GDCB of a) the outer edge detection, b) translated edge curve fitting, c) a zoom for the predicted crack for initial crack and d) a zoom of an analysis during crack propagation.

inner ones since an elastic behaviour with no shear effects is assumed and these surfaces are not affected by the waviness or small defects caused during the crack propagation, having a clearer response.

The crack length obtained using this approach just before propagation starts is a bit longer than the crack length measured using the mark from specimen preparation with the predicted crack length, as seen in Fig. 5.8c. This difference is around 2 mm, which is similar to the values of the correction factor χh defined by Hashemi et al. [109] to determine the effective crack length. Therefore, this image post-processing approach already accounts for

the rotation of the arms at the crack tip.

To determine the displacement profile parameter ω_2 for Method 2a and Method 2b, the near-crack-tip portion of the initially detected outer edges of the specimen arms is used (Fig. 5.8a). In this case, around half of the data points collected for the process to obtain the crack length are used, ensuring enough data points for the fitting process but being as close as possible to the crack tip to minimise the possible dynamic effects. Then, a third-grade polynomial expression is adjusted to each outer arm edge by a curve fitting process and the ω_2 parameter is determined. Finally, the polynomial expressions adjusted to the deflection of the specimen arms, as shown in Fig. 5.8b and 5.8d, are use to obtain the displacement profile $\omega(x)$, and therefore, to impose the prescribed displacements in the FE model used in Method 3.

5.6 Results and discussion

The results of the fracture toughness presented in this section have been normalised by the respective standardised quasi-static DCB value using the CBT data reduction method, $G_{\text{Ic-QS-CBT}}$. The results related to the composite laminate are presented first and then the results of the adhesively bonded joint.

5.6.1 Opening loading rates

Fig. 5.9 summarises some examples of the evolution of the opening loading rates tested, 1, 6 and 30 m/s, and the corresponding displacement rate applied by the tester actuator for both material configurations, the composite laminate and the adhesively bonded joint. The black and red curves show the acceleration ramp of the tester until reaching a constant velocity. The green and blue curves show that the crack opening of the specimens is happening when the actuator reached the predefined constant velocity. It is clear that the start of crack propagations is delayed in the case of the adhesively bonded joint. This can be due to the higher fracture toughness of the adhesive with

respect to the composite one and the use of the same pre-crack length, which implies a higher deflection of the arms for crack propagation in the case of the adhesive. The curves also show some changes in the behaviour of the opening loading rates during the crack propagation, mainly because of the reduction of the arms stiffness when the crack increases.

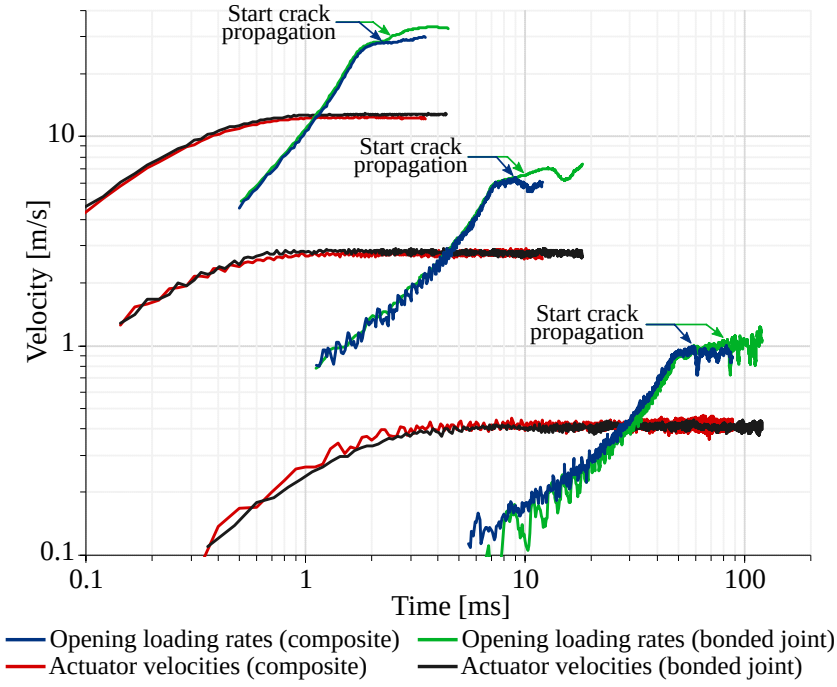

Fig. 5.9: Example of the opening loading rates achieved and the actuator velocities for the high-rate GDCB tests.

5.6.2 Composite fracture toughness

The results of the mode I interlaminar fracture toughness of the composite material for the different loading rates tested are shown in Fig. 5.10. First, this figure is used to compare the results obtained with the quasi-static GDCB (GDCB QS) and the DCB (DCB QS) test methods using the Method 1 data reduction procedure in both cases (Eq. (4.11) for the GDCB and its equivalent equation without the axial-load effect for the DCB). Analysing the DCB QS results, they are slightly higher than the DCB QS-CBT. Even though, it is

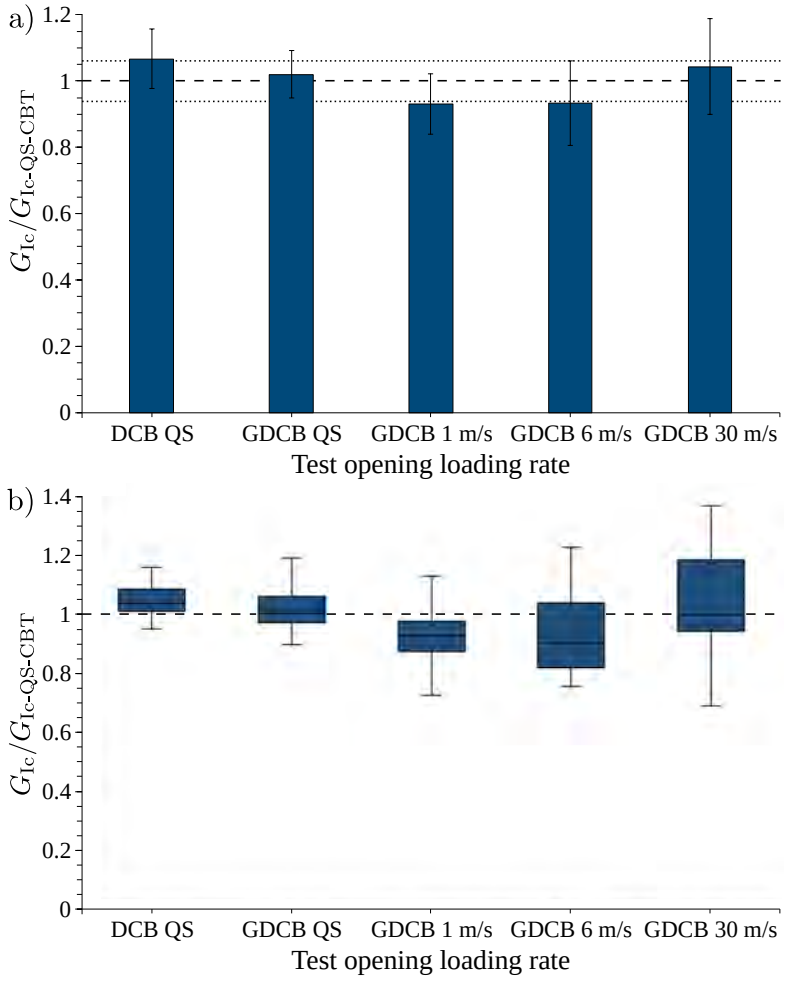

Fig. 5.10: Mode I interlaminar fracture toughness at different loading rates using the Method 1 for the data reduction, showing in a) the mean and the standard deviation, and in b) the distribution of data.

acceptable since the load-independent method can present some differences respect to the CBT method due to the way of collecting the data and the several simplifications introduced in the beam theory [118]. Comparing the GDCB QS and the DCB QS, the results can be considered as equivalent although the variability in the case of the GDCB is higher (Fig. 5.10b) and the mean value is closer to the unit ratio (Fig. 5.10a). Therefore, it can be

considered that the GDCB testing method has been validated to characterise the mode I fracture toughness in composite materials. When analysing the intermediate/high-rate tests, at 1 m/s and 6 m/s the results are below the reference values, i.e., the mean from Fig. 5.10a for each rate is out the DCB QS-CBT range, but the corresponding dispersion (Fig. 5.10b) is higher and falls within the range of the quasi-static values. Analysing the tests at 6 m/s and 30 m/s, there is a clear increase of the dispersion of data, especially in the middle quartiles. For the case of 30 m/s, there is a low minimum value in the first quartile (Fig. 5.10b). In fact, during the experiments it was observed that at this loading rate the initiation values were always lower than for the other loading rates. Although this progressive increase in scatter, the resulting median values (Fig. 5.10a) show that there is no clear rate effect.

A comparison of the different methods used for the data reduction of the GDCB tests with the composite material is presented in Fig. 5.11. The results of the fracture toughness determined with the four different data reduction methods are similar between them and can be assumed as equivalent to the quasi-static ones. In the case of Method 1 and Method 2a, there is a relatively large difference between values at different opening rates. Comparing the mean and the standard deviation of all the methods and velocities (Fig. 5.11a), it can be noticed that Method 1 and Method 2a have a similar behaviour, with a decrease of the results for opening rates of 1 m/s and 6 m/s and an increase at 30 m/s when compared to the QS-CBT value. The results from Method 2b are similar for all the opening rates and close to the QS-CBT. In the case of Method 3, all the mean values are lower than the QS-CBT, with the lowest at 6 m/s. Although in general the results are close to the QS-CBT ones, there is no clear tendency in the variation of the results with the opening loading rate and data reduction method. This may be explained by the accuracy in the analysis of the images to obtain the data for the different data reduction methods. At high displacement rates, the resolution of the images is limited by the test set-up and the cameras used, leading to a high dispersion in the results. Due to the scatter of the data, at this stage it cannot be clearly

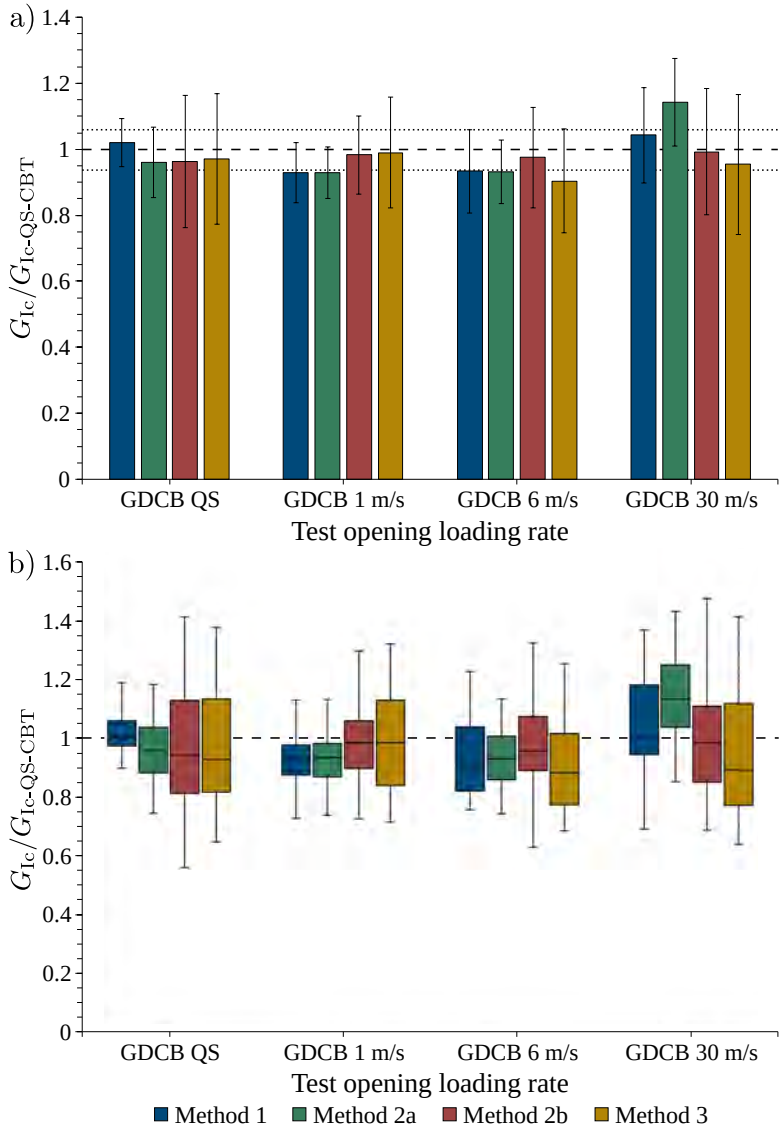

Fig. 5.11: Comparison of data reduction methods for mode I interlaminar fracture toughness at different loading rates, showing in a) the mean and the standard deviation, and in b) the distribution of data.

determined if there is an effect of the loading-rate on the fracture toughness of the material or not. Although the method and the set-up have been proven

to be valid, additional tests with faster and higher resolution cameras are necessary.

When comparing the distribution of data for each method and velocity (Fig. 5.11b), although there is significant scatter in the data for some of the data reduction methods, similar trends can be observed for all cases. There is a tendency to increase the dispersion with the increase of the opening loading rate for Method 1 and Method 2a. However, Method 2b and Method 3 present a high dispersion of data for all the opening rates. Additionally, it can be seen that the crack tip local displacement formulation of Method 2a is the one with the lesser dispersion, meanwhile the crack tip local displacement formulation of Method 2b is the one with higher dispersion in the results. This is linked to the accuracy to read the input parameter for each of the data reduction methods. As explained before and summarised in Tab. 5.1, Method 1 requires three input parameters of which two are associated to tracking at the loading point (opening displacement δ and opening velocity $\dot{\delta}$) and are captured directly from the image analysis with high accuracy. The remaining parameter, the crack length a, is accurately captured by the image post-processing script. This means that Method 1 has a low scattering in the results due to the accuracy of the input data. Method 2a also requires three input parameters of which two of them, the opening displacement δ and the crack length a, are captured as for Method 1, obtaining good accuracy. Meanwhile, the last parameter, the near-crack-tip displacement profile parameter ω_2, is not captured with that high accuracy, promoting a higher scatter. However, since Method 2a involves two parameters captured with good accuracy and one parameter with low accuracy, the results obtained present low scatter. For the case of Method 2b, it depends on only one input parameter, the near-crack-tip displacement profile parameter ω_2, which presents low accuracy and results in the higher scattering in the results. Similarly, Method 3 requires the displacement profile $\omega(x)$ as input parameter, and as in the case of Method 2b, it is captured with low accuracy by the test set-up promoting a high dispersion of the results. As a conclusion, the dispersion in the results of the

different data reduction method is linked not only with the parameters and the associated theory but with the accuracy of the set-up (resolution of the high speed cameras) and the post-processing to capture the required input data.

Fig. 5.12 shows a representative example of the curves of the interlaminar

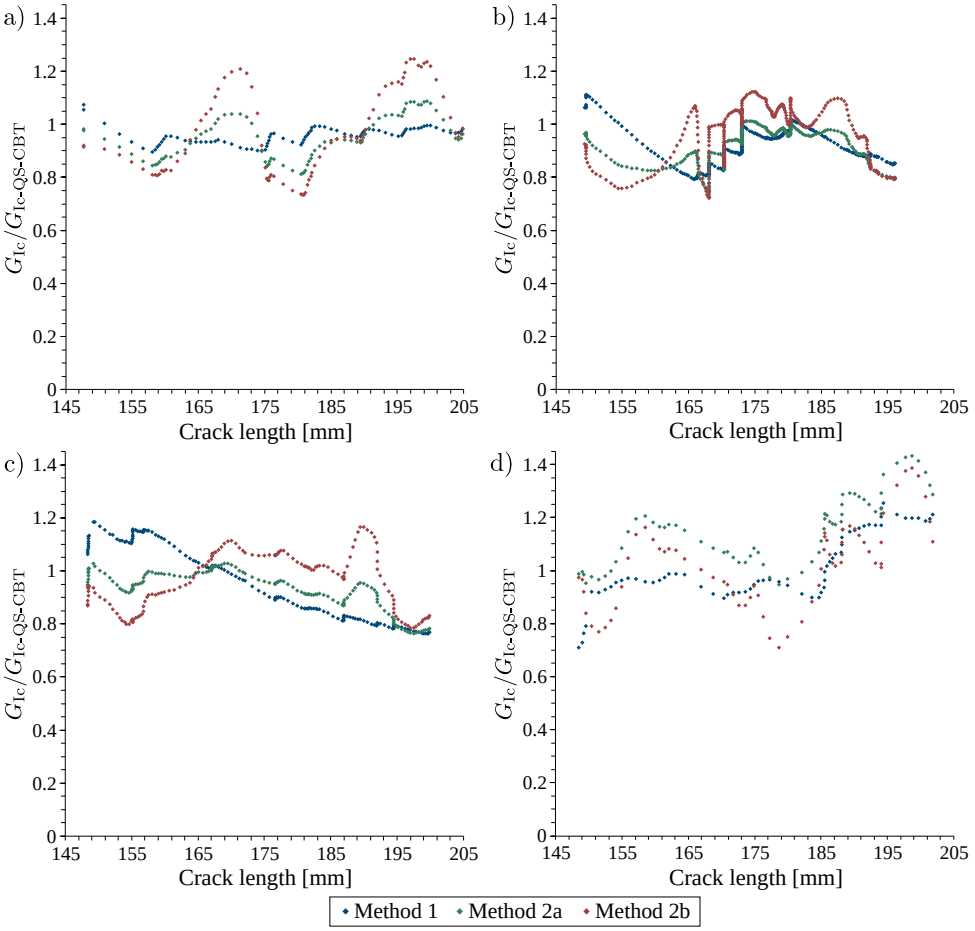

Fig. 5.12: Example of curves of the interlaminar fracture toughness in terms of the crack length for the composite laminate using three different data reduction methods for opening loading rates of a) quasi-static, b) 1 m/s, c) 6 m/s, and d) 30 m/s.

fracture toughness in terms of the crack length for the tested loading rates using Method 1, Method 2a, and Method 2b for the data reduction. It can be seen how the curves of Method 2a tend to have a mean behaviour of the curves of Method 1 and Method 2b, confirming the explanation in the previous paragraph about the influence of the parameters in the dispersion of the results. Additionally, it can be noticed that at high loading rates, i.e., at 30 m/s, the fracture toughness starts with low values and increases with the crack propagation, having a wide range of data and therefore a high dispersion of data. This behaviour can be due to the increase of the inertia effects linked to the large deformation of the arms.

Fig. 5.13 summarises the results of the interlaminar fracture toughness for each of the loading rates in terms of the crack propagation velocities. This figure is obtained by considering the mean value of the fracture toughness and the associated standard deviation for different values of crack propagation velocities for each tester loading rate. In addition, the density distribution for the crack velocities for the tested loading rates, shown in Fig. 5.13a, is included to give an idea of the relationship between the testing opening loading rate and the crack propagation velocity associated. Only the data reduction Method 1, 2a and 2b are used mainly because the Method 3 does not capture the crack length, thus, a crack propagation velocity cannot be assessed. Actually, Method 2b is crack length independent, presenting a similar case as Method 3, however the crack length data from Method 2a is used for Method 2b.

As shown in Fig. 5.13, a wide range of crack propagation velocities can be achieved for each one of the tester loading rates. For the tester loading rate of 1 m/s, crack propagation velocities between 0.05 m/s and 8.5 m/s were reached, having the main range of data between 1.5 and 4 m/s. For the tester loading rate of 6 m/s between 0.25 m/s and 40 m/s of crack propagation velocity, with the main range of data between 10 and 30 m/s. For the tester loading rate of 30 m/s between 4.5 m/s and 70 m/s, with a main range of

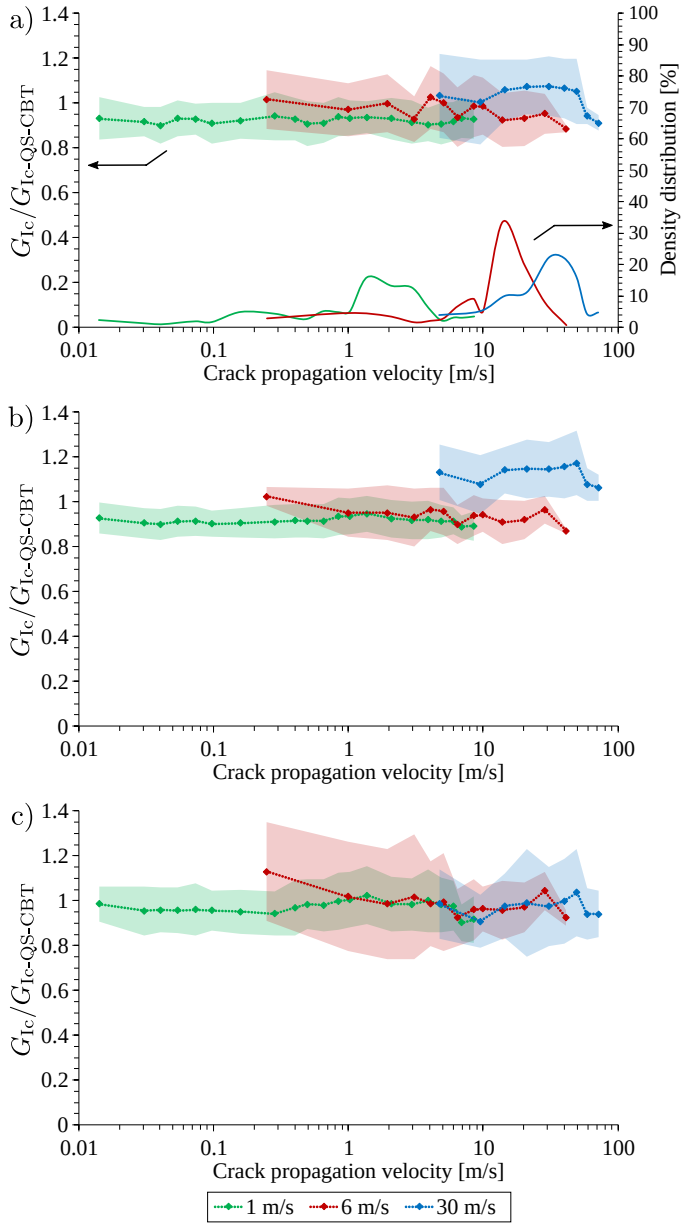

Fig. 5.13: Interlaminar fracture toughness in terms of the crack propagation velocities and the density distribution for the composite laminate using a) Method 1, b) Method 2a, and c) Method 2b. Graph a) also shows the density distribution of data which applies for the three different methods.

data between 25 and 55 m/s. Therefore, the higher the tester loading rate, the lesser the ratio between the crack propagation velocity and the loading rate. In addition, despite the scatter of the fracture toughness in Fig. 5.13a, b, and c, the mean values are similar for the different data reduction methods. It is possible to conclude that for these loading rates there is no effect over the fracture toughness for the composite material used. Thus, comparing the three different method of Fig. 5.13, Method 2b seems to be the one that better eliminates the inertia effect at high loading rates.

5.6.3 Adhesive fracture toughness

For the adhesively bonded joint, the results of the mode I fracture toughness for the different loading rates tested are shown in Fig. 5.14. Similarly to the case of composite material, the figure establishes a comparison between the quasi-static results of the GDCB (GDCB QS) and the DCB (DCB QS) tests when Method 1 is used for the data reduction in both cases (Eq. (4.11) for the GDCB and its equivalent equation without the axial-load effect for the DCB). Analysing the DCB results, they are nearly equivalent to the DCB QS-CBT. When comparing the GDCB QS and the DCB QS, the results are similar. Both of them with a mean value below the QS-CBT one (Fig. 5.14a) and, with a higher dispersion in the case of the GDCB (Fig. 5.14b). This validates, too, the use of the GDCB test method for bonded joints. Moving to the high-rate tests, at 1 m/s the results are above the reference mean value but still in the range of the QS-CBT results. For 6 m/s, there is a decrease of the mean and an increase of the dispersion. Finally, for the case of 30 m/s, there is an increase of the dispersion of data (Fig. 5.14b), especially in the first quartile. This is because during the tests at 30 m/s, the initiation values of crack propagation were really low for this data reduction method. Although having a higher scatter, the median values are in a range where no rate effect can be assumed.

Fig. 5.15 shows a comparison of the different methods used for the data reduction in the case of the adhesively bonded joint. It is noticeable that for

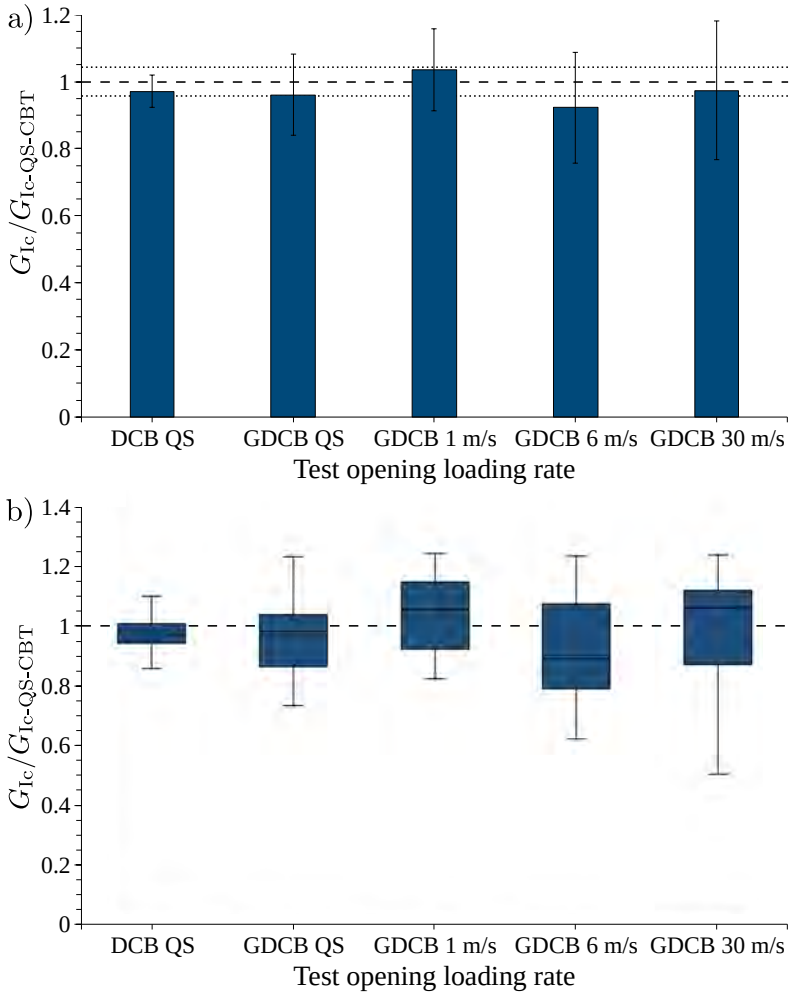

Fig. 5.14: Mode I adhesive fracture toughness at different loading rates using the Method 1 for the data reduction, showing in a) the mean and the standard deviation, and in b) the distribution of data.

this case of adhesively bonded joint, results with Method 3 are not presented. This is because the FE model used for bond joints is the same as for the case of the composite material (model described in Section 5.3). It means that the model does not consider the adhesive layer or its properties. Applying the VCCT method to this model gave values of fracture toughness below half of

the expected ones which indicates the necessity to improve the model, such as considering the adhesive layer and its material behaviour.

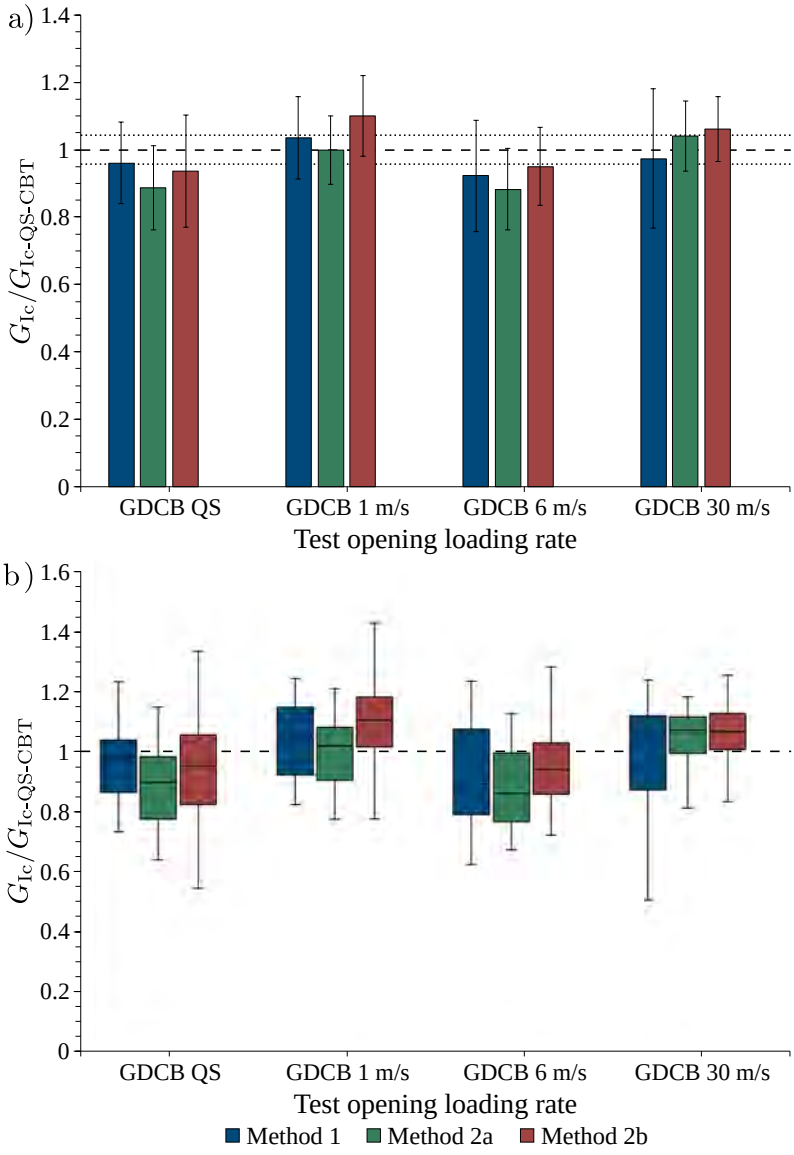

Fig. 5.15: Comparison of data reduction methods for mode I adhesive fracture toughness at different loading rates, showing in a) the mean and the standard deviation, and in b) the distribution of data.

In Fig. 5.15, no clear tendency of the results with respect to the opening rate can be evidenced. The obtained results using Method 1 are below the QS-CBT reference value at QS and 6 m/s, and 30 m/s loading rates. Method 2a presents the lowest mean values at QS and 6 m/s, and an increase of the fracture toughness with respect to the reference for 30 m/s. For Method 2b, a similar behaviour to the results of Method 2a can be seen, with higher mean values in all cases. Method 2a produces always the lowest values while Method 2b corresponds to the highest one except for the quasi-static case. In any case, as mentioned, the three methods result in similar fracture toughness values and within the variability range. For the case of 1 m/s opening displacement, the results are higher than the quasi-static values, but not enough to present a rate effect. Additionally, it can be observed that the dispersion in the results obtained with Method 1 tends to increase with the loading rate. On the contrary, the dispersion in the results for Method 2b is reduced with increasing loading rates. Method 2a presents a similar dispersion for all the cases.

Fig. 5.16 shows a representative example of the curves of the adhesive fracture toughness in terms of the crack length for the tested loading rates using Method 1, Method 2a, and Method 2b for the data reduction. Similar to the case for the composite laminate, the curves of Method 2a tend to present a mean behaviour of the curves of Method 1 and Method 2b. Besides, as in the case of the composite material, the behaviour of the fracture toughness with a low initial value at high opening rates (30 m/s) when using Method 1 can be seen. However, this behaviour is not that relevant for the other two data reduction methods, being possible to better deals with the inertia effects at high loading rates.

Fig. 5.17 shows the variation of the fracture toughness ratio of the adhesively bonded joint versus the crack propagation velocities for each loading rate. Fig. 5.17a also shows the density distribution for the crack velocities for each tested loading rate in the case of the adhesive joint configuration. For the

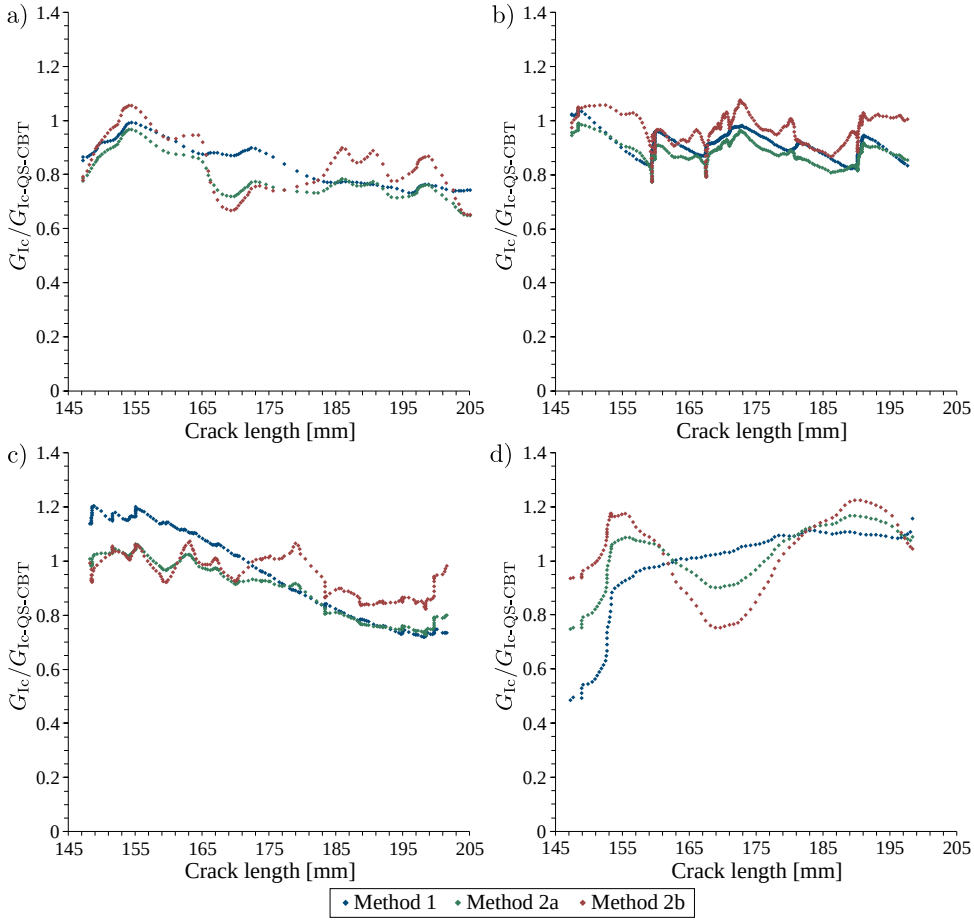

Fig. 5.16: Example of curves of the adhesive fracture energy in terms of the crack length for the bonded joint using three different data reduction methods for opening loading rates of a) quasi-static, b) 1 m/s, c) 6 m/s, and d) 30 m/s.

tester loading rate of 1 m/s, crack propagation velocities between 0.07 m/s and 5 m/s were reached, having the main range of data between 1 and 3 m/s. For the tester loading rate of 6 m/s between 0.08 m/s and 20 m/s of crack propagation velocity, with the main range of data between 9 and 20 m/s. For the tester loading rate of 30 m/s between 1.5 m/s and 50 m/s, with a main range of data between 15 and 40 m/s. In a similar case as the

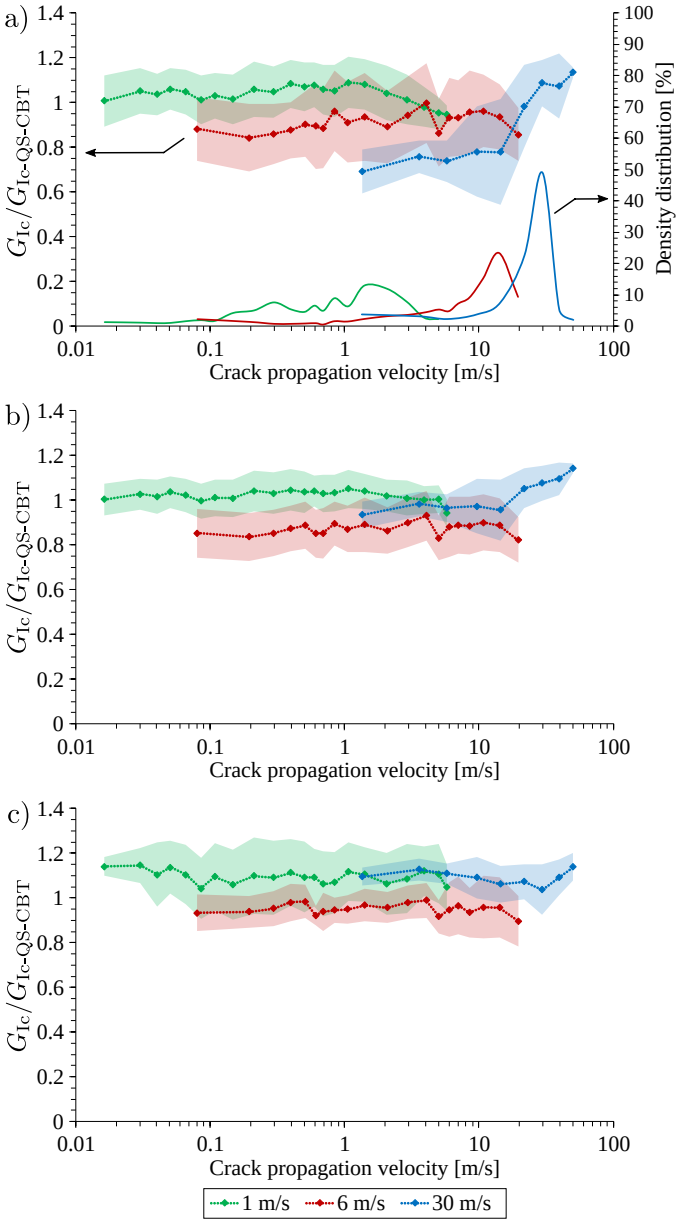

Fig. 5.17: Adhesive fracture toughness in terms of the crack propagation velocities and the data distribution for the bonded joint using a) Method 1, b) Method 2a, and c) Method 2b. Graph a) also shows the density distribution of data which applies for the three different methods.

composite laminate, the higher the tester loading rate the lesser the ratio between the crack propagation velocity and the loading rate. However, lower crack propagation velocities were reached in the bonded joint when compared to the composite laminate. Therefore, it is possible to conclude that the propagation velocity of the crack is slower in the adhesive used.

As an overall, the fracture toughness results shown in Fig. 5.17 present a similar dispersion. For the results using Method 1 (Fig. 5.17a), it seems to be a tendency of decreasing the fracture toughness with the crack propagation velocity and the opening loading rate. However, the low values of the fracture toughness at low crack propagation velocities for the loading rate of 30 m/s can be explain by the low initiation values that are usually at the lower crack propagation velocities, as seen in Fig. 5.16d. In addition, for the adhesive bonded joint tests, the loading rate of 6 m/s produces lower results for the three different data reduction methods. Therefore, despite the scatter, it is possible to conclude that there is no clear effect of the loading rates tested over the adhesive fracture toughness.

6 Methodology for dynamic mode I delamination testing

This chapter summarises the findings of Chapters 3, 4 and 5. Here, as the final result of the thesis, a methodology for dynamic mode I delamination testing in composites or adhesive joints is presented. Coming from the basic definition of methodology, the goal is to help make the research process efficient and reliable by guiding researchers on which method to employ at each step. For this aim, this chapter presents two flow diagrams (Fig. 6.1 and Fig. 6.2) to help selecting the correct options when carrying out mode I delamination tests in composites or adhesively bonded joints.

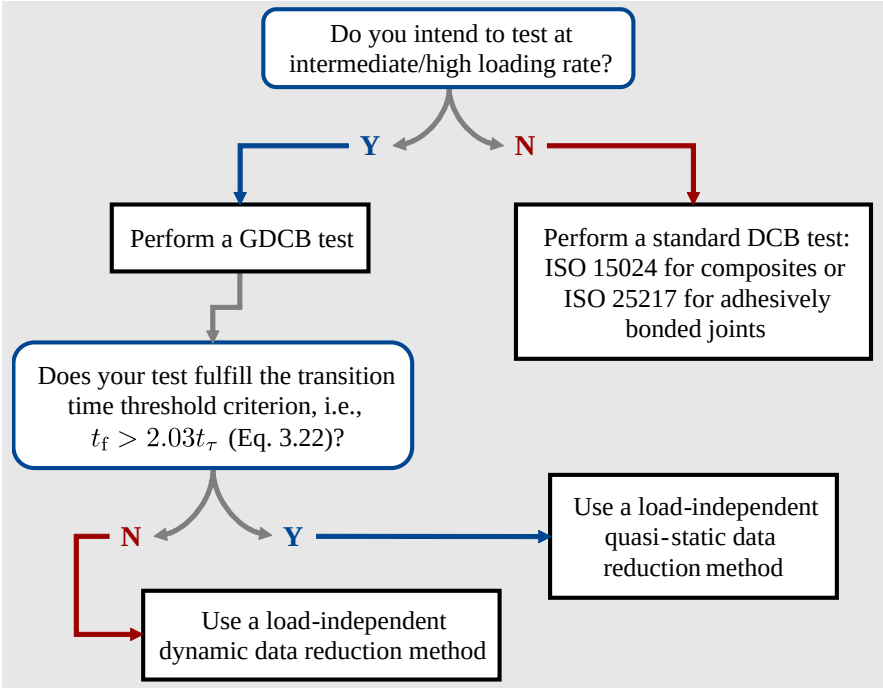

Fig. 6.1: Flow diagram for the mode I fracture toughness testing.

Fig. 6.1 illustrates the flow diagram for the mode I fracture toughness testing as an overall conjunction of the test method and the general data reduction method. This diagram defines when the GDCB test method proposed in Chapter 4 is recommended, and when a quasi-static data reduction scheme can be performed. It is important to remark that, although there are well established standards for the quasi-static mode I testing, the GDCB test method, defined for intermediate/high loading rates, can be also used under quasi-static loading conditions for convenience of test set-up. When using the GDCB method for quasi-static testing, a load-dependent data reduction method can be used as well as the load-independent methods proposed in this thesis for dynamic testing. Additionally, even though the diagram of Fig. 6.1 specifies the use of a quasi-static data reduction method when the transition time threshold criterion is fulfilled, a data reduction method considering the dynamic effects can be used anyway since the dynamic contribution is negligible.

For the case where an intermediate/high loading rate GDCB test method is used and a dynamic data reduction method is needed, a new flow diagram is presented in Fig. 6.2. This diagram shows when the data reduction methods presented in Chapter 5 can be used, depending on the GDCB test set-up (number and resolution of the high speed cameras available).

Since the GDCB is designed for testing at intermediate/high-rates, load-independent data reduction methods should be used. However, the methods can be limited at a certain point by the high speed cameras used in the test set-up. This means that, for example, using the displacement-based method (Method 1) or the crack tip local displacement method (Method 2a) requires two high speed cameras, one to monitor the opening displacement δ and the other one to extract the crack length a and the displacement profile parameter ω_2. Thus, if only one high speed camera is available, these data reduction methods cannot be used (as addressed in Fig. 6.2).

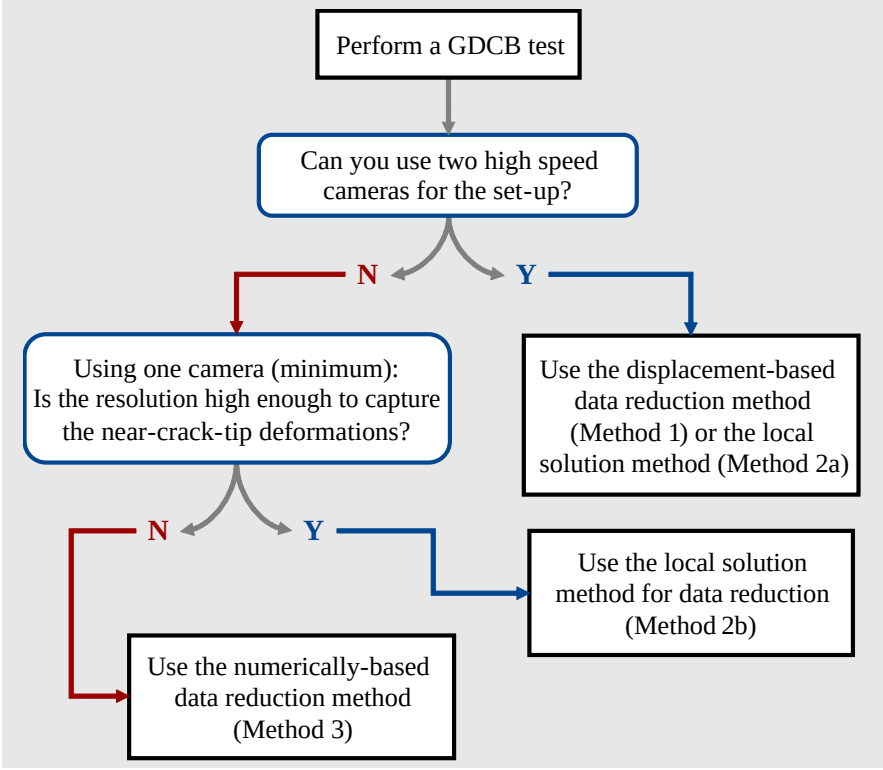

Fig. 6.2: Flow diagram for the data reduction selection for the GDCB test method based on high-speed image recording.

Additionally, a methodology to obtain the mode I fracture toughness in FRPs composite materials and brittle adhesively bonded joints under intermediate/high loading rates using the GDCB test method can be defined by seven general tasks:

(i) Definition: determine the plan for the testing campaign, defining the equipment to be used and the opening velocities to be tested. A servo-hydraulic high speed testing machine is preferred when using the GDCB device. In addition, the number of high-speed cameras to be used for the test set-up must be defined, depending on the availability, since the

data reduction method to be used depends on the number of high-speed cameras and the resolution and set-up to obtain the input data.

(ii) Preparation: prepare the specimens according to the GDCB method description in Chapter 4. This includes the proper selection of the initial crack length as explained in Section 4.2.1.

(iii) Pre-analysis: select the data reduction method to be used according to the transition time threshold criterion and the set-up defined in Task (i) to obtain the output data from the high-speed video recording. This task may be performed after Task (iv) when the time to fracture is unknown, being necessary to test at least one specimen to obtain the value of t_f.

(iv) Testing: perform the tests capturing properly the input data required for the post-processing, paying attention to the testing details defined in Chapter 4. A minimum batch of four specimens per loading rate is recommended.

(v) Image post-processing: perform an analysis of the output data of the tests, i.e., carry out an image analysis of the frames from high speed video to obtain the input values for the data reduction method selected in Task (iii).

(vi) Calculation: using the input data from the image post-processing, perform the data reduction strategy as defined in Chapter 5. Take into account whether or not dynamic considerations are needed for the data reduction method according to Task (iii).

(vii) Analysis of results: interpret the behaviour of the test results, assessing the rate-dependency of the material and the fracture toughness evolution with respect to the crack propagation velocity. Finally, a report of the dynamic testing can be prepared.

Part III

Concluding remarks

Conclusions

7

A methodology for the experimental characterisation of mode I fracture toughness in FRPs composites or adhesively bonded joints under intermediate/high loading rates was proposed. This methodology allows to obtain the rate dependency of the mode I delamination for the tested material. The dynamic mode I delamination methodology proposed is based in three different aspects of analysis: first, a threshold to limit the analysis of dynamic tests using a quasi-static framework; second, the development of a new test set-up for different loading rates to characterise the mode I fracture toughness and solving the main issues found in the literature; and third, the development of well suited data reduction methods for the cases where a quasi-static analysis cannot be performed.

Regarding the first aspect, a transition time concept has been introduced for DCB-type specimens, proposing a time-based threshold criterion to define when the inertia effects can be neglected and a quasi-static based data reduction method can be used. Three different methods to determine the transition time have been proposed: an analytical approach, a numerically-based approach and a graphical method. A dimensional analysis has been carried out using the Buckingham Pi theorem to obtain the numerically-based expression. Additionally, a geometrical scalability study has been performed to validate the use of the graphical method and the numerically-based approach. The numerically-based expression has proved to be a powerful tool to determine the transition time, resulting in smaller differences with respect to the FE simulation in comparison to the expression of the analytical approach.

The effect of the velocity profile and its maximum value on the dynamical response of the system has been also analysed, showing the importance of

the dimensionless parameter D. The transition time has been proved to be independent of the maximum velocity applied when $D = 2$ and up to a certain value when $D = 1$. However, the velocity profile will limit the use of the quasi-static analysis for high values of maximum velocity, especially when a step velocity ($D = 1$) or similar loading is applied.

Thanks to the scalability analysis, and the results of the velocity profile and its maximum value, the graphical method has proved to be useful to define an energy ratio curve for a particular DCB specimen. The obtained curve of energy ratio (U_k/U_e) versus π_1 (tc_o/a_o) can be extrapolated to different DCB specimen configurations, geometries and materials, provided that the π-parameters π_2 ($D = t\dot{\delta}/\delta$) and π_3 (h/a_o) are kept constant.

The proportionality of the time-based threshold criterion has been defined based on a 20% limit of the energy ratio, which corresponds to t_f at least 2.03 times larger than t_τ. The results show that the proposed approach to determine the transition time and the use of the time-based threshold criterion are powerful tools to define when a quasi-static data-reduction scheme can be applied to calculate the mode I fracture toughness in symmetrical opening DCB tests under high loading rates. It is worth mentioning that for the analytical approach, the analysis is restricted to arm bending profiles assumed compliant with the quasi-static beam theory. However, the numerically-based approach should be used when loading at high-rates as it captures accurately the bending profiles of the specimen arms affected by non-linearities.

Regarding the second aspect defined at the beginning of the chapter, a novel test method for the interlaminar fracture toughness in mode I loading at intermediate and high loading rates has been developed. The proposed device, Guided Double Cantilever Beam, solves the issues of asymmetrical loading when using DCB at high loading rates, and it does not require adhesive joints with other parts to carry out the test, allowing for an easy reuse. It is also important to comment that when used with a servo-hydraulic dynamic testing machine, the opening velocity of the arms is constant and that the

negative effects of friction present in other tests are avoided. The GDCB method has been validated under quasi-static loading by comparison with DCB tests. As part of the validation process, an experimental test campaign under intermediate/high loading rates to assess the performance of the device has also been carried out.

From the results of the validation process it can be concluded that the GDCB method is appropriate to be used for dynamic fracture toughness testing in composites. However, for the material used, there is no clear effect of the loading rates over the interlaminar mode I fracture toughness up to 3 m/s tester loading rate. For a loading rate of 10 m/s there is an effect and it must be assessed whether it is due to the type of material and its preparation or the data reduction method used. It is important to remark that the material tested presented stick-slip behaviour and high scatter, which makes it difficult to assess properly the effect of the loading rate. It has been shown that at high loading rates the contribution of the inertia effects over the calculation of the fracture toughness is significant, about 15%.

Now, regarding the third aspect of the dynamic mode I delamination methodology, three different data reduction methods have been proposed in order to assess the data reduction method used initially for the GDCB validation in Chapter 4. The rate-dependency of the mode-I fracture toughness in a thermoset-matrix CFRP composite and an adhesively bonded joint was assessed. The study comparing the three different methods has been performed at different loading rates (from quasi-static to high-rate). The results between the methods presented a similar overall behaviour, but with differences in scattering. No clear rate-dependency for the materials tested has been evidenced with any of the data reduction methods.

The crack tip local displacement method using the equivalent moment and the crack length (Method 2a) is the one that produces lower scattering in the results. Meanwhile, the near-crack-tip formulation of the crack tip local displacement method (Method 2b) is the one that generates a higher scattering.

The numerically-based method (Method 3) results in a similar high scattering as Method 2b for the case of the composite laminate, therefore, the methods dependent of the displacement profile (Method 2b and Method 3) can be improved by improving the resolution of the image acquisition. Although presenting a high scattering, Method 2b is a promising data reduction method for dynamic testing since it is the method that best reduces inertia effects, added to the easy set-up needed, indubitably being dependent of the resolution and accuracy of the high speed camera set-up. In addition, even though there is variability between the mean/measured values of G_{Ic} for the different data reduction methods, these values lay within the range when compared with the QS DCB.

Finally, a methodology for carrying out dynamic mode I tests with the GDCB test set-up has been provided to help other researchers in the characterisation of this property. Besides, the GDCB test method in conjunction with the data reduction methods have proven to work appropriately for opening loading rates between quasi-static to 30 m/s, validating the methodology proposed.

Perspectives & Future work

8

Notwithstanding the satisfactory results of the GDCB test method and the general methodology for the characterisation of the dynamic mode I delamination, and the accomplishment of the objectives proposed at the beginning of this thesis, some improvements from the work done and additional future work can be proposed.

The potential of the transition time and the time-based threshold criterion can be further extended to other test methods related to different modes of fracture, such as the End-Notched Flexure (ENF) or the End-Load Split (ELS) test set-ups for mode II and the Mixed-Mode Bending (MMB) test set-up for mixed-mode testing. In addition, since the criterion has been developed for a DCB test analysis, not all the three methods to determine the transition time can be directly applied to the GDCB. The graphical method to compute the transition time through the energies ratio obtained from a simulation of the GDCB test can be used with accuracy for GDCB if proper simulations of the GDCB test are carried out. However, the analytical and the numerically-based expressions must be improved to account for the kinetic contribution of the axial loading.

In the same way of thinking, the GDCB device can be further extended to other modes of fracture, such as mode II and mixed-mode testing, with some design changes but keeping the main design proposed. Besides, the actual design of the GDCB for the mode I testing can be improved to reduce the required length of the initial crack or to obtain a smoother behaviour during propagation by means of friction reduction.

Concerning the proposed numerical-based method for data reduction, i.e., Method 3, the FE model should be improved when bonded joint are analysed,

such as modelling the adhesive layer with its elastic properties and thickness, and include its material behaviour (visco-elasto-plastic).

Other different data reduction strategies can be explored, such as the use of DIC to improve the accuracy of the crack tip location during propagation or the deformation profile near the crack tip. Additionally, the measurement of the rotation profile near the crack tip can be studied in order to avoid the use of the second derivative of the deformations for the crack tip local displacement data reduction method.

Despite the good performance of the GDCB device and the data reduction method proposed, further studies considering different material can be carried out. Materials with known loading rate dependency, such as the case of thermoplastic FRPs composites or other types of adhesives for the bonded joints, are suggested.

As part of the understanding of the rate sensitivity of the fracture toughness in different materials, the local heating at the crack tip for high loading rates can be studied. It will be necessary to explore the capabilities of high speed infra-red thermal cameras or bonded thermocouples to capture the temperature changes at high rates.

Knowing the rate-dependency of the materials, a cohesive element formulation that takes into account the dynamic effects studied experimentally can be developed to improve numerical models for FE analysis. All this, taking into account the different formulations developed in the research group (AMADE). This will help in the simulation and design of composite structures with high crack propagation rates.

Bibliography

[1] M. May, Measuring the rate-dependent mode I fracture toughness of composites – A review, Composites Part A: Applied Science and Manufacturing 81 (2016) 1–12. doi:10.1016/j.compositesa.2015.10.033.

[2] J. S. Neumayer, Characterisation and simulation of adhesively bonded joints with laminated adherends for crash applications, Phd thesis, Technischen Universität München, 2017.

[3] M. May, Numerical evaluation of cohesive zone models for modeling impact induced delamination in composite materials, Composite Structures 133 (2015) 16–21. doi:10.1016/j.compstruct.2015.07.032.

[4] G. C. Jacob, J. M. Starbuck, J. F. Fellers, S. Simunovic, R. G. Boeman, The effect of loading rate on the fracture toughness of fiber reinforced polymer composites, Journal of Applied Polymer Science 96 (2005) 899–904. doi:10.1002/app.21535.

[5] N. Sela, O. Ishai, Interlaminar fracture toughness and toughening of laminated composite materials: a review, Composites 20 (1989) 423–435. doi:10.1016/0010-4361(89)90211-5.

[6] A. Brunner, B. Blackman, P. Davies, Mode i delamination, in: D. Moore, A. Pavan, J. Williams (Eds.), Fracture Mechanics Testing Methods for Polymers, Adhesives and Composites, volume 28 of *European Structural Integrity Society*, Elsevier, 2001, pp. 277–305. doi:10.1016/S1566-1369(01)80038-8.

[7] N. Nasuha, A. I. Azmi, C. L. Tan, A review on mode-i interlaminar fracture toughness of fibre reinforced composites, Journal of Physics: Conference Series 908 (2017) 012024. doi:10.1088/1742-6596/908/1/012024.

[8] A. Siddique, S. Abid, F. Shafiq, Y. Nawab, H. Wang, B. Shi, S. Saleemi, B. Sun, Mode i fracture toughness of fiber-reinforced polymer composites: A review, Journal of Industrial Textiles 50 (2021) 1165–1192. doi:10.1177/1528083719858767.

[9] ISO 15024:2001, Fibre-reinforced plastic composites — Determination of mode I interlaminar fracture toughness, GIC, for unidirectionally reinforced materials, Standard,

International Standardization Organization, Geneva, CH, 2001.

[10] ASTM D5528-13, Standard Test Method for Mode I Interlaminar Fracture Toughness of Unidirectional Fiber-Reinforced Polymer Matrix Composites, Standard, ASTM International, West Conshohocken, PA, 2013. doi:10.1520/D5528-13.

[11] JIS K 7086:1993, Testing methods for interlaminar fracture toughness of carbon fibre reinforced plastics, Standard, Japanese Standards Association, 1993.

[12] H. Körber, Mechanical response of advanced composites under high strain rates, Ph.D. thesis, Faculdade de Engenharia - Universidade do Porto, 2010.

[13] R. Sierakowski, Strain Rate Behavior of Metals and Composites, in: Convegno IGF XIII Cassino 1997, Gruppo Italiano Frattura, Cassino, Italy, 1997.

[14] G. C. Jacob, J. M. Starbuck, J. F. Fellers, S. Simunovic, R. G. Boeman, Strain rate effects on the mechanical properties of polymer composite materials, Journal of Applied Polymer Science 94 (2004) 296–301. doi:10.1002/app.20901.

[15] H. Hsiao, I. Daniel, Strain rate behavior of composite materials, Composites Part B: Engineering 29 (1998) 521–533. doi:10.1016/S1359-8368(98)00008-0.

[16] H. M. Hsiao, I. M. Daniel, R. D. Cordes, Strain Rate Effects on the Transverse Compressive and Shear Behavior of Unidirectional Composites, Journal of Composite Materials 33 (1999) 1620–1642. doi:10.1177/002199839903301703.

[17] M. Hosur, J. Alexander, U. Vaidya, S. Jeelani, High strain rate compression response of carbon/epoxy laminate composites, Composite Structures 52 (2001) 405–417. doi:10.1016/S0263-8223(01)00031-9.

[18] Q. Bing, C. Sun, Modeling and testing strain rate-dependent compressive strength of carbon/epoxy composites, Composites Science and Technology 65 (2005) 2481–2491. doi:10.1016/j.compscitech.2005.06.012.

[19] J. Wiegand, Constitutive modelling of composite materials under impact loading, Ph.D. thesis, Oxford University, UK„ 2009.

[20] H. Koerber, J. Xavier, P. Camanho, High strain rate characterisation of unidirectional carbon-epoxy im7-8552 in transverse compression and in-plane shear using digital image correlation, Mechanics of Materials 42 (2010) 1004–1019. doi:10.1016/j.mechmat.2010.09.003.

[21] M. Ploeckl, P. Kuhn, J. Grosser, M. Wolfahrt, H. Koerber, A dynamic test methodology for analyzing the strain-rate effect on the longitudinal compressive behavior of fiber-reinforced composites, Composite Structures 180 (2017) 429–438. doi:10.1016/j.compstruct.2017.08.048.

[22] J. Harding, L. M. Welsh, A tensile testing technique for fibre-reinforced composites at impact rates of strain, Journal of Materials Science 18 (1983) 1810–1826. doi:10.1007/BF00542078.

[23] N. Taniguchi, T. Nishiwaki, H. Kawada, Tensile strength of unidirectional CFRP laminate under high strain rate, Advanced Composite Materials 16 (2007) 167–180. doi:10.1163/156855107780918937.

[24] A. Gilat, R. K. Goldberg, G. D. Roberts, Experimental study of strain-rate-dependent behavior of carbon/epoxy composite, Composites Science and Technology 62 (2002) 1469–1476. doi:10.1016/S0266-3538(02)00100-8.

[25] G. H. Staab, A. Gilat, High Strain Rate Response of Angle-Ply Glass/Epoxy Laminates, Journal of Composite Materials 29 (1995) 1308–1320. doi:10.1177/002199839502901003.

[26] M. M. Shokrieh, M. J. Omidi, Investigation of strain rate effects on in-plane shear properties of glass/epoxy composites, Composite Structures 91 (2009) 95–102. doi:10.1016/j.compstruct.2009.04.035.

[27] J.-L. Tsai, C. Sun, Strain rate effect on in-plane shear strength of unidirectional polymeric composites, Composites Science and Technology 65 (2005) 1941–1947. doi:10.1016/j.compscitech.2005.01.013.

[28] C. A. McCarroll, High Rate Fracture Toughness Measurement of Laminated Composites, Ph.D. thesis, Imperial College London, 2011.

[29] P. Kuhn, G. Catalanotti, J. Xavier, P. Camanho, H. Koerber, Fracture toughness and crack resistance curves for fiber compressive failure mode in polymer composites under high rate loading, Composite Structures 182 (2017) 164–175. doi:10.1016/j.compstruct.2017.09.040.

[30] P. Kuhn, G. Catalanotti, J. Xavier, M. Ploeckl, H. Koerber, Determination of the crack resistance curve for intralaminar fiber tensile failure mode in polymer composites under high rate loading, Composite Structures 204 (2018) 276–287. doi:10.1016/j.compstruct.2018.07.039.

[31] B. M. Leite, L. F. M. Leite, V. L. Reis, M. V. Donadon, N. N. A. da Silveira, Strain rate effects on the intralaminar fracture toughness of composite laminates subjected to compressive load, Composite Structures 186 (2018) 94–105. doi:10.1016/j.compstruct.2017.11.091.

[32] L. F. M. Leite, B. M. Leite, V. L. Reis, N. N. Alves da Silveira, M. V. Donadon, Strain rate effects on the intralaminar fracture toughness of composite laminates subjected to tensile load, Composite Structures 201 (2018) 455–467. doi:10.1016/j.compstruct.2018.06.040.

[33] G. Catalanotti, P. Kuhn, J. Xavier, H. Koerber, High strain rate characterisation of intralaminar fracture toughness of gfrps for longitudinal tension and compression failure, Composite Structures 240 (2020) 112068. doi:10.1016/j.compstruct.2020.112068.

[34] S. Yoo, D. Dalli, G. Catalanotti, N. Toso, F. Kessel, H. Voggenreiter, Dynamic intralaminar fracture toughness characterisation of unidirectional carbon fibre-reinforced polymer composites using a high-speed servo-hydraulic test set-up, Composite Structures 295 (2022) 115838. doi:10.1016/j.compstruct.2022.115838.

[35] M. Laffan, S. Pinho, P. Robinson, A. McMillan, Translaminar fracture toughness testing of composites: A review, Polymer Testing 31 (2012) 481–489. doi:10.1016/j.polymertesting.2012.01.002.

[36] J. Hoffmann, H. Cui, N. Petrinic, Determination of the strain-energy release rate of a composite laminate under high-rate tensile deformation in fibre direction, Composites Science and Technology 164 (2018) 110–119. doi:10.1016/j.compscitech.2018.05.034.

[37] W. J. Cantwell, M. Blyton, Influence of Loading Rate on the Interlaminar Fracture Properties of High Performance Composites - A Review, Applied Mechanics Reviews 52 (1999) 199. doi:10.1115/1.3098934.

[38] A. Jadhav, E. Woldesenbet, S.-S. Pang, High strain rate properties of balanced angle-ply graphite/epoxy composites, Composites Part B: Engineering 34 (2003) 339–346. doi:10.1016/S1359-8368(03)00003-9.

[39] F. Jiang, K. S. Vecchio, Hopkinson Bar Loaded Fracture Experimental Technique: A Critical Review of Dynamic Fracture Toughness Tests, Applied Mechanics Reviews 62 (2009) 060802. doi:10.1115/1.3124647.

[40] J. Tsai, C. Guo, C. Sun, Dynamic delamination fracture toughness in unidirectional polymeric composites, Composites Science and Technology 61 (2001) 87–94. doi:10.1016/S0266-3538(00)00197-4.

[41] A. Aliyu, I. Daniel, Effects of Strain Rate on Delamination Fracture Toughness of Graphite/Epoxy, in: Delamination and Debonding of Materials, ASTM International, 100 Barr Harbor Drive, PO Box C700, West Conshohocken, PA 19428-2959, 1985, pp. 336–336–13. doi:10.1520/STP36313S.

[42] M. Colin de Verdiere, A. Skordos, A. Walton, M. May, Influence of loading rate on the delamination response of untufted and tufted carbon epoxy non-crimp fabric composites/Mode II, Engineering Fracture Mechanics 96 (2012) 1–10. doi:10.1016/j.engfracmech.2011.12.011.

[43] W. Feng, K. Reifsnider, G. Sendeckyj, T. Chiao, G. Rodericks, W. Stinchcomb, L. de Vore, D. Hunston, W. Bascom, Effects of Lay-Up, Temperature, and Loading Rate in Double Cantilever Beam Tests of Interlaminar Crack Growth, Journal of Composites Technology and Research 5 (1983) 118. doi:10.1520/CTR10810J.

[44] S. Marzi, A. Rauh, R. M. Hinterhölzl, Fracture mechanical investigations and cohesive zone failure modelling on automotive composites, Composite Structures 111 (2014) 324–331. doi:10.1016/j.compstruct.2014.01.016.

[45] S. Mall, G. Law, M. Katouzian, Loading Rate Effect on Interlaminar Fracture Toughness of a Thermoplastic Composite, Journal of Composite Materials 21 (1987) 569–579. doi:10.1177/002199838702100607.

[46] A. Smiley, R. Pipes, Rate Effects on Mode I Interlaminar Fracture Toughness in Composite Materials, Journal of Composite Materials 21 (1987) 670–687. doi:10.1177/002199838702100706.

[47] T. Kusaka, M. Hojo, Y.-W. Mai, T. Kurokawa, T. Nojima, S. Ochiai, Rate dependence of mode I fracture behaviour in carbon-fibre/epoxy composite laminates, Composites Science and Technology 58 (1998) 591–602. doi:10.1016/S0266-3538(97)00176-0.

[48] B. R. K. Blackman, J. P. Dear, A. J. Kinloch, H. Macgillivray, Y. Wang, J. G. Williams, P. Yayla, The failure of fibre composites and adhesively bonded fibre composites under high rates of test. Part I Mode I loading - experimental studies, Journal of Materials Science 30 (1995) 5885–5900. doi:10.1007/BF01151502.

[49] C. Sun, C. Han, A method for testing interlaminar dynamic fracture toughness of

polymeric composites, Composites Part B: Engineering 35 (2004) 647–655. doi:10.1016/j.compositesb.2004.04.006.

[50] M. Colin de Verdiere, A. Skordos, M. May, A. Walton, Influence of loading rate on the delamination response of untufted and tufted carbon epoxy non crimp fabric composites: Mode I, Engineering Fracture Mechanics 96 (2012) 11–25. doi:10.1016/j.engfracmech.2012.05.015.

[51] K. Low, S. Teng, M. Johar, H. Israr, K. Wong, Mode i delamination behaviour of carbon/epoxy composite at different displacement rates, Composites Part B: Engineering 176 (2019) 107293. doi:10.1016/j.compositesb.2019.107293.

[52] S. I. Thorsson, A. M. Waas, J. Schaefer, B. Justusson, S. Liguore, Effects of elevated loading rates on mode I fracture of composite laminates using a modified wedge-insert fracture method, Composites Science and Technology 156 (2018) 39–47. doi:10.1016/j.compscitech.2017.12.018.

[53] M. Isakov, M. May, P. Hahn, H. Paul, M. Nishi, Fracture toughness measurement without force data – application to high rate dcb on cfrp, Composites Part A: Applied Science and Manufacturing 119 (2019) 176–187. doi:10.1016/j.compositesa.2019.01.030.

[54] B. R. K. Blackman, A. J. Kinloch, Y. Wang, J. G. Williams, The failure of fibre composites and adhesively bonded fibre composites under high rates of test. Part II Mode I loading - dynamic effects, Journal of Materials Science 31 (1996) 4451–4466. doi:10.1007/BF00366341.

[55] B. Blackman, A. Kinloch, F. Rodriguez Sanchez, W. Teo, J. Williams, The fracture behaviour of structural adhesives under high rates of testing, Engineering Fracture Mechanics 76 (2009) 2868–2889. doi:10.1016/j.engfracmech.2009.07.013.

[56] G. Hug, P. Thévenet, J. Fitoussi, D. Baptiste, Effect of the loading rate on mode I interlaminar fracture toughness of laminated composites, Engineering Fracture Mechanics 73 (2006) 2456–2462. doi:10.1016/j.engfracmech.2006.05.019.

[57] D. A. Dillard, D. J. Pohlit, G. C. Jacob, J. M. Starbuck, R. K. Kapania, On the Use of a Driven Wedge Test to Acquire Dynamic Fracture Energies of Bonded Beam Specimens, The Journal of Adhesion 87 (2011) 395–423. doi:10.1080/00218464.2011.562125.

[58] S. Oshima, H. Ishida, T. Kusaka, T. Takeda, Experimental characterization of dynamic crack growth behavior in cfrp adhesive interface, Advanced Composite

Materials 27 (2018) 397–411. doi:10.1080/09243046.2017.1401336.

[59] M. Riezzo, M. Simmons, B. Russell, F. Sket, V. Martínez, C. González, Dynamic characterisation of interlaminar fracture toughness in carbon fibre epoxy composite laminates, Composites Part A: Applied Science and Manufacturing 126 (2019) 105597. doi:10.1016/j.compositesa.2019.105597.

[60] Shuangyan Xu, D. Dillard, Determining the impact resistance of electrically conductive adhesives using a falling wedge test, IEEE Transactions on Components and Packaging Technologies 26 (2003) 554–562. doi:10.1109/tcapt.2003.817646.

[61] Y. Yamagata, X. Lu, Y. Sekiguchi, C. Sato, Experimental investigation of mode I fracture energy of adhesively bonded joints under impact loading conditions, Applied Adhesion Science 5 (2017) 7. doi:10.1186/s40563-017-0087-7.

[62] S. Oshima, A. Yoshimura, Y. Hirano, T. Ogasawara, Experimental method for mode i fracture toughness of composite laminates using wedge loaded double cantilever beam specimens, Composites Part A: Applied Science and Manufacturing 112 (2018) 119–125. doi:10.1016/j.compositesa.2018.05.036.

[63] H. Liu, X. Meng, H. Zhang, H. Nie, C. Zhang, Y. Li, The dynamic crack propagation behavior of mode i interlaminar crack in unidirectional carbon/epoxy composites, Engineering Fracture Mechanics 215 (2019) 65–82. doi:10.1016/j.engfracmech.2019.05.004.

[64] B. Blackman, A. Kinloch, F. Rodriguez-Sanchez, W. Teo, The fracture behaviour of adhesively-bonded composite joints: Effects of rate of test and mode of loading, International Journal of Solids and Structures 49 (2012) 1434–1452. doi:10.1016/j.ijsolstr.2012.02.022.

[65] J. Neumayer, P. Kuhn, H. Koerber, R. Hinterhölzl, Experimental determination of the tensile and shear behaviour of adhesives under impact loading, The Journal of Adhesion 92 (2016) 503–516. doi:10.1080/00218464.2015.1092387.

[66] M. Lißner, E. Alabort, B. Erice, H. Cui, B. Blackman, N. Petrinic, On the dynamic response of adhesively bonded structures, International Journal of Impact Engineering 138 (2020) 103479. doi:10.1016/j.ijimpeng.2019.103479.

[67] N. Ben Salem, J. Jumel, M. Budzik, M. Shanahan, F. Lavelle, Analytical and experimental investigations of crack propagation in adhesively bonded joints with the mixed mode bending (mmb) test part i: Macroscopic analysis and digital image

correlation measurements, Theoretical and Applied Fracture Mechanics 74 (2014) 209–221. doi:10.1016/j.tafmec.2014.05.006.

[68] ISO 25217:2009, Adhesives — Determination of the mode I adhesive fracture energy of structural adhesive joints using double cantilever beam and tapered double cantilever beam specimens, Standard, International Standardization Organization, Geneva, CH, 2009.

[69] J. C. Simon, Response and Failure of Adhesively Bonded Automotive Composite Structures under Impact Loads, Master of science thesis, Virginia Polytechnic Institute and State University, 2004.

[70] D. J. Pohlit, Dynamic Mixed-Mode Fracture of Bonded Composite Joints for Automotive Crashworthiness, Master of science thesis, Virginia Polytechnic Institute and State University, 2007.

[71] T. L. Anderson, Fracture mechanics : fundamentals and applications, CRC Press, 2005.

[72] N. Perez, The Energy Principle, in: Fracture Mechanics, Springer International Publishing, Cham, 2017, pp. 227–256. doi:10.1007/978-3-319-24999-5_6.

[73] J. Rice, Thermodynamics of the quasi-static growth of Griffith cracks, Journal of the Mechanics and Physics of Solids 26 (1978) 61–78. doi:10.1016/0022-5096(78)90014-5.

[74] R. M. Christensen, A rate-dependent criterion for crack growth, International Journal of Fracture 15 (1979) 3–21. doi:10.1007/BF00115904.

[75] H. W. Haslach, A non-equilibrium thermodynamic model for the crack propagation rate, Mech Time-Depend Mater 14 (2010) 91–110. doi:10.1007/s11043-009-9094-9.

[76] J. Berry, Some kinetic considerations of the Griffith criterion for fracture—I: Equations of motion at constant force, Journal of the Mechanics and Physics of Solids 8 (1960) 194–206. doi:10.1016/0022-5096(60)90038-7.

[77] J. Berry, Some kinetic considerations of the Griffith criterion for fracture—II: Equations of motion at constant deformation, Journal of the Mechanics and Physics of Solids 8 (1960) 207–216. doi:10.1016/0022-5096(60)90039-9.

[78] L. B. Freund, Dynamic Fracture Mechanics, Cambridge University Press, Cambridge, 1990. doi:10.1017/CBO9780511546761.

[79] T. Chen, C. M. Harvey, S. Wang, V. V. Silberschmidt, Dynamic interfacial fracture of a double cantilever beam, Engineering Fracture Mechanics 225 (2020) 106246. doi:10.1016/j.engfracmech.2018.11.033.

[80] T. Chen, C. M. Harvey, S. Wang, V. V. Silberschmidt, Delamination propagation under high loading rate, Composite Structures 253 (2020) 112734. doi:10.1016/j.compstruct.2020.112734.

[81] G. Kotsinis, T. Loutas, Strain energy release rate under dynamic loading considering shear and crack tip root rotation effects, European Journal of Mechanics - A/Solids 92 (2022) 104435. doi:10.1016/j.euromechsol.2021.104435.

[82] J. Kalthoff, J. Beinert, S. Winkler, Measurements of Dynamic Stress Intensity Factors for Fast Running and Arresting Cracks in Double-Cantilever-Beam Specimens, in: Fast Fracture and Crack Arrest, ASTM International, 100 Barr Harbor Drive, PO Box C700, West Conshohocken, PA 19428-2959, 1977, pp. 161–161–16. doi:10.1520/STP27387S.

[83] T. Nakamura, C. Shih, L. Freund, Analysis of a dynamically loaded three-point-bend ductile fracture specimen, Engineering Fracture Mechanics 25 (1986) 323–339. doi:10.1016/0013-7944(86)90129-3.

[84] T. Nakamura, C. Shih, L. Freund, Three-Dimensional Transient Analysis of a Dynamically Loaded Three-Point-Bend Ductile Fracture Specimen, in: Nonlinear Fracture Mechanics: Volume I Time-Dependent Fracture, ASTM International, 100 Barr Harbor Drive, PO Box C700, West Conshohocken, PA 19428-2959, 1989, pp. 217–241. doi:10.1520/STP26778S.

[85] ISO 12135:2016, Metallic Materials – Unified Method of Test for the Determination of Quasistatic Fracture Toughness, Standard, International Standardization Organization, Geneva, CH, 2016.

[86] ISO 12737:2010, Metallic Materials — Determination of plane-strain fracture toughness, Standard, International Standardization Organization, Geneva, CH, 2010.

[87] ISO 148:2016, Metallic Materials — Charpy pendulum impact test — Part 1: Test method, Standard, International Standardization Organization, Geneva, CH, 2016.

[88] D. R. Ireland, Critical Review of Instrumented Impact Testing, in: M. Dawes (Ed.), International Conference on Dynamic Fracture Toughness, The Welding Institute, London, UK, 1976, pp. 47–62.

[89] W. Böhme, Dynamic Key-Curves for Brittle Fracture Impact Tests and Establishment

of a Transition Time, in: Fracture Mechanics: Twenty-First Symposium, ASTM International, 100 Barr Harbor Drive, PO Box C700, West Conshohocken, PA 19428-2959, 1990, pp. 144–156. doi:10.1520/STP18993S.

[90] J. F. Kalthoff, On the measurement of dynamic fracture toughnesses - a review of recent work, International Journal of Fracture 27 (1985) 277–298. doi:10.1007/BF00017973.

[91] A. T. Zehnder, A. J. Rosakis, Dynamic fracture initiation and propagation in 4340 steel under impact loading, International Journal of Fracture 43 (1990) 271–285. doi:10.1007/BF00035087.

[92] T. Yokoyama, K. Kishida, A novel impact three-point bend test method for determining dynamic fracture-initiation toughness, Experimental Mechanics 29 (1989) 188–194. doi:10.1007/BF02321374.

[93] G. Sunny, V. Prakash, J. J. Lewandowski, Dynamic Fracture of a Zr-based Bulk Metallic Glass, Metallurgical and Materials Transactions A 44 (2013) 4644–4653. doi:10.1007/s11661-013-1810-z.

[94] M. Shazly, V. Prakash, S. Draper, Dynamic Fracture Initiation Toughness of a Gamma (Met-PX) Titanium Aluminide at Elevated Temperatures, Metallurgical and Materials Transactions A 40 (2009) 1400–1412. doi:10.1007/s11661-009-9823-3.

[95] C. F. Martins, M. A. Irfan, V. Prakash, Dynamic fracture of linear medium density polyethylene under impact loading conditions, Materials Science and Engineering: A 465 (2007) 211–222. doi:10.1016/j.msea.2007.02.010.

[96] R. L. Jones, P. C. Davies, Experimental characterisation of dynamic tensile and fracture toughness properties, Fatigue & Fracture of Engineering Materials and Structures 12 (1989) 423–437. doi:10.1111/j.1460-2695.1989.tb00550.x.

[97] ASTM E23-18, Standard Test Methods for Notched Bar Impact Testing of Metallic Materials, Standard, ASTM International, West Conshohocken, PA, 2018. doi:10.1520/E0023-18.

[98] S. Henschel, L. Krüger, Dynamic crack initiation measurements in a four-point split Hopkinson bending device, Engineering Fracture Mechanics 133 (2015) 62–75. doi:10.1016/j.engfracmech.2015.05.020.

[99] K. C. Koppenhoefer, R. H. Dodds, Constraint effects on fracture toughness of impact-loaded, precracked Charpy specimens, Nuclear Engineering and Design 162 (1996) 145–158. doi:10.1016/0029-5493(95)01151-X.

[100] Y. Takashima, F. Minami, Influence of impact velocity on transition time for v-notched charpy specimen, Quarterly Journal of the Japan Welding Society 35 (2017) 80s–84s. doi:10.2207/qjjws.35.80s.

[101] A. G. Dutton, R. A. W. Mines, Analysis of the Hopkinson Pressure Bar loaded Instrumented Charpy Test using an inertial modelling technique, International Journal of Fracture 51 (1991) 187–206. doi:10.1007/bf00045806.

[102] E. Buckingham, On physically similar systems; illustrations of the use of dimensional equations, Phys. Rev. 4 (1914) 345–376. doi:10.1103/PhysRev.4.345.

[103] Dassault Systèmes Simulia Corp., Abaqus Analysis User's Manual, in: Abaqus documentation 6.14, Simulia Worldwide Headquarters, Providence, RI, USA, 2014.

[104] A. Soto, E. V. González, P. Maimí, J. A. Mayugo, P. R. Pasquali, P. P. Camanho, A methodology to simulate low velocity impact and compression after impact in large composite stiffened panels, Composite Structures 204 (2018) 223–238. doi:10.1016/j.compstruct.2018.07.081.

[105] A. Soto, E. V. González, P. Maimí, F. Martín de la Escalera, J. R. Sainz de Aja, E. Alvarez, Low velocity impact and compression after impact simulation of thin ply laminates, Composites Part A: Applied Science and Manufacturing 109 (2018) 413–427. doi:10.1016/j.compositesa.2018.03.017.

[106] M. L. Benzeggagh, M. Kenane, Measurement of mixed-mode delamination fracture toughness of unidirectional glass/epoxy composites with mixed-mode bending apparatus, Composites Science and Technology 56 (1996) 439–449. doi:10.1016/0266-3538(96)00005-X.

[107] A. Soto, E. V. González, P. Maimí, A. Turon, J. R. Sainz de Aja, F. Martín de la Escalera, Cohesive zone length of orthotropic materials undergoing delamination, Engineering Fracture Mechanics 159 (2016) 174–188. doi:10.1016/j.engfracmech.2016.03.033.

[108] J. G. Williams, On the calculation of energy release rates for cracked laminates, International Journal of Fracture 36 (1988) 101–119. doi:10.1007/BF00017790.

[109] S. Hashemi, A. J. Kinloch, J. G. Williams, The analysis of interlaminar fracture in uniaxial fibre-polymer composites, Proceedings of the Royal Society of London. Series A, Mathematical and Physical Sciences 427 (1990) 173–199.

[110] S. Awtar, A. H. Slocum, E. Sevincer, Characteristics of beam-based flexure modules,

Journal of Mechanical Design 129 (2006) 625–639. doi:10.1115/1.2717231.

[111] P. Liu, P. Yan, A modified pseudo-rigid-body modeling approach for compliant mechanisms with fixed-guided beam flexures, Mechanical Sciences 8 (2017) 359–368. doi:10.5194/ms-8-359-2017.

[112] J. Williams, Large displacement and end block effects in the 'dcb' interlaminar test in modes i and ii, Journal of Composite Materials 21 (1987) 330–347. doi:10.1177/002199838702100403.

[113] S. Medina, E. González, N. Blanco, Transition time threshold for double cantilever beam specimens under high loading rates, Engineering Fracture Mechanics 249 (2021) 107754. doi:10.1016/j.engfracmech.2021.107754.

[114] E. González, P. Maimí, J. Sainz de Aja, P. Cruz, P. Camanho, Effects of interply hybridization on the damage resistance and tolerance of composite laminates, Composite Structures 108 (2014) 319–331. doi:10.1016/j.compstruct.2013.09.037.

[115] J. Artero-Guerrero, J. Pernas-Sánchez, J. López-Puente, D. Varas, Experimental study of the impactor mass effect on the low velocity impact of carbon/epoxy woven laminates, Composite Structures 133 (2015) 774–781. doi:10.1016/j.compstruct.2015.08.027.

[116] E. Rybicki, M. Kanninen, A finite element calculation of stress intensity factors by a modified crack closure integral, Engineering Fracture Mechanics 9 (1977) 931–938. doi:10.1016/0013-7944(77)90013-3.

[117] J. Renart, N. Blanco, E. Pajares, J. Costa, S. Lazcano, G. Santacruz, Side clamped beam (scb) hinge system for delamination tests in beam-type composite specimens, Composites Science and Technology 71 (2011) 1023–1029. doi:10.1016/j.compscitech.2010.10.005.

[118] W. Xu, Z. Guo, A simple method for determining the mode i interlaminar fracture toughness of composite without measuring the growing crack length, Engineering Fracture Mechanics 191 (2018) 476–485. doi:10.1016/j.engfracmech.2018.01.014.